GLASS CERAMICS FROM A SOUTH AFRICAN PULVERISED FUEL ASH

by

M.J Kirby

A thesis submitted for the degree of Master of Science in Applied Science to the Faculty of Engineering at the University of Cape Town.

Department of Civil Engineering
University of Cape Town

April 1991

ACKNOWLEDGMENTS

I would like to thank a number of people for their assistance during the writing of this thesis:

- Professor R.O. Heckroodt, my supervisor, for his help, guidance and patience,
- Dane Gernecke, Charlie Bruintjies and William Williams of the Electron Microscope Unit,
- The Department of Geology for the X-ray diffraction facilities,
- Bernard Greaves, for the photographic work,
- John Williams, for help in the laboratory,
- E.W Randall of the Department of Chemical Engineering,
- and the students and staff of the Materials Research Group.
- The Foundation of Research Development of the CSIR is gratefully acknowledged for their financial assistance.

CONTENTS

LIST of FIGURES

LIST of TABLES

1. INTRODUCTION

The generation of electricity by the combustion of pulverised coal produces large quantities of coal ash (PFA). The disposal of this ash has become a matter of concern due to the unsightly and hazardous nature of the PFA, and it has been the subject of intense investigations into its suitability as a raw material. Many uses have been proposed for the PFA. When used as landfill or mining backfill, the attraction is the low cost of the material. Other uses, as in the concrete industry, use PFA because of the improvements in quality of the resultant product.

PFA has been suggested as a raw material for the production of wear resistant materials. The PFA is composed in the main of SiO_2 and Al_2O_3, and is a suitable material for the production of alumino-silicate ceramic materials, which are known to be tough and wear resistant.

To establish the suitability of PFA from the Lethabo Power Station as a raw material, a project to prepare glass ceramic materials from the PFA was started. The conversion of the PFA to a glass ceramic material is a complex process involving many stages, and the processing at each stage will affects the final properties of the material.

It is not possible in a short project such as this to examine all the factors which exert some control on the process, and so a small subset of these parameters was selected for study, namely the effect of added oxides on the crystallisation behaviour.

Glass items which crystallise on holding at high temperatures commonly do so by growth of crystals from the surface of the item. This results in a material that is mechanically weak, due to the highly oriented microstructure that results.

Nucleating agents can be used to obviate this. By providing sites for crystal growth in the bulk of the sample, they induce the crystallisation of fine grained ceramics with good mechanical properties.

This study examines the effect of TiO_2, P_2O_5, and a mixture of iron and chrome oxides on the crystallisation of the glass prepared using PFA. The effect of these oxides was evaluated by examination of the microstructure of the crystalline specimens, and the kinetics of crystallisation were analysed by fitting data obtained by isothermal crystallisation of the specimens to the Avrami equation. Finally, the mechanical properties of the materials were tested by solid particle erosion, and the materials ranked against a selection of other materials used for their wear resistance.

2. PULVERISED FUEL ASH (PFA)

2.1 Provenance

Coal is South Africa's primary energy source. Large reserves of low grade coal are available in the RSA. Of some 58 billion tons of recoverable coal reserves in the RSA (Figure 1), 96% are bituminous coal, with a high ash content, used for gasification or combustion. In 1985, 210 million tons of coal were mined, of which 125 million tons were consumed locally. More than 90% of this coal is used for fuel by ESKOM, ISCOR, and other industries, and for gasification by SASOL. ESKOM alone burned 60 million tons of coal in 19 power stations, to generate 20 GW of electricity. A further 18 GW of coal-fired power stations are under construction (Alberts, 1987).

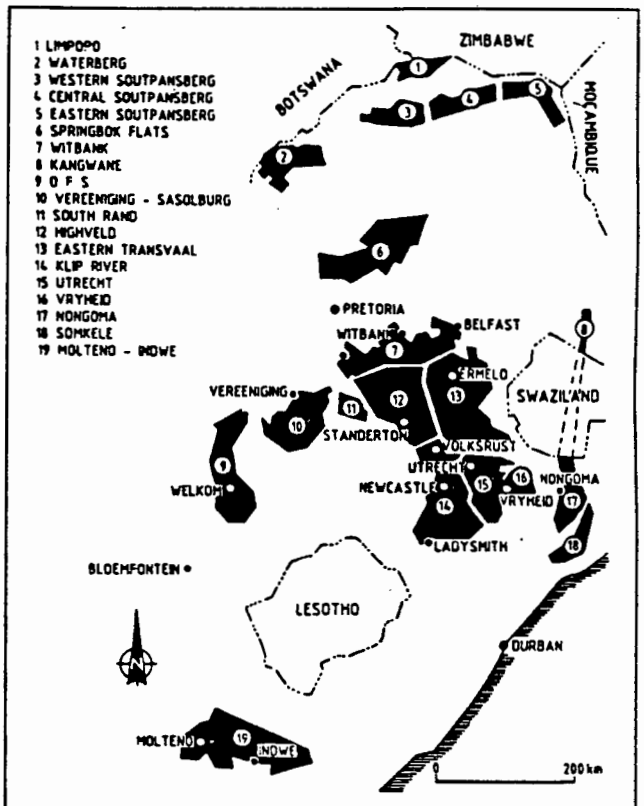

Figure 1: Coalfields of South Africa. (Alberts, 1987)

Coal-fired power stations in the RSA burn about 60 million tons of low grade coal each year, producing 18 million tons of coal ash per annum. The Lethabo power station alone burns 12 million tons of pulverised coal per annum, and with an ash content of 38% this necessitates the disposal of 4.8 million tons of Pulverised Fuel Ash (PFA) each year. At present some 250 million tons of ash lies in heaps in the Eastern Transvaal and is both unsightly and a source of pollution. The PFA

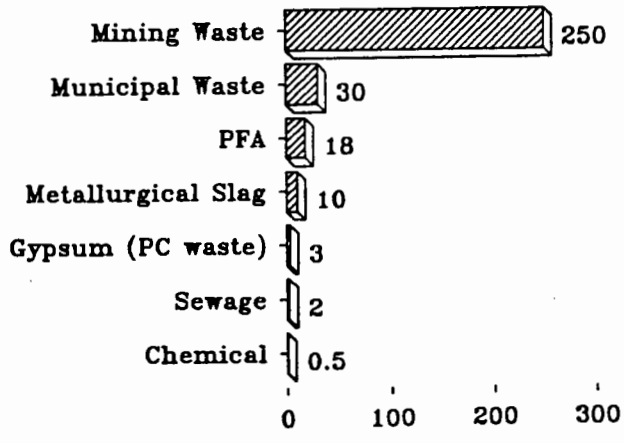

Figure 2: Waste production in the RSA. (Million tons / year : 1985) (Alberts, 1987)

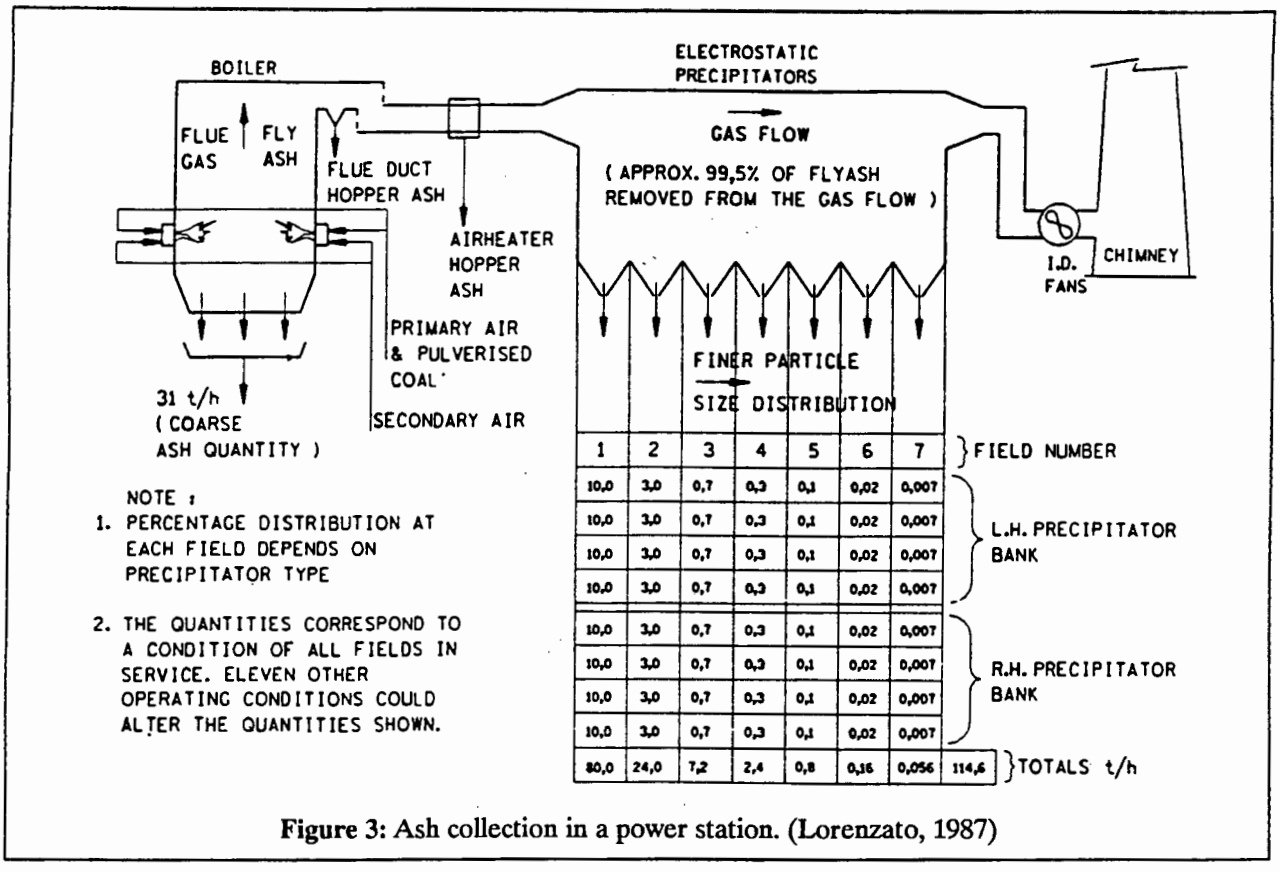

Figure 3: Ash collection in a power station. (Lorenzato, 1987)

produced is the third most abundant source of waste material in the RSA (Figure 2).

Combustion of coal in a boiler gives rise to two types of ash: large particles removed from the bottom of the boiler known as grate ash or bottom ash, and finer particles removed from the boiler via the flue gases, known as Fly Ash or PFA. The PFA is extracted from the flue gases by a series of extractors, usually electrostatic precipitators (Boswell, 1987; Lorenzato, 1987). Figure 3 illustrates in diagrammatic form the operation of a power plant, showing the point of collection of the ash.

To investigate the potential of PFA as a resource, a government sponsored program was launched to examine the suitability of PFA as a raw material for industrial processes. This approach has been successful in many countries; for example in the USA where PFA is now considered the nations' sixth most abundant resource.

2.2 Physical Properties of South African PFA

2.2.1 Chemical Composition

The chemical composition of the coal supplied to a power station has the largest influence on the composition of PFA. Other factors are the conditions within the boiler, which affects the unburnt coal content, as well as the design and efficiency of the precipitators collecting the PFA. The plant design and the operating efficiency of

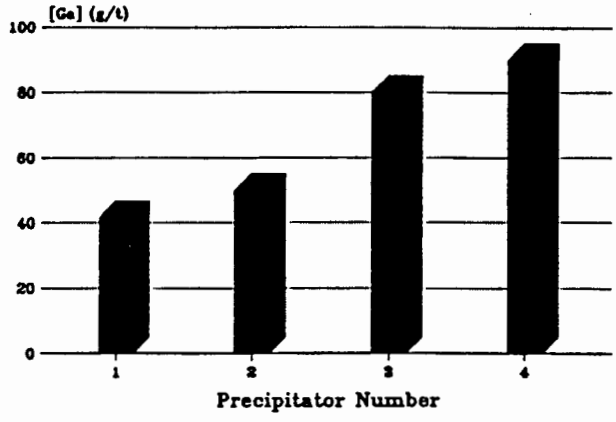

Figure 4: Variation in trace element composition across fields in a power station (Marshall, 1987)

the precipitators affect the type and thus the composition of the PFA collected in each precipitator field.

An extensive study of ash from a number of South African power stations (Willis, 1987) investigated the variation of elemental composition. Table 1 gives typical concentration ranges for the composition of ash samples from a range of power stations. In addition to analysing the bulk composition of ash from these power stations, they analysed samples of PFA from different precipitator fields in each plant. The variation in composition of the PFA from the Matla power station with field of collection is shown in Table 2.

Table 1: Major Element Compositions of PFA bulk samples from some South African Power Stations. (Willis, 1987)

Per Cent Oxide by mass.						
Oxide	Lethabo	Matla	Kriel	Indanga	Camden	Arnot
SiO_2	50.77	38-50	55-61	39	53-63	51-58
Al_2O_3	35.23	25-32	26-29	34	25-27	15-25
CaO	4.36	8.7-15	7.9-12	7.4	6.3-7.0	7.5-10
Fe_2O_3	3.41	3.4-5.0	2.9-3.2	4.7	4.8-5.4	5.7-13
TiO_2	1.67	1.4-1.7	1.5-1.7	1.3	1.3-1.5	1.0-1.4
MnO	0.01	0.04-0.05	0-0.04	0.01	0.04-0.05	0.02
P_2O_5	0.74	0.63-2.9	0.74-1.9	0.96	0.38-0.89	0.4-1.7
S	N/A	0.23-0.5	0.15-0.22	0.49	0.15-0.34	0.18-0.7
MgO	1.2	2.0-3.5	1.9-2.8	1.7	1.7-2.0	1.7-2.6
K2O	0.46	0.8-1	0.6-1	0.5	0.48-0.51	0.55-0.7
Na_2O	0.28	0.5-1	0.3-0.5	0.2	0.16-0.21	0.35-0.87

The only significant variations in the composition of the ash are between grate ash and PFA. The PFA from each precipitator shows little variation in the major

element composition. Trace element variability is greater, particularly among the volatile elements (Figure 4). Generally, composition is not strongly dependent on the point of collection.

With reference to Table 1, some generalization may be made:

i) The ash is high in SiO_2 and Al_2O_3

ii) Other oxides of significance are Fe_2O_3, CaO, and MgO, which together with SiO_2 and Al_2O_3 comprise more than 95% of the PFA.

2.2.2 Mineralogy

The major mineralogical components of PFA are quartz, mullite and glass (Willis, 1987). The mullite content is determined by the Al_2O_3 content of the coal and the combustion conditions. The quartz content of the ash is controlled by the large particle size of the quartz which causes it to collect predominantly in one precipitator. The variation in glass content is largely dependent on cooling conditions in the exhaust.

Table 2: The composition of coal ash, grate ash, and PFA from different precipitators in the Matla Power Station. (Willis, 1987).

Oxide	Ash		Ash from Precipitator #			
Mass %	Coal	Grate	1	2	3	4
SiO_2	47	48	47	45	45	44
Al_2O_3	29	22	26	26	27	28
CaO	10	9.4	9.1	10	10	9.6
Fe_2O_3	3.4	4.8	3.6	3.8	3.7	3.6
S	3.3	0.19	0.37	0.47	0.56	0.61
MgO	2.7	2.1	2.1	2.5	2.8	2.8
TiO_2	1.8	1.3	1.5	1.5	1.6	1.7
P_2O_5	1.1	0.54	1.2	1.8	2.3	2.6
K_2O	0.78	0.89	0.93	0.94	0.97	0.99
Na_2O	0.45	0.38	0.57	0.64	0.68	0.70

Flanagan (1977) described the sequence of events involved in the formation of PFA. This is diagrammatically illustrated in Figure 5. Coal combustion starts with the volatilisation of the organic components. This results in a skeletal char structure which supports the mineral inclusions. As the char skeleton burns away, the inclusions fuse together and leave large ash particles.

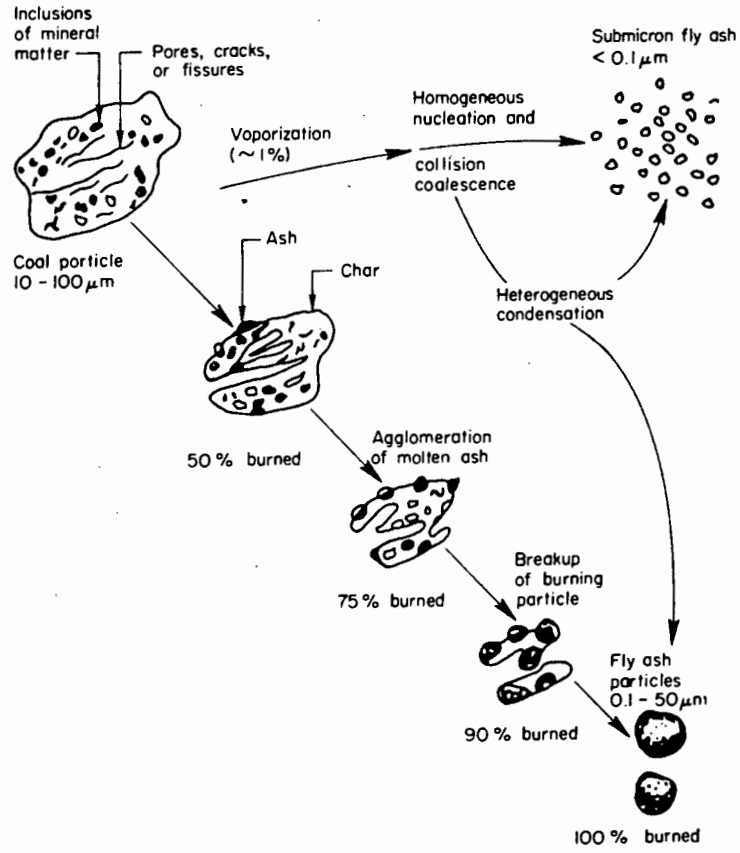

Figure 5: Combustion of coal, leading to the formation of PFA

PFA forms due to the volatilisation and subsequent recrystallisation of ash components. There are three stages to ash volatilisation, depending on the temperature of the ash. Vaporisation of alkali metals, sublimation or volatilisation

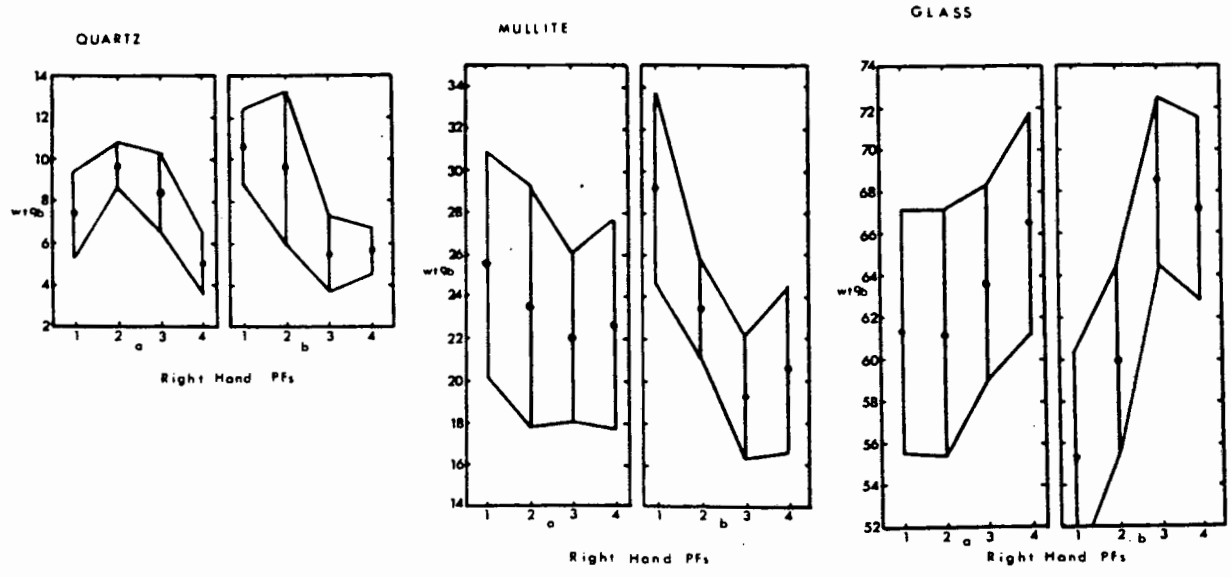

Figure 6: The mineral content of the ash varies with the field of collection (pf : precipitator field). (Lesch, 1987)

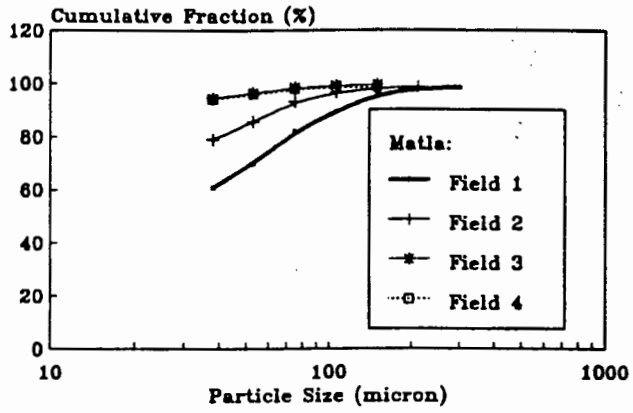

Figure 7: Particle size distribution of selected PFA samples. (Boswell, 1987).

of heavy metal salts, and volatilisation of SiO_2 occur as the temperature increases (above 1630°C). These vapours nucleate and grow on existing particles as they condense, and these particles become the PFA.

The extent of crystallisation is very dependent on cooling conditions, and thus on the field of collection of the ash (Lesch, 1987). Figure 6 shows the variation in mineral content among the precipitator fields for quartz, mullite, and glass respectively. The later fields collect finer particles, which cool more rapidly, and will be less crystallised. The variation in the extent of crystallisation is not reflected in variations in composition.

2.2.3 Particle Size Distribution

The PFA is a fine powder in the 2-100 micron range (Figure 7). The material is largely spherical, consisting of a mix of solid spheres, cenospheres, pleospheres and sphere aggregates (Lauf, 1986). The particle size distribution varies with the field from which it is collected. The range becomes finer in later fields. This gives rise to inhomogeneities in the ash. Transport leads to settling and stratification of the composition. Poor sampling of the ash may lead to larger variations in composition than expected.

2.3 Disposal of PFA

Disposal of 18 million tons of PFA per annum is a costly, high maintenance problem due to the abrasive nature of the ash (Heckroodt, 1987) and the high level of maintenance required by the ash dumps (Boswell, 1987). In South Africa, ash is transported to ash-disposal sites (ash dumps) close to the production site.

As of 1985, an estimated 250 million tons of ash was stored in ash dumps around SA, illustrated in Figure 7. A brief calculation shows that 250 million tons of coal occupies a volume of some 200 million m^3. Even in a layer 10 meters high this is still an enormous usage of otherwise valuable land (approximately 4500 m^2).

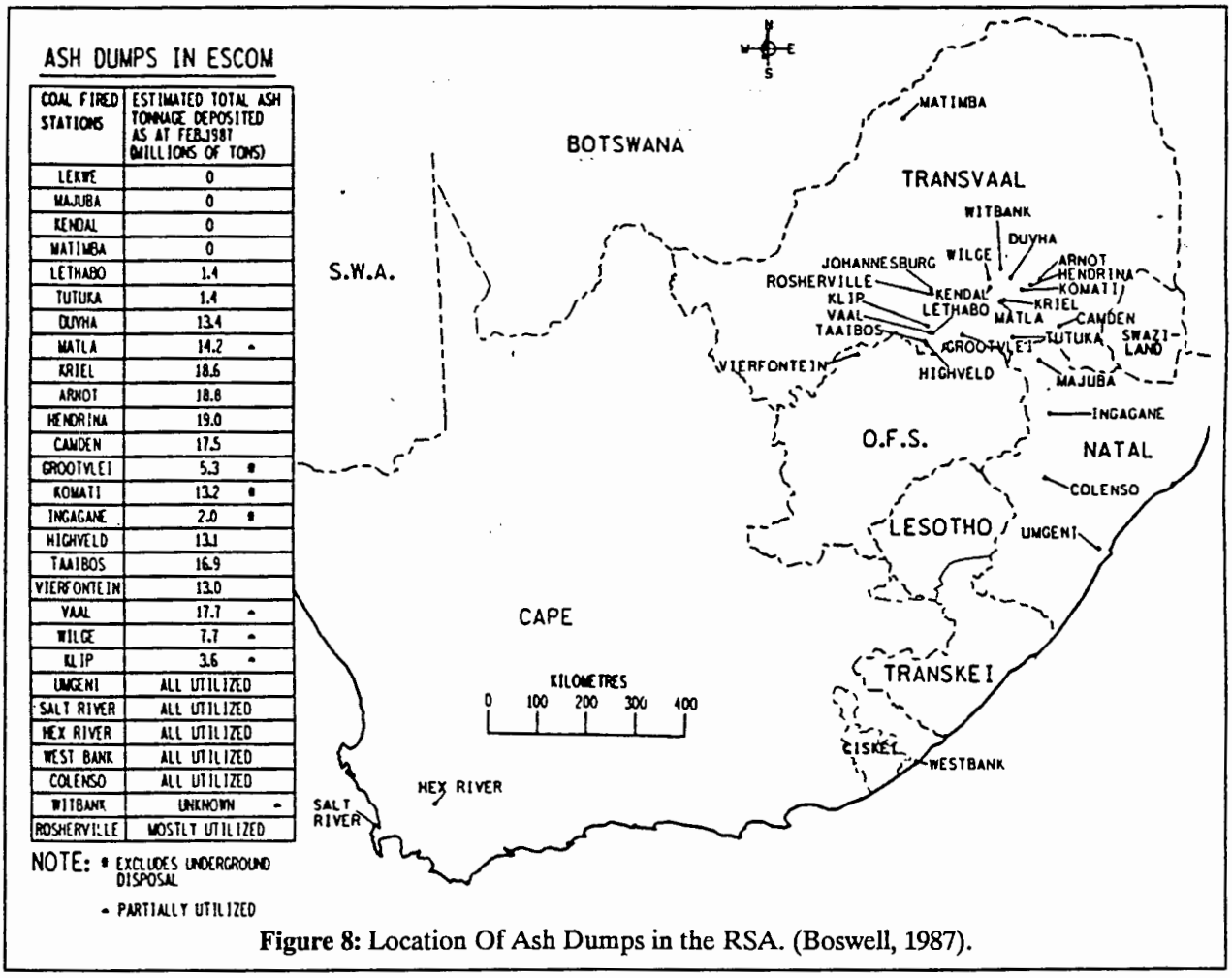

Figure 8: Location Of Ash Dumps in the RSA. (Boswell, 1987).

This has serious consequences in terms of land use, water pollution, and environmental degradation. PFA is not friendly to the environment. Aside from the potential contamination of ground water by run-off from dumps (Orren, 1987), there is considerable disruption of the habitat of the local fauna and flora, and dust pollution is common. Although these may be ameliorated by careful siting and design of ash dumps (Smith, 1987), it is only possible to minimize the effect to a certain extent. These problems are lessened as weathering of the material occurs and plant growth becomes more established.

2.4 Utilisation of PFA

PFA usage may be classified into low-, medium-, and high technology applications depending on the nature of the process and the extent to which the PFA is altered.

Low technology utilization has as its basis a low cost per ton of the ash, for example in applications such as structural landfill or backfill. Medium technology uses are typified by the use of PFA as a cement extender or concrete additive. High technology uses involve extensive processing of PFA, for which the technology may yet be undeveloped.

The possible economic benefits of using PFA increase with the level of technology; but so does the level of investment. At present, the existence of high quality alternative sources of raw materials discourages high technology uses of the PFA.

The extent to which PFA is utilised varies from country to country. Table 3 compares the usage of PFA in the RSA with that in a few other industrialised nations. Only countries with low ash production have been able to achieve near-complete utilization of PFA. The major obstacle to complete utilization is the huge volume of the ash produced: few commercial processes operate on a scale which consumes 60 million tons of raw material per annum.

Table 3: Global Production and Usage of Pulverised Fuel Ash.

Country	Year	Ash Prod Mt	% Used	a	b	c	d	e	Source
RSA	85	18	0.5	0.1					Kruger (1987)
USA	85	65.1	27.4	5.1	1.5	0.5	0.83	0.9	Faber (1987)
Israel	85	0.36	90	0.2	0.1				Lavie (1987)
Italy	85	1.5	55	0.7	0.15				Sandrelli (1987)
UK	85	12	27	3.5	0.9			0.13	Smith (1987)
FRG	85	7	80	0.8	0.7	0.14		0.36	Zelowski (1987)
Japan	85	4	36	1.0	0.14	0.07	0.07	0.14	Wakabayashi (1987)

Legend :
a) Cement and Concrete.
b) Structural Landfill.
c) Road Base.
d) Coal Mining (Backfill).
e) Miscellaneous Use.

PFA has a diversity of uses. Large tonnages are consumed by the cement and concrete industry (Davis, 1987) and by the construction industry as landfill (Clark, 1987). The coal mining industry has used PFA as a backfill material to increase the amount of coal extracted from a seam (Wagner, 1987).

Many novel and innovative uses have been proposed for PFA. Among these are the use of PFA as a raw material for the extraction of alumina (Burnett, 1987; Heinichen, 1987; Verbaan, 1987) and other elements, and as a source for iron ore (Bronkala, 1987).

Another promising application is the use of PFA to produce wear resistant materials. Production of such materials requires further processing of the PFA, usually with other materials added. A well established production route is the conversion of PFA to a glass, followed by crystallisation to produce a glass ceramic material. Due to the relevance of this topic, we give greater detail to this application.

2.5 Glass Ceramic and Erosion Resistant Materials

The production of tiles and other wear-resistant surfaces from blast-furnace slag is an established process. The high CaO content of such slags makes them very suitable since they do not require large additions of other materials to produce suitable glasses. Figure 9 illustrates the production process.

PFA from the RSA, while containing a similar assemblage of elements in its makeup, has a considerably lower concentration of fluxing oxides such as MgO and CaO. Since these act to lower the melting temperature of the system, the PFA from South African sources is far more refractory than blast-furnace slags. Production of a glass with a composition similar to one prepared with blast-furnace slag requires the addition of metal oxides.

A number of researchers have prepared ceramic materials which are mechanically tough and wear resistant using PFA as a raw material.

Karayakin (1975) combined 100 parts of ash and 40 of limestone to produce a workable glass. Addition of 1-2% of Cr_2O_3 ensured bulk nucleation of the glass, while the addition of an unspecified quantity of sodium sulphite prevented reduction of the iron in the glass. The major crystalline phase in the glass was a pyroxene. The author (Karayakin, 1980) used ash mixed with (variously) dolomite, limestone, and blast-furnace slag, and melted the batch to form glass. Heat-treatment of the glass at 950°C produced glass ceramics with mechanical properties that exceeded those produced by a comparable (slag-based) glass ceramic ('slag-sitall') produced industrially.

Bek (1981) produced tiles by mixing PFA with clay, pressing the result into moulds, and firing the moulded articles at temperatures around 1050°C. The tiles produced have a high abrasion resistance when compared to 'standard' (unspecified) tiles.

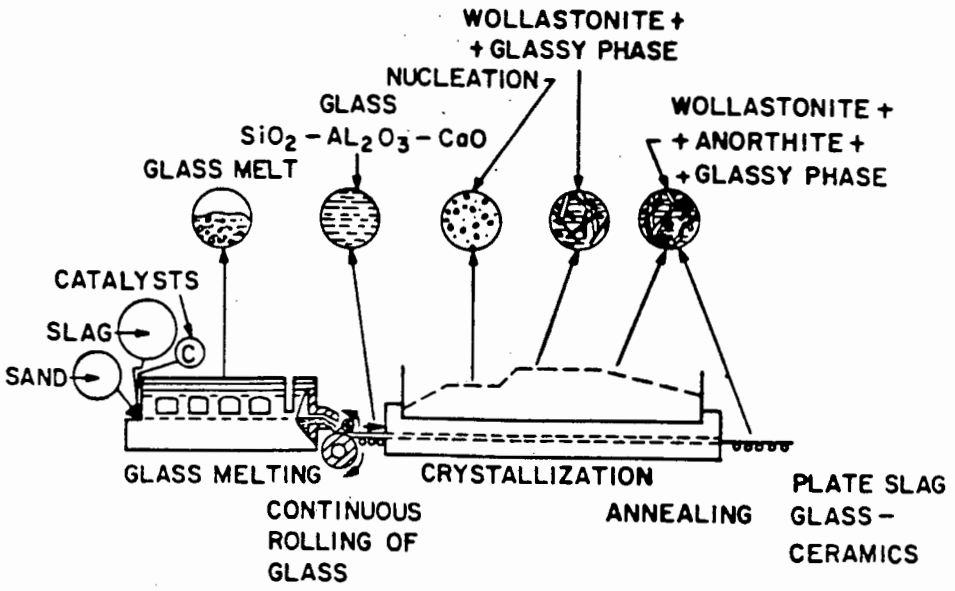

Figure 9: The production of glass ceramic materials from blast-furnace slag. (After Rabinovich, 1982).

Rabinovich (1982) produced glass ceramic materials by melting coal ash with additions of dolomite. Various ash samples, among them a sample of ash from coal sourced in the RSA, produced ceramic materials under the right conditions. An assortment of crystallisation catalysts were used, among them TiO_2, apparently the most successful for ash-based ceramics. He does not state explicitly whether the nucleating agent was added, or give concentrations, and the presence of TiO_2 may be due to that in the ash. The glass was melted at 1550°C and crystallised at 750°C.

PFA from an Illinois (USA) utility melted and recrystallised without the need of additives (Deguire, 1984). Heat treatment of the glass at 1150°C for 4 hours produced a partially crystalline material (23% crystalline). This was attributed by Deguire to the low concentration of TiO_2 present in the material. An alternative explanation is that depletion of iron bearing oxides from the glass results in an increase in the viscosity of the residual glass, slowing growth to negligible levels.

Manz (1984) reports the use of (CaO rich) PFA to prepare tiles by wet pressing and sintering of the material. The body was pressed to 31 MPa, dried, and fired at 1075°C. Tiles so produced meet the ASTM specification for tiles.

Two ash sources, one low in CaO and the other high, combine to give a body suitable for pressing and sintering (Stavreka, 1987). Tiles made from this body and sintered at 1050°C - 1300°C have good mechanical properties.

No reports are available describing the large-scale production of ceramic tiles or sheet from PFA. Unlike blast-furnace slag, the raw material for a flourishing industry producing erosion resistant materials (Pavlushkin, 1982; Veasey, 1973), PFA based glass ceramics do not appear to be in widespread use.

This may be attributed to two factors. Firstly, processes for the production of glass ceramics from blast-furnace slag are established, while the technology for PFA must still be developed. Secondly, the advantages of PFA over blast-furnace slag are small. Both materials are low-cost by-products of industrial processes. The blast-furnace slag requires few additions; conversely, PFA allows a wider range of compositional modification due to the low level of modifier oxides.

From a raw material viewpoint, PFA has little more to offer when compared to blast-furnace slag, it's major advantage is the fine powder form in which it is available. It is not surprising that there is little drive for the replacement of the blast-furnace slag in wear resistant materials by PFA.

The glass content is important in glass formation, due to the lowered energy requirements for melting when glass is present. The mineralogy of the ash is not very important in determining the glass-forming ability of the PFA except in as far as higher proportions of glass are conducive to easy melting. Many ashes contain some level of Fe-bearing phases which may have significance in terms of the nucleation of species in the glass ceramics.

3. GLASS CERAMIC MATERIALS

Glass ceramics are polycrystalline ceramic materials produced by the crystallisation of glass. The crystalline phase derives entirely from the growth of crystals from the glass phase, distinguishing the materials from ceramics produced using traditional sintering processes. Glass ceramic materials are in the majority crystalline, with little or no residual glass.

Workers have been aware for centuries of the tendency for glass to crystallise if held at elevated temperatures for extended periods. These materials tend to be mechanically weak, so the occurrence was regarded as an undesirable problem and much effort has been expended in the search for glasses that resist devitrification.

In the 1960's, Stookey showed that it was possible to produce a polycrystalline material with superior mechanical properties by the crystallisation of glass under controlled conditions. These conditions include the provision of nucleation sites throughout the material, and a heat treatment cycle tailored to the glass.

The normal production process for glass ceramics is a multi-stage process, starting with the production of the melt, followed by cooling and annealing the glass, and a two stage heat treatment to nucleate and crystallise the glass.

Glass ceramics are generally prepared using silicate-based glasses, in which the glass is composed in large part of SiO_2. Due to the very high viscosity of silica glass, other oxides are added to change the viscosity of the glass. For example, alkali oxides (Na_2O, Li_2O), alkali earth oxides (CaO, MgO) and borates (B_2O_3) may be added to lower the viscosity and improve the working range of the melt, while alumina (Al_2O_3) increases viscosity and decreases the working range.

For straight-forward production of the glass and items cast from the glass, the composition should allow working and fining (removal of entrained gases) at 1400°C - 1500°C. The viscosity/temperature behaviour of the glass controls the temperature range over which the glass is workable (the working range) and is dependent on the composition of the melt.

Some glass compositions are inherently stable, while others devitrify spontaneously on cooling. Stability during cooling and rapid crystallisation during heat-treatment are almost mutually exclusive and a nucleating agent is often used to resolve this problem by providing finely disseminated heterogeneous nuclei throughout the material. These nuclei appear when the glass is heat treated and provide an alternative, low-energy path for nucleation and subsequent growth of crystals.

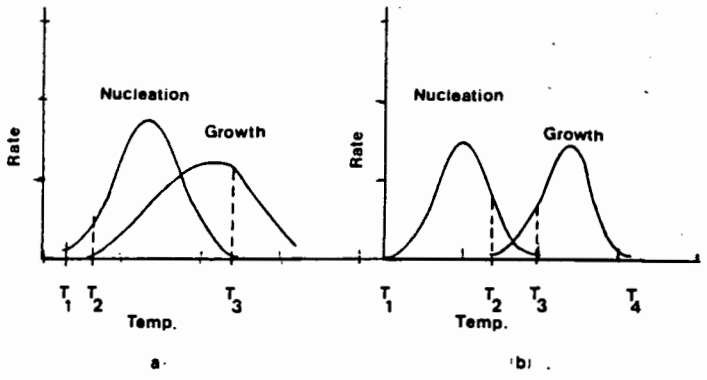

Figure 10: Nucleation and growth in a viscous liquid. (McColm, 1984)

The nucleating material should be stable in the glass during the melting phase, and form nuclei readily during the nucleation phase. The materials used as nucleating agents fall into several categories: metallic sulphides and other insoluble salts, metal colloids, and metal oxides soluble in the glass. The viscosity of the melt during crystallisation of a glass strongly affects the mode of the crystallisation, and oxides which affect viscosity have a commensurate effect on diffusion and thus the crystallisation rate of the glass.

The initial formation of nuclei is followed by growth on these nuclei at a higher temperature. The microstructure of the material will in a large measure be controlled by the type and concentration of these nuclei. There is a correlation between the concentration of nuclei and the grain size of the resultant material. The temperature cycle chosen will depend on temperature linked parameters, *viz.* the rate of nucleation, the rate of crystal growth, and the viscosity-temperature relationship of the glass.

For controlled growth, the temperatures of peak nucleation and peak growth rate should overlap as little as possible (Figure 10b). If these temperatures overlap (Figure 10a), growth occurs at the expense of the formation of new nuclei, leading to coarsening of the microstructure.

Conventional glass forming equipment may be used to shape articles prior to crystallisation. Close control over tolerances is possible due to the small dimensional changes during crystallisation, and low porosity and high uniformity of properties in the finished article stem from the homogeneous nature of glassy materials.

The enhanced properties of glass ceramics stem from the low glass content of the material and the low stress in the glass-to-ceramic interface. This is particularly so where the grain size of the crystalline phase is small due to the relationship between strength and grain size shown in Figure 11.

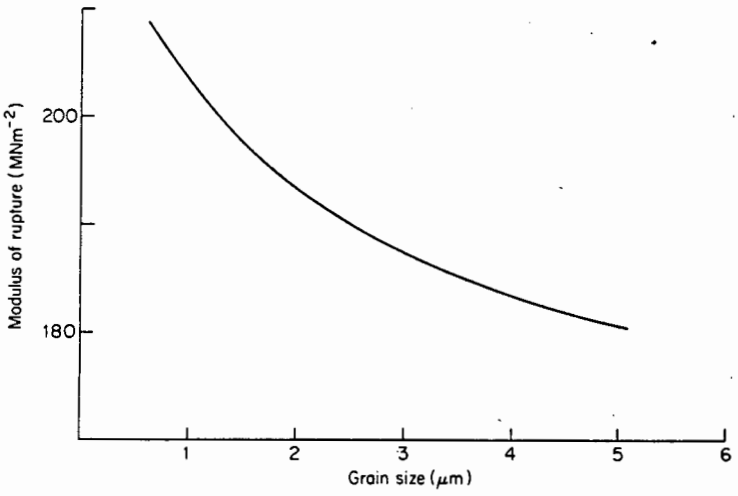

Figure 11. Modulus of rupture as a function of grain size. (McMillan, 1979)

A number of factors influence the properties of the glass ceramic material and should be controllable. Among these are the properties of the crystalline phase, the grain size distribution of the crystalline phases, the nature of the intergranular bonding in the material, the crystal orientation (texture) of the final product, the fraction of crystalline phase, and the distribution of the glassy phase.

The mechanical properties of a glass ceramic material are affected most by the microstructure (Hing, 1975). The most important parameters are the grain size of the crystals and the porosity of the material (Rice, 1977). Differences in composition between the crystals and residual glass phase will also have significant effects on the mechanical properties of the material (McMillan, 1974).

3.1 Nucleation

Nucleation of a new phase may happen by a homogeneous or heterogeneous route, depending on the conditions. Homogeneous nucleation is rare in silicate melts, as the energy barrier to the formation of a new phase is large in such systems. Heterogeneous nucleation reduces the energy requirement by providing a low energy site upon which growth may begin.

Heterogeneous nucleation in glass ceramics is accomplished via one of two routes. Reduction of a glass which contains metal ions supplies nucleation sites by precipitating colloidal metal particles in the glass. Alternatively, the addition of a second, often immiscible, oxide to a glass may lead to the production of a finely dispersed crystalline phase. This crystalline phase acts as the nucleation sites for the major phase on further heat treatment, in a similar fashion to the colloidal metal particles.

The optimum temperature for nucleation varies with the composition of the melt, the nucleating agent used, and the history of the melt. Too low a temperature will require long nucleation times. Nuclei form via diffusion of ions, and slow diffusion at low temperatures will cause slow nucleation. Too high a temperature will lead to rapid growth on the nuclei as they are formed. The first nuclei formed will experience a disproportionate amount of growth, leading to a coarse microstructure.

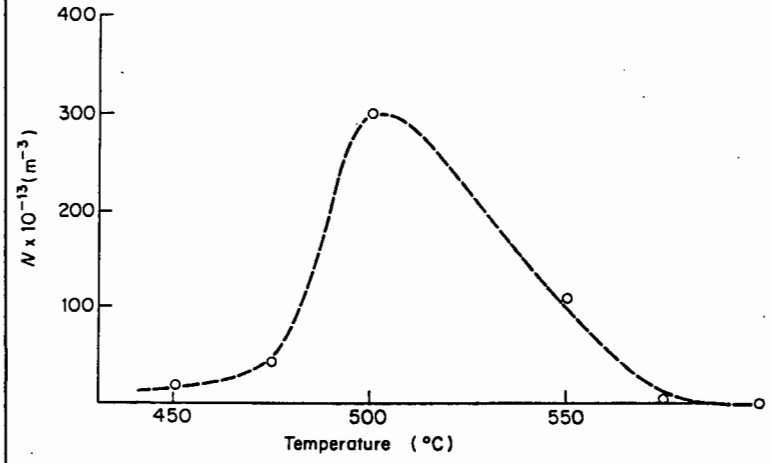

Figure 12: The relationship between nuclei density (N) and temperature (Hing, 1973).

The existence of an optimum temperature for nucleation has been demonstrated clearly by Harper *et al.* (1970; 1972) and Hing (1973) who observed the relationship between nuclei density and temperature shown in Figure 12.

Crystal growth in glasses occurs via either surface or bulk heterogeneous nucleation. Under surface nucleation, growth starts at heterogeneities on the surface of the glass. Crystal growth then occurs into the specimen. This leads to a microstructure characterized by large, oriented grains. If a large number of small, dispersed sites for crystal growth exist throughout the glass, crystallisation will occur throughout the sample, avoiding problems due to shrinkage of the crystals and partitioning of the oxides in the glass.

3.1.1 Thermodynamics of Nucleation

A fundamental analysis of the processes involved in nucleation and growth evolved through the efforts of, *inter alia*, Becker (1935; 1938), Vonnegut (1947), and Turnbull and Vonnegut (1952). For the sake of simplicity in derivation, we assume spherical nuclei, but the treatment is similar for other shapes.

There are two important features in this model:

i) A thermodynamic barrier to nucleation exists due to the changes of state required.

ii) There exists a critical radius for nuclei, below which radius they are unstable and tend to redissolve.

An expression for the change in energy for the transformation of a liquid to a solid can be is derived from the changes in state that occur. The formation of a new surface and the change in molar volume associated with the change of phase both affect the free energy of the system. This change in energy may be expressed as a function of the size and surface area of the new sphere: (for a spherical region)

$$\Delta G_r = 4\pi r^2 \eta_{sl} + (4/3)\pi r^3 \Delta G_v \qquad [1]$$

where ΔG_r = energy required for formation of new phase.
ΔG_v = energy required for change of state of particle of radius r.
r = radius of particle.
η_{sl} = interfacial energy.

Some of the new regions which form are able to grow to a critical radius (r^*), above which their energy decreases with size and they become stable. The regions smaller than r^* are termed embryos, and have a free energy higher than an equivalent volume of the matrix, while those larger than r^* are nuclei, and are energetically stable with respect to the matrix. By differentiation of [1] it can be seen that the critical radius is a function of the composition of the melt, as this will affect the free energy and interfacial energy:

$$r^* = \frac{-2\ \eta_{sl}}{\Delta G_r} \qquad [2]$$

Thus the ease of formation of nuclei from a matrix depends on the magnitude of the thermodynamic barrier to nucleation and on the radius of the critical nuclei .

There will always be embryos in a system due to the increase in the entropy of mixing in a system associated with their formation. The growth of embryos is a stochastic process associated with thermal agitation; as a result the number of embryos of a given size (N_r) in a melt is an exponential function of temperature:

$$N_r = \frac{N \exp\ [\ -\Delta G_v\ ]}{kT} \qquad [3]$$

N = Avogadro's number.
k = Boltzman const.

The presence of an interface with different surface energy assists nucleation. Nucleation in the presence of a different surface is heterogeneous nucleation. Vonnegut (1952) expressed the effect of the interface as:

$$\Delta G_{hom} = \Delta G_{het}\ (f(\theta)) \qquad [4]$$

where θ = "contact angle" or wetting angle, and (for spherical nuclei)

$$f(\theta) = \frac{((2+\cos(\theta))(1-\cos(\theta)))}{4} \qquad [5]$$

θ is determined by the surface tensions:

$$\phi_{HL} = \phi_{SH} + \phi_{SL}\cos(\theta) \qquad [6]$$

where :

ϕ_{HL} = interfacial energy between heterogeneous nuclei and melt.
ϕ_{SH} = interfacial energy between heterogeneous nucleus and primary crystal phase
ϕ_{SL} = interfacial energy between crystal phase and melt

The ability of a particle to act as a site for heterogeneous nucleation will depend on the similarity in the lattice spacing for the nucleating and the crystalising species (the lattice registry). McMillan states that disregistry should be no more than 15% in the low index planes of the nucleation catalyst and nucleated phase for nucleation in supercooled melts (McMillan, 1979). An effective nucleating agent requires the following:

i) Low interfacial tension between nuclei catalyst and primary crystal phase. This will give a low value of $f(\theta)$, causing a drop in the activation energy of the process.

ii) Similar crystal structures, with lattice disregistry less than 15%.

3.1.2 Metallic dispersions

Many metallic species can exist as a colloidal solution in a glass. Copper, silver, and gold are examples of this, and are well established as nucleating agents (Weyl, 1951). Copper, soluble in silicate melts under oxidising conditions, exists as Cu^{2+} ions in solution, and may be reduced to the elemental state on the addition of stannous oxide (SnO). This atomic copper will grow via diffusion when the glass is heat-treated,

giving a ruby colour to the glass ('striking'). Silver, gold, and platinum, while less soluble in glass than copper, can also be reduced to the metallic state. Gold and platinum are particularly susceptible to reduction and the metallic form predominates in the melt, forming colloidal dispersions with no further treatment needed.

Irradiation of glass containing cuprous ions with a suitable dose of radiation of an appropriate wavelength causes the reduction to a metallic state in a two step process: (Dalton, 1947)

$$Cu^{+} + h\mu \rightarrow Cu^{2+} + e^{-},$$

followed by: $$Cu^{+} + e^{-} \rightarrow Cu^{0} \qquad [7]$$

This will increase the concentration of the metallic atoms in the glass, producing nuclei for growth. If a soak at an appropriate temperature follows, diffusion of ionic species to the metallic clusters allows their growth via a nucleation and growth process. This will increase the number of viable nuclei in the system.

3.1.2.1 Nucleation by metallic dispersions

Stookey (1950) reported the first occurrence of controlled crystallisation in glass. Photosensitive glasses in the Li_2O-SiO_2 system containing Au became opaque due to the crystallisation of $Li_2O.2SiO_2$ crystals following irradiation and heat treatment. Irradiation of the glass produced metallic colloids, which were able to act as nucleation sites for the growth and nucleation of silicate crystals.

Stookey (1956) showed that crystal growth of a Li_2O-Al_2O_3-SiO_2 glass nucleated by photosensitive Au, Ag, and Cu could produce a completely crystallised, polycrystalline material with good mechanical properties. Concentration of the metal species used varied from 0.001 to 0.1 per cent. Submicroscopic particles of metal (metallic colloids) were precipitated and acted as nucleation sites for the crystallisation of a silicate phase.

Rindane (1962) studying platinum-nucleated $Li_2O.4SiO_2$ glasses using XRD, noted an enhanced rate of crystallisation as well as a uniform distribution of crystals. The optimum platinum concentration varied with the nucleation temperature, between 0.004% and 0.011% of platinum. Above 0.025% platinum, the proportion of $Li_2O.2SiO_2$ in the crystalline material dropped. He attributed the nucleating ability of platinum to the close registry of the <111> platinum and the <200> $Li_2O.2SiO_2$ lattice planes, a disregistry of less than 5%.

The structure of the glass ceramics formed via this nucleation route is very sensitive to the radiation dose. Miles (McMillan 1979) examined the modulus of rupture (bend strength) and grain size of an Au-nucleated Li_2O-Al_2O_3-SiO_2 glass ceramic. An optimum strength of 230 Nm^{-2} was obtained after 40 minutes of radiation, for a grain size of approximately 1 micron. Longer or shorter times produced materials with lower breaking strength. This was ascribed to the two step nucleation procedure described earlier. Irradiation converts ions to atomic species, which act as nucleation sites for growth of metallic clusters. Ionic species diffuse to these sites during heat treatment, and are reduced to the metallic state. Over exposure diminishes the concentration of ionic species to a level where diffusion becomes insignificant, and the embryos cannot grow to the required critical radius.

3.1.3 Phase Separation in Oxide Glass

The process of phase separation in silicate glasses has consistently been shown to improve the properties of the glass ceramics. Structural reasons for the separation into two phases (a process sometimes known as metastable immiscibility) are not fully understood, although the thermodynamic basis is clear. McMillan proposes two reasons for separation: a structural incompatibility between the network structures of the two phases, and a difference in charge between two glass network forming species (McMillan, 1979).

The Goodman theory of glass structure allows an alternative explanation (Goodman, 1987). Highly strained crystallites, corresponding in composition to the equilibrium phases present, make up the glass network. A complex glass will have more than one network of crystallites present, and these networks will provide the basis for phase separation.

Many glass systems separate into two non-crystalline states on heating (James, 1975). This involves a small scale shift in the composition of the glass, which will affect the crystallisation kinetics and the morphology of the growing phases.

Phase separation may occur via a nucleation and growth or via a spinodal decomposition mechanism (Cahn, 1965). Spinodal decomposition is a process in which new phases form without an interface between the two phases, with the result that there is no barrier to nucleation as in traditional nucleation and growth processes. The result of both processes (spinodal decomposition and nucleation and growth) will be two phases in equilibrium. There will be differences in the morphology of the two phases, described in Table 4.

Table 4: Morphology of glasses after phase separation. (McMillan, 1979).

	Nucleation and Growth	Spinodal Decomposition
Phase composition	Nucleated phase composition constant with time (at fixed temperature).	Composition changes continually with time.
Interface	Sharply defined always.	Initially diffuse but ultimately becomes sharp.
Morphology	Nucleating phase is spherical. Particles are random in size and have low connectivity.	Second phase is generally non-spherical and threadlike, with regular spacing and high interconnectivity

During cooling a glass will cross the phase composition in which phase separation occurs via nucleation and growth before that due to of spinodal decomposition. Nucleation and growth will thus tend to be the more common route to phase separation. If the glass remains homogeneous on cooling to room temperature, phase separation by spinodal decomposition may occur on re-heating in preference to nucleation and growth.

McMillan (1979) demonstrated the relationship between nucleation time, nuclei density and grain size of crystallised product. A clear optimum time was shown, after which coarsening of the microstructure occurred. There was no correlation between the final microstructure and either the nucleation density or the size of the phase separated microstructure. McMillan suggested that crystal nuclei arise in the matrix of the two-phase structure. Initially these nuclei increase in number, but later decrease due to coarsening. Phase separation in a glass increases the viscosity of the glass and thereby lowers the diffusion rates in the glass, which slows the coarsening process (Ostwald ripening) acting to decrease the number of nuclei as time passes. Thus it appears that phase separation does not act to generate nuclei, but merely to preserve them.

3.1.4 Oxide Nucleation

No definitive mechanism for the process of nucleation has been proposed. Different combinations of glass forming oxides and other added oxides undergo events up to the stage of complete crystallisation in different sequence (Ohlberg, 1962). There are similarities, and all the observations may be explained in terms of a general mechanism.

Many glass systems undergo phase separation into two glassy phases below the liquidus temperature. This separation of glass into two phases is associated with increased nucleation. Metal oxides used as nucleating agents appear to act via an initial glass-in-glass phase separation (James, 1975).

Phase separation on a fine scale acts to lower the energy barrier for nucleation of a new crystalline phase. The composition of the phases changes toward the equilibrium crystalline composition.

The mechanism of the phase separation affects the concentration profile that develops. A sharply defined interface formed by nucleation and growth will give rise to a zone adjacent to the interface depleted in some components relative to the bulk. This region will be closer in concentration to the equilibrium crystalline composition than the bulk, and crystallisation begins in this depleted zone. In spinodal decomposition, the material would be less likely to crystalize at the 'interface' than in the bulk, as the regions with composition closest to the equilibrium value will be at maximum separation, i.e. in the centre of the phase separated region.

The effect of phase separation is easy to visualise if one considers glass structure in terms of the Goodman model (Goodman, 1986; 1987). The structure in the "strained crystallite" is that of the equilibrium crystalline phase. As phase separation proceeds, and the glass becomes depleted in impurities, the crystalline lattice will become more substantial, and detectable crystallinity will appear.

3.1.4.1 Phosphorous Pentoxide

P_2O_5 successfully nucleates glasses of the type LiO-SiO_2 (LS), as well as more complex glasses. The nucleating ability of P_2O_5 appears to be due to the formation of lithium phosphate species following glass in glass phase separation (James, 1970; Headley, 1984; Hametter, 1987).

The addition of P_2O_5 to a glass markedly alters its immiscibility behaviour (Matusita, 1975), and results in marked changes in the extent and morphology of phase separation in the glass (James, 1970). Substitution of 1 mol% of P_2O_5 for SiO_2 in a 30%-70% LS glass increased the number density and volume fraction of the phase separated regions considerably (James, 1970).

Associated with changes in the immiscibility and phase separation are changes in the crystallisation of the glass. Harper (1972) demonstrated the ability of P_2O_5 to affect the microstructure and kinetics of crystallisation of the glass ceramic material. A marked reduction in the grain size of the material occurred when 1 mol% of P_2O_5 was substituted for SiO_2 in 30%-70% LS glass. The paper shows a considerable

change in the crystallisation rate. However, due to the loss of the legend in the figure of interest, it is not clear if the rate increased or decreased. McMillan (1982) noted that P_2O_5 decreased the rate of crystallisation.

The change in the microstructure is associated with a change in the number of nuclei produced during heat-treatment (Harper, 1972; Hing, 1973). An optimum heat treatment temperature for a 30% Li_2O - 69% SiO_2 - 1% P_2O_5 glass was shown, with a nuclei density approximately 300 times higher than in a P_2O_5-free glass (Harper, 1970).

McMillan (1974a) confirmed the existence of an optimum temperature for nucleation, and showed that a diffusion-controlled coarsening process (Ostwald ripening) eliminated a large proportion of the nuclei during crystallisation, as proposed earlier by Hing (1973). McMillan (1974) showed that optimum nucleation conditions produced glass ceramics with the most fine-grained microstructure.

The mechanism for the crystallisation behaviour of a glass nucleated by P_2O_5 was only recently elucidated (Headley, 1984). Headley (1984) confirmed early suggestions by, *inter alia*, James (1975) that lithium phosphate species were important in the nucleation process. Direct observation of the nucleation of lithium silicate species by crystals of Li_3PO_4 were made using TEM. To grow nuclei suitably large for viewing by TEM, they used a nucleation temperature of 1000°C, which developed crystalline nuclei imaged easily using TEM.

Examination of the crystallographic orientation of the crystals in the glass showed an orientation relationship between the Li_3PO_4 crystals and the species growing on them, a requirement for nucleation catalysis. According to Headley (1984), the sequence of crystallisation in this glass is as follows:

i) Lithium phosphate (Li_3PO_4) crystals form during nucleation. The temperature and length of this stage fixes the number and size of the nuclei.

ii) On further heating, lithium metasilicate (Li_2SiO_3) crystallises on the {120} faces of Li_3PO_4 crystals with an orientation relationship (Figure 12(b)).

iii) Crystobalite and some lithium disilicate ($Li_2Si_2O_5$) grow at higher temperatures. Crystobalite nucleates only on the {120} faces of the Li_3PO_4, with an orientation relationship (Figure 12(a)). $Li_2Si_2O_5$ nucleates on {120} and {010} faces (Figure 12(c) and (d)).

The calculated degree of misfit is between -5,3% to 3,8%, much lower than the commonly quoted requirement of 15% registry (McMillan, 1979).

Addition of P_2O_5 to a LS melt affects both the kinetics of the crystallisation process and the microstructure of the product. Ray (1987) has shown that addition of P_2O_5 to a melt decreases the critical cooling rate for glass formation. The nucleating agent appears to slow the crystallisation process in the LS glass used. This is attributed to a change in the mechanism of crystallisation of the glass. McMillan (1979) states that addition of P_2O_5 to a LS melt decreases the crystal size, while also decreasing the rate of crystallisation.

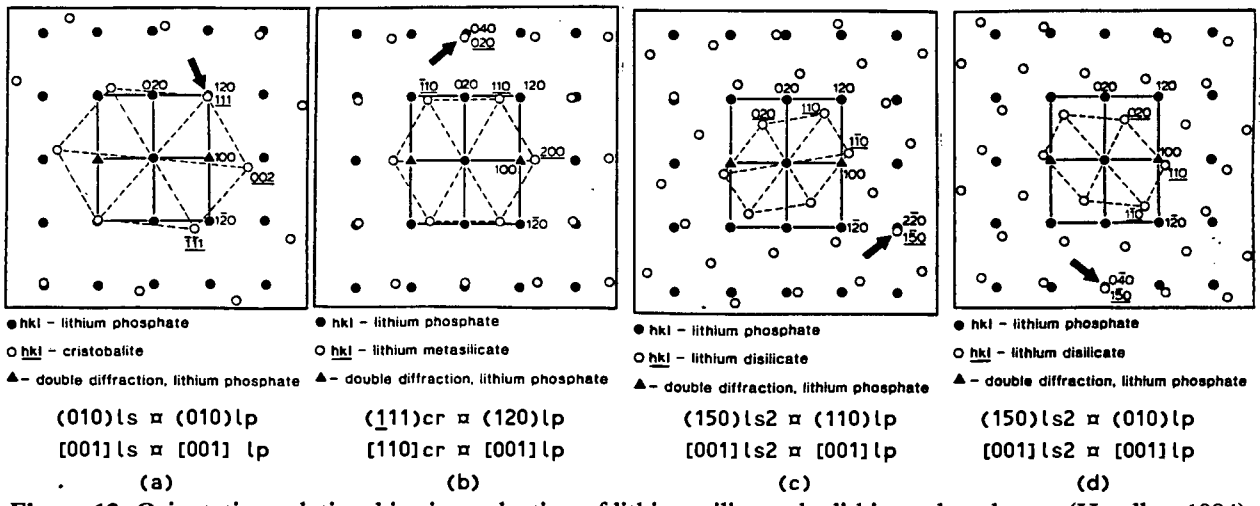

Figure 13: Orientation relationships in nucleation of lithium silicates by lithium phosphates. (Headley, 1984)

P_2O_5 has been used to good effect in other complex glass systems (McMillan, 1972). It has been most effective in systems containing significant amounts of Li_2O, due to formation of lithium phosphate species. It is anticipated that in glasses containing little or no alkali earth oxides, P_2O_5 would be ineffective.

3.1.4.2 Titanium Dioxide

This is probably the most widely used nucleating agent for silicate glass ceramics. The ability of TiO_2 to nucleate glasses in the Li_2O-Al_2O_3-SiO_2 (LAS) system has long been commercially exploited in the production of such materials as CorningWare (Barry, 1979).

TiO_2 is effective as a nucleating agent in conjunction with a suitable divalent metal oxide (McMillan, 1979). These combine with the TiO_2 to give titanates with the general formula $RO.TiO_2$. These titanates have a close-packed hexagonal structure *cf* ilmenite (McMillan, 1979). Oxides which have proved effective include iron, cobalt, cadmium, zinc, nickel, manganese and magnesium (Stookey, 1960; Barry, 1979; Scheidler, 1989).

It has been known for a long time that TiO_2 produces a glass-in-glass phase separation in a glass melt. Ohlberg (1962) showed that phase separation was the first step in the crystallisation of $MgO\text{-}Al_2O_3\text{-}SiO_2$ (MAS) glasses containing TiO_2. Other authors who have noted the occurrence of phase separation in TiO_2 nucleated glasses during heat treatment include Zdaniewski (1973; 1975; 1978), Hing (1973), Barry (1978), DeVekey (1975), Hayward (1987) and Maier (1987; 1988).

Addition of TiO_2 to a glass will increase the viscosity of the glass (Matusita, 1975). In addition, the onset of phase separation is often associated with large increases in the viscosity of the glass (Mazurin, 1970).

Barry (1978) showed that adding TiO_2 caused considerable changes in the crystallisation process. He noted that a $MgO\text{-}Al_2O_3\text{-}SiO_2$ glass with a cordierite composition was poorly nucleated without TiO_2, and that increasing the TiO_2 content improved the efficiency of nucleation. The change in crystallisation behaviour with the addition was evident from the DTA trace as the more efficient nucleation produced larger crystallisation exotherms.

Little work has been done to establish the effect of TiO_2 on crystallisation kinetics. In one of the few studies dealing with this aspect, TiO_2 added to a $Li_2O\text{-}SiO_2$ glass (Ray, 1987) had little effect on the crystallisation rate.

The ability of TiO_2 to act as a nucleating agent is affected by its oxidation state. Thus the atmosphere in the furnace, and the redox conditions within the melt may affect the quality of the product. TiO_2 may readily be reduced to Ti^{3+}, or even Ti^{2+}. Neither of these species form titanates of the type required.

The concentration of the TiO_2 is also significant. TiO_2 is very soluble in glass, and is easily assimilated into many silicate lattices. There will be a concentration below which no titanates form, due to the solubility of the TiO_2. Successful nucleation in materials containing TiO_2 is generally achieved when the TiO_2 content is above 5% (Davies, 1970; Gutzow, 1977; Maier, 1988). In the $Li_2O\text{-}Al_2O_3\text{-}SiO_2$ system, TiO_2 contents of approx 1% appear effective, especially in conjunction with ZrO_2 (Maier, 1987; Barry, 1978).

(A) Nucleation in $Li_2O\text{-}Al_2O_3\text{-}SiO_2$ glasses containing TiO_2 and ZrO_2.

Commercial glass ceramic systems based on the $Li_2O\text{-}Al_2O_3\text{-}SiO_2$ (LAS) system are used to produce glass ceramics with a low coefficient of thermal expansion for use in, *inter alia*, cooking ware and telescope mirrors. These crystallise to give phases based on the silica polymorphs keatite and quartz (Barry, 1979). Typical of these material are Zerodur, CorningWare and Hercuvit. These glass ceramics are commonly

nucleated by the addition of TiO_2 alone, or a mixture of TiO_2 and ZrO_2 (Scheidler, 1989).

Many authors have noted that the nucleating ability of TiO_2 in Li_2O-Al_2O_3-SiO_2 (LAS) glasses is improved when ZrO_2 is added (Stewart, 1972; Barry, 1978). Much work in the LAS system has been done with a combination of these oxides.

Partridge (1982) examined the process of crystallisation in a LAS glass nucleated with TiO_2 and ZrO_2. He summarised earlier work by Ray (1968) and Beall (1969) and proposed the mechanism summarised here.

i) Glass-in-glass phase separation produces a phase substantially enriched in ZrO_2 and TiO_2.

ii) This precedes crystallisation of cubic zirconia ($ZrTiO_4$) in the enriched phase.

iii) The major phase, β-eucryptite, is nucleated on the cubic crystals.

Examining the microstructure of LAS glass ceramics, Chen (1982) found precipitates containing TiO_2 and ZrO_2, with a structure approximating to gahnite ($ZnAlO_4$). These were assumed to have acted as nucleation sites.

Maier (1987), using a HRTEM (high resolution TEM) method to examine the nucleation of glass ceramics in the LAS system by TiO_2 and ZrO_2, showed that $(Zr,Ti)O_2$ crystallites form on heating the glass. These crystallites then act as nuclei for the β-quartz solid solution (the major phase). The quartz crystals grew with a $ZrTiO_4$ crystal at the center, but the small size of the crystals precluded a measurement of the orientation relationship. The authors state that the epitaxy between $ZrTiO_4$ and the β-quartz is the critical step in initiating silicate growth.

(B) Nucleation in MgO-Al_2O_3-SiO_2 glasses

Working with glasses of the MgO-Al_2O_3-SiO_2 (MAS) system, Maier (1988) established the following mechanism for the nucleation of the glass by TiO_2.

Phase separation precedes the formation of a TiO_2-containing phase in the phase separated regions. Titanates with a pseudo-brookite structure (Mg_x Al_{2-2x} Ti_xO_5; $x=0.8$) form initially. Silicates then grow around this "spinel" structure. However, the overall degree of crystallisation is low. Epitaxy between the titanate and silicate crystals is not evident, and growth of silicates is assumed to be initiated by depletion of MgO and Al_2O_3 in the glass, enriching the glass with respect to SiO_2.

In MAS glasses containing ZrO_2 in addition to TiO_2, cubic zirconia ($ZrTiO_4$) is formed and acts as the nucleating phase. These crystallites are smaller, and the grain size in the crystallised material finer, than when nucleated by TiO_2 alone.

(C) Nucleation in glasses manufactured using industrial by-products

Blast furnace slags, power station ash, and many other types of industrial wastes have compositions that fall within the MgO-CaO-Al_2O_3-SiO_2 (MCAS) system. This system has been widely used to prepare a class of materials known as "slag ceramics" (Topping, 1976) used as low cost wear resistant materials. The most commonly used material has been blast furnace slag, usually composed of calcium and magnesium alumino-silicates. Comprehensive reviews of the manufacture of such materials are given by Topping (1976), Veasey (1973) and Pavlushkin (1982).

Research on glass in the MCAS system prepared from pure components (DeVekey, 1970; Topping, 1976) has shown that TiO_2 is able to produce bulk nucleation during heat treatment. Nucleation control in glasses prepared from blast furnace slags or other silicate containing wastes is similarly possible by adding TiO_2, and some examples are described below.

Davies (1970) used TiO_2 alone and in combination with chromite (chrome ore) to nucleate glasses prepared from blast furnace slag. A combination of 6% TiO_2 and 0.5% chrome ore was found to be an extremely effective nucleating agent, judged by the extent to which the material crystallised on heating.

Researchers in the USSR have gone to considerable efforts to produce 'slag-sitalls' from blast furnace slag or power station ash. Pavlushkin (1982) discusses the production of such materials from various sources of raw material in the USSR. Some of these materials are produced by the addition of up to 15% of TiO_2 or mixtures of TiO_2 and Cr_2O_3.

3.1.4.3 Iron Oxides

Iron oxides, particularly in combination with chromium oxides, have been used very successfully to nucleate glasses prepared from industrial by-products. Veasey (1973) reviewed their production, noting that Fe_2O_3 is commonly added to these melts to promote nucleation. According to the author, 'slag-cerams' or 'slag-sitalls' have been produced in large amounts using Fe_2O_3 in conjunction with other oxides to nucleate the glass.

No mechanism for the nucleation of the glass by iron oxides has been given. Kirsh (1989) suggested that the nucleating phases are spinel-type structures. These

would be solid solutions between the species $MgFe_2O_4$ and $MgAl_2O_4$ ($Mg(Al,Fe)_2O_3$).

A common observation is the importance of the ferrous/ferric ratio on the crystallisation behaviour of the glass. The effect of iron oxides on the properties of the glass has, however, not been widely investigated.

Kirsch (1989) reports on the production of a ceramic in the MCAS system from model glasses. The importance of the Fe^{2+}/Fe^{3+} ratio is shown, and it was noted that the type and concentration of nucleant could change the type of crystal formed.

Similarly, Davies (1970) investigated the ability of iron oxides as nucleation catalysts in a $MgO\text{-}CaO\text{-}Al_2O_3\text{-}SiO_2$ (MCAS) glass prepared using blast furnace slag. The extent and type of the crystallisation was found to be very sensitive to the state of oxidation of the iron oxides, i.e. the Fe^{2+}/Fe^{3+} ratio. With an optimum ratio, glass ceramics with low porosity and fine crystalline structure could be crystallised. Davies reported a complex dependance of crystallisation rate on the oxidation state of the melt and the iron content.

Additions of Fe_2O_3 and FeO to a MCAS glass reduced the viscosity, and increased the rate of crystallisation of the melt (Williamson 1969). Further, as the ratio of Fe^{2+}/Fe^{3+} increased, the crystallisation rate increased to an extent which could not be explained by the lowering of viscosity alone.

3.1.4.4 Chrome Oxides

Many commercial 'slag-ceramics' or 'slag-sitalls' produced using industrial waste as a raw material are nucleated using Cr_2O_3, either directly, or more commonly by chrome ore, usually chromite ($CrFe_2O_4$). Kirsch (1989) suggested that Cr_2O_3 promotes nucleation by the formation of spinels, similar to the $Mg(Al,Fe)_2O_4$ solid solutions that form in iron catalysed glasses.

Pavlushkin (1982) reviews the production of 'slag-sitalls' from industrial by-products, and it is clear that the addition of chromite is the most commonly used method of nucleation in the USSR. The use of this material in a wide variety of glass systems is described.

Pavlushkin (1982) describes work by Motsareva which established some parameters for nucleation by Cr_2O_3. The glass composition, especially the 'basicity' (ratio of metal oxides to $SiO_2 + Al_2O_3$) of the glass, was shown to be a controlling factor. In glasses with basicity greater than 1, Cr_2O_3 could nucleate the glass. This was attributed to the presence of Cr^{5+} and Cr^{6+} ions in these glasses. High valence ions

have a tendency to form species of the type [R_2O_7] which encourage the formation of the major phase.

Davies (1970) noted the ability of Cr_2O_3, added as chromite, to nucleate a glass prepared from blast furnace slag. He found that the chrome ore was less effective if the glass was melted in an oxidising environment, while under reducing conditions a fine-grained product resulted from heat treatment.

3.1.4.5 Mixed oxides

A recurrent theme in the literature is the enhanced nucleation resulting from a combination of two or more oxides as a nucleating agent.

The synergistic interaction of TiO_2 and ZrO_2 in LAS glasses has been noted by several authors (Steward, 1972; Barry, 1979; Maier, 1987; Scheidler, 1989). This is attributed to formation of crystallites of the composition [$ZrTiO_4$] which are very effective at nucleating silicates.

Another well known interaction is between chrome and iron oxides (Carter, 1986). This may give rise to chromites ($FeCr_2O_4$), and in fact many glasses are nucleated by the addition of chrome ore, or chromite, which provides spinel nuclei directly. Spinel group minerals are often mentioned as nucleation sites for silicates (Shelestak, 1978; Pavlushkin, 1982). Iron ores often contain magnetite [FeO Fe_2O_3], a spinel.

Davies (1970) investigated the effect of a large number of mixed oxide nucleating agents on the crystallisation of a MCAS glass prepared from blast furnace slag. Combinations such as TiO_2 + Cr_2O_3, TiO_2 + MgO, and chromite + magnetite proved to be more effective nucleating agents than single oxides. Davies attributed this largely to better control of the oxidation state of the nucleating oxide by selective oxidation of one of the couple, a concept known as an electron buffer.

Researchers in the USSR have also used combinations of oxides. Pavlushkin (1982) mentions the use of, *inter alia*, mixtures of TiO_2 + Cr_2O_3, Cr_2O_3 + P_2O_5, and TiO_2 + P_2O_5. All of these gave improved crystallisation in a particular application.

The material 'silceram' (Carter, 1986) is manufactured from blast furnace slag nucleated by iron and chrome oxides.

In summary, it may be said that many of the combinations of oxides that have been successful are able to form crystals of the spinel type. The combination of control of the redox environment and formation of suitable nuclei probably accounts for the successful combination of two oxides.

3.2 Crystal Growth

Irrespective of the route taken to give finely disseminated nuclei suitable for further growth, the heat treatment used to grow the crystals is of great importance. The optimum heat treatment cycle is a function of the composition of the glass. Crystal growth in silicate glass ceramics occurs at higher temperatures than does nucleation, largely due to the slower diffusion of the silicate species involved in crystallisation of the major species.

3.2.1 Thermodynamics of Crystal Growth

The rate of crystal growth is affected by the rate at which the glass rearranges to the lattice structure of the crystalline form, and the rate at which heat can be extracted from the interface.

Structural rearrangement is largely controlled by the energy difference between the crystal and glass phase. An activation energy (ΔG_{Ea}) is needed for an atom to cross the interface from liquid to solid (McMillan, 1979). The growth rate of the interface can be derived, and this treatment is summarised by McMillan (1979). The growth rate (U) is affected by a number of factors as shown below:

$$U = a_o \nu \left[\frac{-\Delta G_{Ea}}{RT}\right] \left[1 - \exp\left(\frac{\Delta G}{RT}\right)\right] \qquad [8]$$

where:

U	=	growth rate
a_o	=	interatomic spacing
ν	=	vibrational frequency of atom at glass crystal interface
R	=	gas constant
T	=	absolute temperature (K)
ΔG	=	energy difference between glass and crystal
ΔG_{Ea}	=	activation energy

In silicate melts, growth occurs on an atomically rough interface (McMillan, 1979) due to the high energy associated with the interface. Atoms landing on atomically smooth interface will be unstable energetically, and will tend to rejoin the melt. Alternative site for growth are needed.

A common mechanism for growth is one in which atoms add at step sites provided by screw dislocations intersecting the interface (Christian, 1975). Only a small fraction (f) of the total possible number of sites are available.

This fraction can be calculated, as below:

$$f \simeq \frac{\Delta t}{2\pi T_m} \qquad [9]$$

Δt = degree of undercooling
T_m = melting point

The growth rate equation must be modified to take this into account:

$$U = f\, a_o\, \nu \left[\frac{-\Delta G_{Ea}}{RT}\right] \left[1 - \exp\left(\frac{\Delta G}{RT}\right)\right] \qquad [10]$$

An alternative equation may be derived to show the effect of viscosity on the growth rate.

The viscosity of the glass is modified by the temperature of the glass and the composition of the melt. Changes in viscosity alter the growth rate of crystals in the glass. Viscosity controls the rate of diffusion of species to and away from the interface. Viscosity and diffusion are related by the Stokes-Einstein equation:

$$D = RT / 3\pi N \eta a_o \qquad \text{ie} \quad D \propto 1/\eta \qquad [11]$$

where:
a_o = interatomic separation
ν = vibrational frequency of atom at glass crystal interface
N = Avogadro's number
η = viscosity.

and diffusion is controlled by the composition of the melt:

$$D = a_o^2\, \nu \exp\left[-\Delta G_{Ea}/RT\right] \qquad [12]$$

The temperature dependence of the growth rate is clearly illustrated by substitution of equations [11] and [12] into equation [10], which yields:

$$U = fRT \left[1 - \exp\left(\frac{\Delta G}{RT}\right)\right] / 3\pi N (a_o)^2 \eta \qquad [13]$$

The interaction between viscosity, composition and growth rate was demonstrated by McMillan (1969). The addition of small amounts of Li_2O to a ZnO-Al_2O_3-SiO_2 glass caused large changes in the growth rate of the major phase. This is shown in Table 5.

Table 5: The variation of growth rate with viscosity.

$\%Li_2O$	Viscosity (poise @ 800°C)	Growth Rate (micron / sec)
0	5.4×10^7	0.067
1	-	0.75
3	3.2×10^4	5.9

Both the free energy change and the viscosity increase as the degree of undercooling increases. The initial large increase in growth rate, due to an increase in free energy, is offset as the viscosity increase begins to dominate. This gives rise to the shape of the typical growth rate curve.

3.2.2 Crystal growth morphology

The crystal growth morphology of a system depends on a number of interacting factors, which include:

- The type of system
- The diffusion rates of the species present
- The temperature of crystal growth
- The temperature gradient at the interface between glass and solid
- The type of nucleation in the system

The temperature gradient of the interface may be a critical factor in the crystallisation of some systems. If removal of heat from the interface is sufficiently slow, a temperature increase at the interface will occur and the growth rate will be affected. The morphology of the growth may also be affected by the temperature profile of the interface. If the temperature at the interface rises above the temperature of the liquid, protrusions formed by statistical fluctuations in the growth process will be unstable, and a dendritic or spherulitic growth may result.

Uhlmann (1971) describes the significant factor in determining morphology as the entropy of fusion (S). Materials with low entropies of fusion ($S < 2R$) have non-faceted interfaces and grow isotropically (R is the gas constant).

Materials with a large entropy of fusion ($S > 4R$) show anisotropic growth. Close packed planes have atomically smooth interfaces, while less closely packed planes are

rough on an atomic scale. Typically these materials have large differences in the rate of growth rate between the rough and smooth interfaces.

In materials with a large entropy of fusion, crystallisation at large undercoolings may cause the nucleation of new crystals having different orientation at or in advance of the growth front. This can lead to spherulitic growth of crystals. Spherulitic growth is favoured by conditions giving rise to low molecular mobility such as high viscosity of the glass and the presence of impurities in the melt.

3.2.2.1 Spherulitic growth

Spherulites form by the growth of fibrous crystals radiating outward from a center. They may have circular geometry or a sheaf-like appearance, and result in a microstructure that is not conducive to the achievement of high mechanical strength.

McColm (1983) states that spherulitic or dendritic growth is the common growth morphology when nuclei are greater than two microns apart. The crystals grow as fibres in a residual glass matrix. Spherulite fibres have the appearance of being "fine and twisted", and dendrites have straight fibres.

Spherulitic growth is commonly found in systems where the composition of the early crystals differs from that of the bulk. This results in depletion of some components of the glass at the interface. Under these conditions, growth at protrusions predominates, particularly at the tip where depletion is less severe. Growth of branches on the protrusion will be controlled by competition with other branches and growth becomes spherulitic.

Keith *et al* (1963) relates the occurrence of spherulitic growth to the ability of the crystals to branch during crystallisation. They also regard impurities as essential, as these concentrate at the advancing interface and reduce the extent of diffusion and therefore growth rate. Analysis of growth rates via kinetic data indicated that the crystallisation was controlled by the rate at which new fibres are nucleated.

It is sometimes possible to convert the (undesirable) spherulitic morphology to a more desirable lath or needle-like form by further heat treatment (McMillan, 1979).

3.3 A model for isothermal transformation of glass: The Avrami equation

Silicate glasses invariably crystallise via a nucleation and growth process, irrespective of the mechanism by which nuclei are formed. A consequence of this is the existence of an interface between the glass and the ceramic. This interface divides the

crystalline and non-crystalline regions of the specimen and has a fixed rate of movement through the specimen while the conditions are held constant.

The rate at which a glass specimen crystallises can be gauged by observing the extent of crystallisation of a material held at a fixed temperature for a known time, a process known as isothermal heat treatment.

A theoretical treatment of the kinetics of interfacial reactions occurring as a result of isothermal heat treatment evolved through the efforts of Johnson and Mehl (1939) and Avrami (1941). This has become known as the Johnson-Mehl-Avrami equation, or the Avrami equation. An abbreviated form of the derivation, summarised by Christian (1975), is given in Appendix 8.8.

Avrami proposed the use of an equation with a general form, valid under conditions discussed below:

$$\xi = 1 - \exp(-kt^n) \qquad [14]$$

where:
k and n are constants
ξ = fraction crystallised
t = time since start of reaction

This equation was derived for 3-dimensional growth on nucleation sites in a material. Under these conditions of growth, the exponent (n) may take values between three and four. An exponent of three implies that nucleation does not occur during growth.

Christian (1975) has shown that the above equation is valid for crystal growth in the presence of surfaces which interfere with the free growth of the new phase. The general expression for the volume transformed remains valid for two-dimensional ($2 \leq n \leq 3$) and one-dimensional growth ($1 \leq n \leq 2$).

There are some assumptions in the Avrami equation whose applicability to the crystallisation of a glass should be examined.

(i) The exponent of the Avrami equation is affected by the rate of formation of nuclei in the specimen. For three-dimensional growth on nuclei, the exponent may take a value between three and four. A value of four corresponds to a constant rate of formation of nuclei during the crystal growth process, while a value of three implies that all nuclei are formed early in the reaction and the nucleation rate is effectively zero.

This latter case corresponds to the situation in a crystallising glass ceramic where the temperatures of nucleation and crystal growth are well separated. This is the desirable situation.

(ii) The growth rate is assumed to be isotropic. This is almost always true in crystallisation of glass melts.

(iii) The Avrami equation has theoretical validity only for transformation by interfacial growth. Glass crystallises by means of a definite interface between the crystalline and non-crystalline regions, which moves through the glass as the reaction proceeds to completion.

The Avrami equation has physical significance only while all assumptions hold true. The condition of complete site saturation of all nucleation sites at an early stage is particularly important.

The Avrami equation is approximately valid for the early stages of diffusion controlled precipitation reactions, and a wide range of experimental work has attempted to give physical significance to the value of n in reactions of this type. The applicability of the equation has also been extended to systems where the nucleation rate is not zero. There is, however, no theoretical basis for the application of this equation to any reaction that does not conform to the assumptions above.

4. EXPERIMENTAL TECHNIQUES

4.1 Raw materials for glass manufacture

The Pulverised Fuel Ash (PFA) used in this study was from the Lethabo power station in the Transvaal. The ash, collected in all the fields and known as "mixed ash", was made available to UCT for use in experimental work. The major element composition of the PFA is given in Table 6 while a more complete analysis is given in Appendix 8.1. The physical properties of the PFA are discussed in Section 2.2. Other oxides used were reagent grade chemicals, with the exception of the industrial grade calcite ($CaCO_3$) used to provide CaO. This material is known to contain a small amount (1-2% by mass) of $MgCO_3$.

4.2 Glass Melting

Specimens of approximately 100 grams of glass were prepared by melting the blended batch for 4 hours at 1550°C in an alumina crucible, after which the glasses were cast and then annealed at 750°C for a further 4 hours. The glass melt was cast into moulds at room temperature. Two types of moulds were used, a brass finger mould used to cast glass rods and a set of steel blocks used to cast glass slabs. To prevent adhesion of the glass, the moulds were painted with graphite powder.

The glass is fairly aggressive and limited erosion of the crucible was noted. This resulted in some increase in the Al_2O_3 content of the glass. Crucible erosion occurred to a different extent in different glasses, but the increase in the alumina content of the different glasses was not calculated.

4.3 Microstructural Analysis

Comparisons between the microstructure of specimens are fraught with problems, particularly when there are large variations in the morphology of the crystalline species, as in the specimens prepared during this study. To avoid the difficulties inherent in a qualitative description of the microstructure, a measurement was taken of the intercept length distribution of the phases made visible by etching polished sections of the materials. This value is significant, as the measured intercept length distribution is directly related to the grain size distribution of the material, (although analytical treatments expressing this relationship are only available for simple shapes) and relationships between grain size and mechanical properties of ceramic materials have been demonstrated many times. This allows the intercept length distribution, along with the average intercept length, to be used as a meaningful parameter for comparison of materials.

Specimens were obtained from the cast glass by cutting specimens of about 1x1x1 cm using a diamond saw. Each sample for microstructural analysis was prepared in the same manner: heat treatment for the desired time, followed by mounting, grinding and polishing. The specimen was then etched to reveal the microstructure, which was examined using optical or scanning electron microscopy. Micrographs of the surface features were taken and used for microstructural analysis. Intercept lengths were measured by means of a lineal analysis system using a grid superimposed on the photograph to provide the reference lines. This produced a data set consisting of measured line segments calibrated for the magnification of the photograph. The data was collected using a semi-automatic digitising system along the lines of those described by Frith (1983), comprising a digitising tablet with custom software developed for the purpose. Data was transferred to a spreadsheet for storage and manipulation. The intercept length distribution is presented as a cumulative frequency histogram, which allows easy comparison between the distributions of different samples, and summarised by calculation of a mean intercept length (MIL).

Specimen preparation procedures were standardised, and will not be discussed at any length as details of the methods are given in the Appendices, along with a short description of both the data produced and the software used to produce the data.

A standard heat treatment cycle was used to crystallise the samples for microstructural analysis. This was composed of an initial nucleation heat treatment at 800°C for one hour (60 minutes), followed by a crystallisation heat treatment of predetermined time at 950°C. Heating and cooling rates were kept constant at 20°C per minute, within the limits imposed by the furnace. The rapid heating rates used imposed thermal stresses on the specimens in the furnace, sometimes resulting in cracking of the material.

Microscopy, in particular SEM, was carried out under a fixed set of optical or electron-optical conditions, to prevent distortions in the magnification. The magnification bar recorded on the SEM micrographs was calibrated against standards of known size across the range of magnifications used.

4.4 The Measurement of Crystallisation Rate

The determination of the rate at which a glass item crystallises is important, as it provides information necessary for control of the microstructure and prescribes the heat treatment cycle needed to crystallise an article. Crystallisation rates obtained under certain conditions can provide information about the processes occurring during crystallisation.

Although the measurement of the growth rate of a ceramic to glass interface can provide important information about the crystallisation of the glass, it does not provide a complete picture of the processes occurring in a crystallising specimen. A more complete description of the crystallisation rate of the specimen is provided by a parameter which is affected by the number of nuclei present in the specimen, as well as the rate and type of growth on those nuclei. Any bulk property that changes steadily with the degree of crystallinity may be used to acquire such data. Suitable indicators include density (Rabinovich, 1982), impedance (Harper, 1970), and measurements of the volume fraction crystallised.

The volume fraction crystallised may be conveniently measured by means of *inter alia*, XRD analysis of powdered specimens. Methods of quantitative XRD analysis to determine the crystalline content of a crystalline material have been reported by Ohlberg (1962), Cervinka (1976) and Kim (1989). The basis for the application of XRD to quantitative determination rests on the observation that the volume fraction of a phase is reflected directly in the intensities of the peaks due to that phase (Klug, 1974).

To investigate the rate of crystallisation of the glasses prepared with PFA as a raw material, a group of samples of comparable size were cut from each glass. Every specimen was given an isothermal heat treatment at 950°C, after which the specimens were powdered and the XRD spectra recorded. These procedures are described in the Appendices.

The area and height of selected peaks in the XRD spectra of the heat treated specimens were determined using software written for that purpose. The same set of peaks were used to analyse all the samples of a given glass composition across the heat treatment series, and where possible the same peaks were used for each glass.

The samples were assumed to be wholly crystalline after 6000 minutes of heat treatment at 950°C, a premise supported by the appearance of the XRD spectra and the micrographs of the polished and etched specimens. The extent of crystallisation of the specimens at each sample time was calculated relative to that of the specimen at 6000 minutes.

The devitrification of a glass progresses by the advance of a crystalline interface into a glassy matrix and is well suited to description by the Avrami equation. Crystallisation data for each glass was fitted to the Avrami equation described below, the procedure being described fully in Appendix 8.7.

The Avrami expression

$X = (1-\exp(-kt^n)$ where

n = dimension of growth
k = rate constant
X = fraction crystallised

may be cast into a more convenient form:

$$\ln(-\ln(1-X)) = \ln(k) + n\ln(t) \qquad [15]$$

A plot of $\ln(-\ln(1-X))$ versus $\ln(t)$ allows the evaluation of (k) and (n) using a least-squares method. The equation should be applied only to data points collected while growth is in progress.

The theoretical treatment in Appendix 8.8 gives (for unobstructed growth on a fixed number of nuclei):

$$k = (4\pi^{v}I/3)\,T^3 \qquad [16]$$

The value of k provides a direct measurement of the rate at which the glass crystallises. As can be seen, this is composed of two factors: the rate at which growth occurs (T), and the number of sites on which growth occurs (^{v}I). This value will be constant for a glass where the composition of the residual glass does not change.

The constant (n) can be used to distinguish among growth processes. The 'dimension of growth' refers to constraints in the directions in which crystal growth can occur (Christian, 1975). For the conditions under which the equation is derived the following interpretation can be made:

3-dimensional growth:	n≈3
2-dimensional growth:	n≈2
1-dimensional growth:	n≈1
Surface nucleation:	n≈1

The change in growth processes from a 1-dimensional to a 3-dimensional mechanism which occurs in the glasses studied here, is significant. It marks a change from surface nucleation of the specimens to bulk nucleation and results in changes to the microstructure which have marked effects on the mechanical properties.

4.5 Erosion

To compare the erosion resistance of the materials, a number of materials were tested alongside the PFA based glass ceramics prepared in this study. These included a range of commercially available wear resistant materials, including cast basalt and alumina.

In addition, specimens were cut from glass ceramic tiles manufactured commercially and using Lethabo PFA as a raw material, (supplied by courtesy of Ash Resources (Pty) Ltd.). A specimen of 'Silceram' was also made available, by courtesy of Ash Resources. This material is of interest as it would provide direct competition in the marketplace for materials of the type prepared in this study. These specimens are described in greater detail in Appendix 8.3.

The wear resistance was evaluated using an accelerated erosion test of the particle-gas stream variety as described by Karlsen (1985). This uses compressed air to impact particles of silicon carbide onto the surface to be tested. A fixed mass of particles is used, and the mass loss of the specimen measured. The mass lost is an indication of the wear resistance and may be used to rank materials. Greater detail of the experimental methods is described in Appendix 8.4.

Erosion of brittle surfaces by hard particles is a complex process involving brittle fracture and plastic deformation of the target surface as a result of the impact. Two theories have evolved which model erosion resistance in terms of the physical properties of the materials used.

These models, by Evans *et al* (1978), and Ruff (1979), start from different approaches to produce very similar models, as seen below:

$$\text{Evans (1978):}\quad W \propto V_o^{3.2}\, R_p^{3.7}\, \rho_p^{0.25}\, K_c^{-1.3}\, H^{-0.25} \qquad [17]$$

$$\text{Ruff (1979):}\quad W \propto V_o^{2.4}\, R_p^{3.7}\, \rho_p^{1.2}\, K_c^{-1.3}\, H^{0.11} \qquad [18]$$

Where

V_o = initial particle velocity
R_p = radius of particle
ρ_p = density of particle
K_c = fracture toughness of target
H = hardness of target.

The values of V_o, R_p and ρ_p are held as constant as possible in the testing of these materials, and variations in wear rate are attributed to changes in the fracture toughness and hardness of the material only.

5. EXPERIMENTAL RESULTS

The production of glass ceramic materials using blast-furnace slag is an established process (Ponton, 1986). Typical applications for these materials are as wear-resistant tiles and surfaces. Studies have shown that other by-products of industrial processes may be used to form similar wear resistant materials (Pavlushkin, 1982; Veasey 1973; Topping 1976). Among these materials is Pulverised Fuel Ash (PFA), produced by the combustion of coal for electrical power.

This project was undertaken to investigate the feasibility of producing glass ceramic materials using PFA from a South African power station as a raw material. An initial study examined the conditions under which the PFA would form a glass (Kirby, 1987). This study details the results of an investigation of the crystallisation behaviour of suitable glass composition selected from this initial study.

The physical properties of ceramics crystallised from glass improve when a material able to form sites for heterogeneous nucleation is incorporated into the glass. Metal oxides of various types are known for their ability to nucleate silicate glasses, and the effect of such metal oxides on the crystallisation of the glass prepared from PFA was evaluated by comparing the microstructure and crystal growth rate of the materials.

A preliminary investigation of a large range of glasses, with a variety of nucleating agents and a limited variation in composition was undertaken. Appendix 8.2 summarises the compositions used, and describes briefly the suitability of each glass. A small number of compositions were selected from this list for further study, either as representative materials of a class or due to the good physical properties of the crystalline material. Table 6 lists these materials, which this study discusses in detail.

Table 6: Nominal Composition of the materials used in this study (mass percent of oxide)

	SiO_2	Al_2O_3	CaO	Fe_2O_3	Cr_2O_3	TiO_2	P_2O_5
PFA	50.8	35.2	4.4	3.4	-	1.7	0.5
Base	25.7	17.8	52.8	1.7	-	0.8	0.1
T2	25.4	17.6	52.2	1.7	-	1.8	0.1
T10	23.3	16.2	47.9	1.6	-	10.0	0.1
D4	24.4	17.0	50.2	4.0	2.4	0.8	0.1
F	25.7	17.8	52.8	1.7	-	0.8	0.6
E2	23.2	16.1	47.7	1.6	-	10.0	0.6

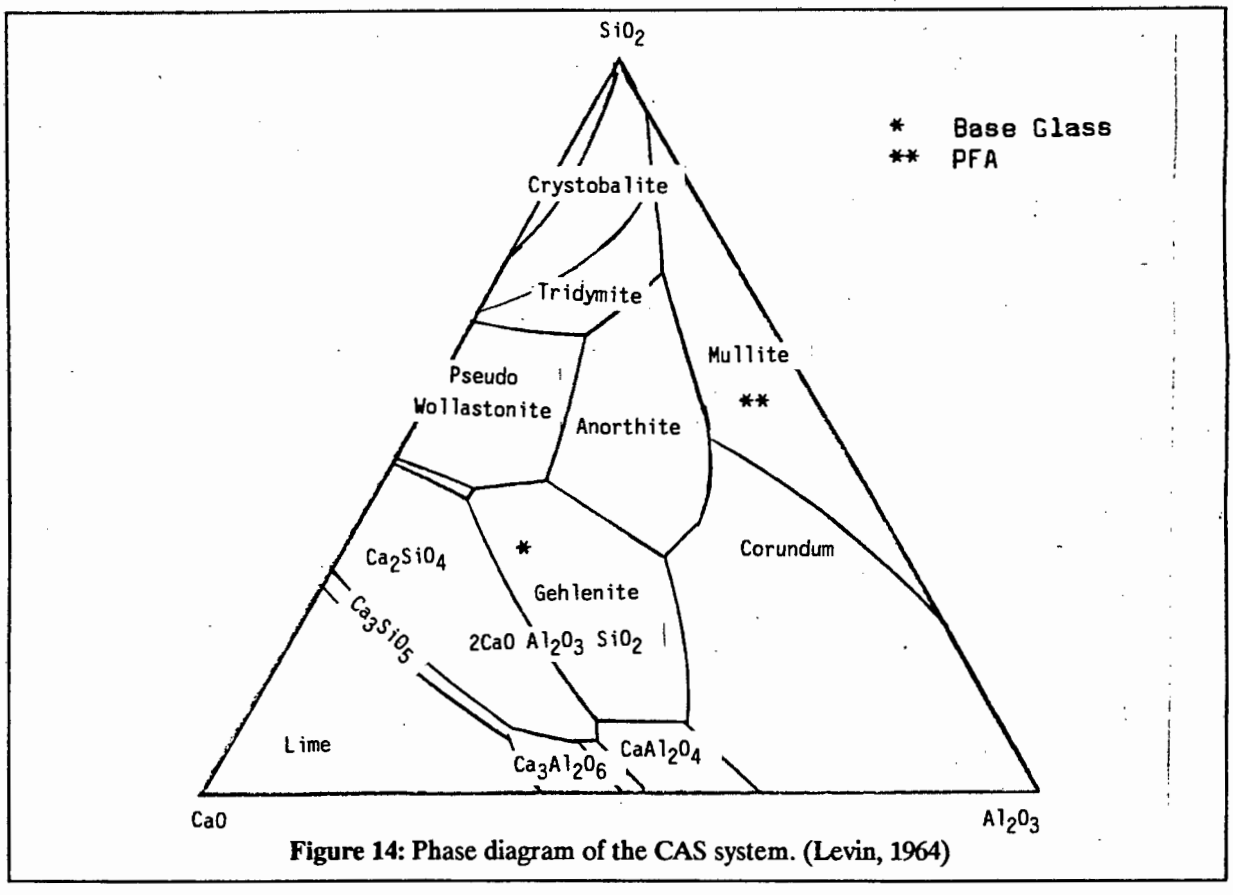

Figure 14: Phase diagram of the CAS system. (Levin, 1964)

5.1 Composition of the Glass.

Previous work has shown that the Lethabo PFA is very refractory (Kirby, 1987), being composed mostly of SiO_2 and Al_2O_3 (Table 6). Attempts to melt the PFA without added oxides were unsuccessful. At 1550°C, the material vitrifies just enough to show signs of bloating, but remains far from becoming a pourable glass. To adjust the composition of the PFA to a batch more suitable for glass formation requires a fluxing agent; this is usually an alkali or alkali-earth oxide in silicate melts. This 'network modifier' has a large influence on the properties of the final product.

This study used CaO as the flux. Glass ceramics in the CaO-Al_2O_3-SiO_2 system have good wear resistance (Kirsch, 1988), and research has shown that bulk nucleation of the such glasses by metal oxides is possible (Davies, 1970; Pavlushkin, 1982; Kirsch, 1988). In addition, CaO is cheap and easily available as the carbonate, a convenient form for introducing the flux into the glass.

An important parameter affecting the selection of a composition suitable for glass formation when using industrial by-products is the 'Acid/Base ratio' (A/B), which is calculated according to Humphreys (1970):

$$A/B = \frac{SiO_2 + Al_2O_3}{CaO + MgO + Fe_2O_3 + A_2O} \quad [19]$$

$$(A_2O = Na_2O + K_2O)$$

Glass batches suitable for melting have A/B ratios of 0.8 - 1.2 (Manz, 1984), whereas the calculated A/B ratio for Lethabo PFA is around 8. Figure 14 displays the PFA composition on a CaO-Al_2O_3-SiO_2 (CAS) phase diagram.

The earlier study, intended to establish the viability of PFA as a raw material for glass fibre manufacture, describes the preparation and melting of series of glass batches containing 30-55% by mass of CaO and the balance PFA. We selected one of these glass batches, with an A/B ratio of 0.6, for use in this study on the basis of its low viscosity compared to the other melts (Kirby, 1987). Table 6 identifies this composition as the Base Glass (glass B), as does the phase diagram in Figure 14.

The CaO content of this glass is such that it borders on being an 'invert' glass, in which the modifier content exceeds the 'network former' content (McMillan, 1982). The high CaO content lowers the chemical resistance of the material, and disruption of the silicate network can adversely affect the physical properties of the material. Despite the high CaO content of the glass chosen for use in this study, no effects of this nature were noted.

5.2 The Base Glass (Glass B)

The term 'Base glass' refers to the glass prepared using only calcite and PFA, mixed and melted using standard methods. This glass is a basis for comparing the efficiency with which the glass specimens are nucleated, having no additives to influence the crystallisation process. Table 7 gives the composition of this glass, with the composition of the PFA provided for comparison.

Table 7: Nominal Composition of batch used to prepare Base glass. (mass percent)

	SiO_2	Al_2O_3	CaO	Fe_2O_3	Cr_2O_3	TiO_2	P_2O_5
PFA	50.8	35.2	4.4	3.4	-	1.7	0.5
Base	25.7	17.8	52.8	1.7	-	0.8	0.1

5.2.1 Physical properties of the glass

As cast, the glass is black due to the high iron content of the PFA. It has a glass transition point at about 750°C, and a softening point at about 850°C, as seen from the thermal expansion curve (Figure 15). The thermal expansion of the glass between 150°C and 700°C was measured as 8.99×10^{-6} °C^{-1}. The high glass transition point requires that the glass be annealed at 750°C.

Differential Thermal Analysis (DTA) on a powdered sample of the glass showed an exothermic reaction starting 920°C and peaking at 960°C (Figure 16). McMillan (1979) attributes this exotherm to the onset of crystallisation in the glass, and on this basis we chose a temperature of 950°C as the crystallisation temperature for all crystal growth heat treatments.

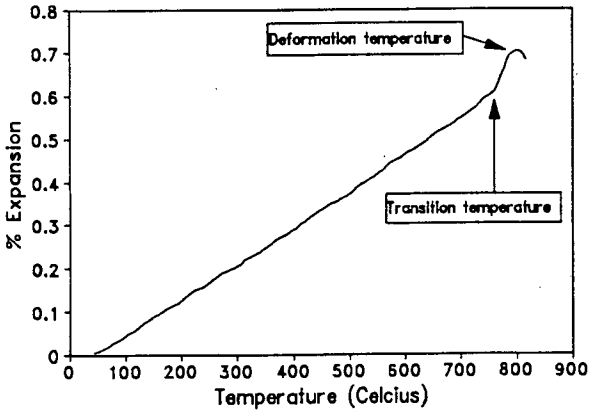

Figure 15: Thermal expansion of the Base glass.

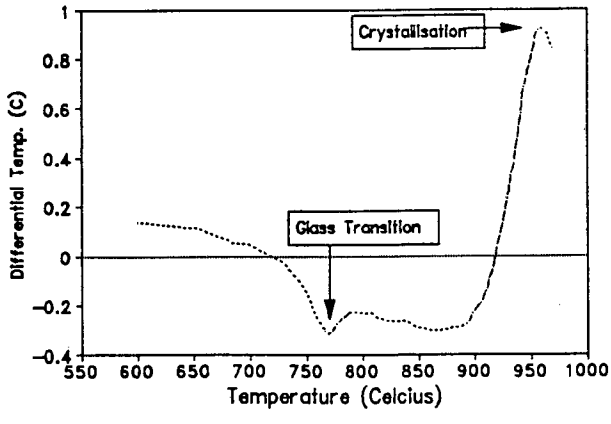

Figure 16: DTA trace of the Base Glass.

Figure 17: Polished and etched section of Base glass.

5.2.2 Devitrification of the glass

Heat treatment of a specimen of the Base glass at 950°C produced a light coloured ceramic which had devitrified mainly from the surface (Figure 17). The oriented

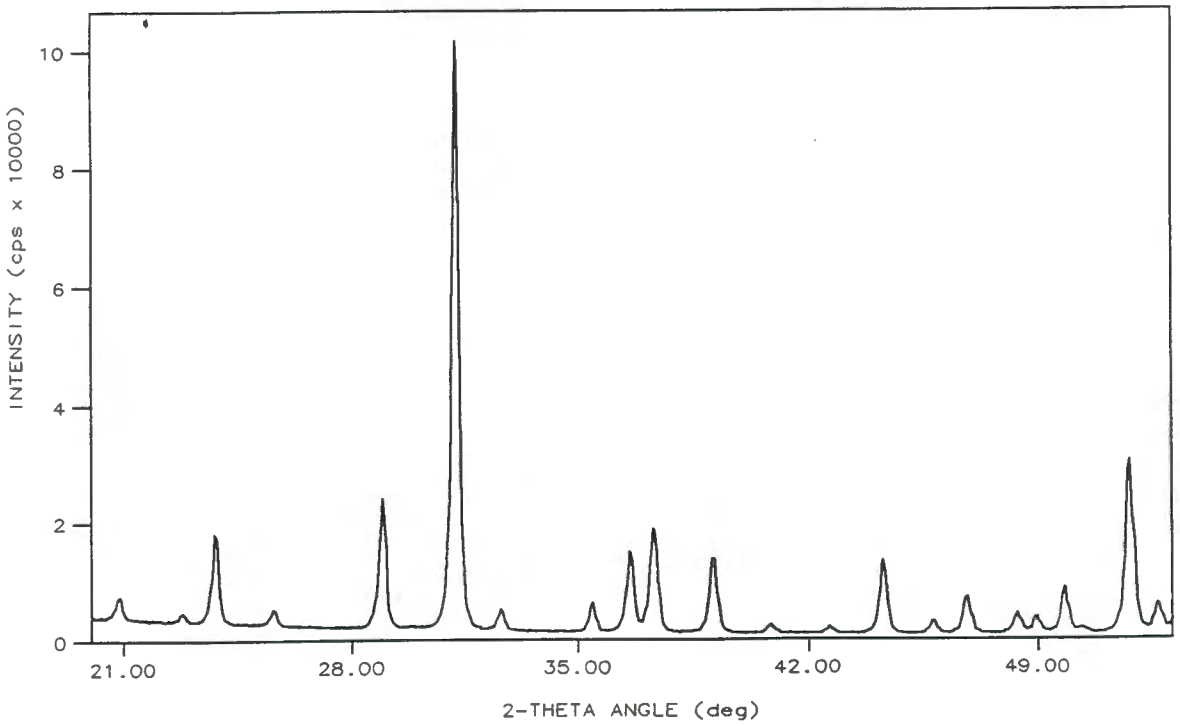

Figure 18: XRD spectrum of fully crystallised Base glass (after 6000 minutes at 950°C)

microstructure of the material was visible even on the macro scale. Shrinkage of the glass and segregation of elements during crystallisation resulted in porosity along the centre line of the sample, and the specimen contained many inter-granular cracks attributed to shrinkage during crystallisation.

The crystalline phase identified in the material during the crystallisation process was gehlenite ($Ca_2[Al_2SiO_7]$), identified using the JCPDS index card no. 4-0960. Gehlenite is one end-member of the melilite series, the other being åkermanite ($Ca_2[MgSi_2O_7]$). The composition of a member of this series may be described in terms of the proportion of the end members, for example [Gehlenite 50%; Åkermanite 50%] is written as (G_{50}/A_{50}).

Melilite ($Ca_2[(Mg,Al,Si)_3O_7]$) is a solid solution series in which $[MgO_4]^{6-}$ and $[SiO_4]^{4-}$ tetrahedra substitute for $[AlO_4]^{5-}$ tetrehedra in the unit cell (Deer, 1964). Substitution is possible across the complete compositional range, and at no stage do two phases appear. Changes in position and intensity of the peaks of the XRD spectra reflect changes in the composition of the material. Comparison of the XRD spectrum of ceramic B (Figure 18) with the JCPDS cards for the melilite series showed that the material contains somewhere between 0 and 25% of åkermanite; that is a Mg^{2+} content of between 0 and 3% by mass, a composition written as G_{75}/A_{75}.

The rate at which the glass devitrifies was measured by isothermal heat treatment of samples for fixed times up to 6000 minutes (Appendix 8.4). Figure 19 shows how the XRD spectrum develops during the heat treatment process. Before heat treatment,

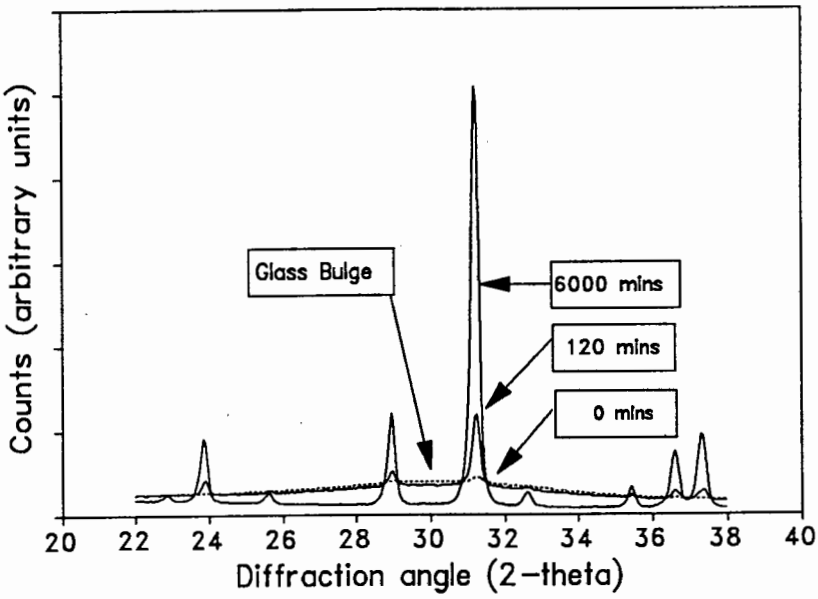

Figure 19: Development of the XRD spectrum for the Base Glass during heat treatment.

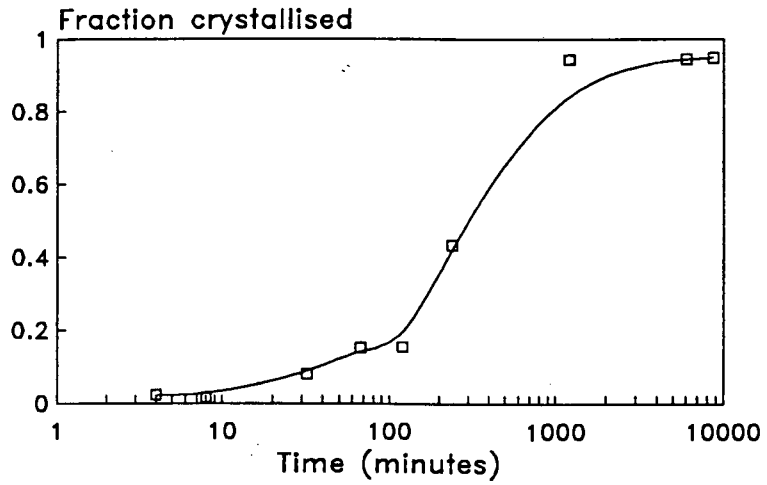

Figure 20: Change in extent of crystallisation with time for Base glass.

the XRD spectrum of the glass contains only the glass bulge centered at about 30° 2-theta. As heat treatment begins, and crystallisation occurs, peaks appear and increase in intensity, while the size of the glassy bulge decreases.

By using the intensity of the peaks of the XRD spectrum as a measure of the degree of crystallisation, the increase in the crystalline fraction of the specimen during heat treatment of the specimen can be plotted. Figure 20 displays the data for the Base glass, which shows that crystallisation took approximately 60 minutes to begin and

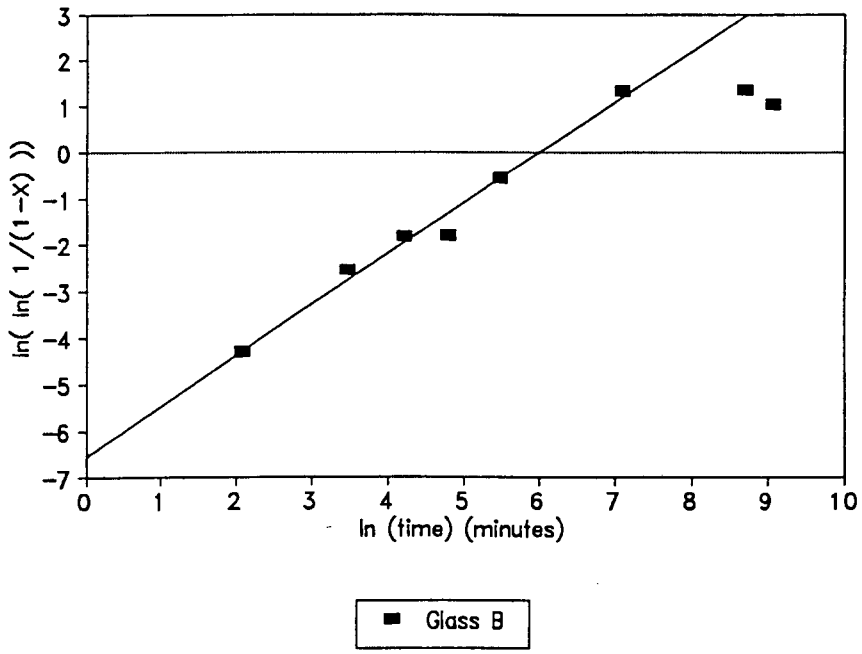

Figure 21: Avrami plot for crystallisation of Base Glass.

finished after 1200 minutes of heat treatment at 950°C.

The kinetic parameters obtained by fitting the data to the Avrami equation (see Figure 21) gave the Base glass a value for the Avrami exponent (n) of about 1 (Table 8). This implies either surface nucleation of the Base Glass or 1-dimensional growth on a fixed number of nucleation sites, as discussed in Appendix 8.8. Surface nucleation is a special case of 1-dimensional growth (Christian, 1975; McFarlane, 1986). Examination of the crystalline specimen using an optical microscope shows clearly that crystallisation begins by surface nucleation of the crystalline phase, with subsequent growth of crystals into the body of the glass (Figure 17).

5.2.3 Microstructure of the Crystalline material

Surface nucleation of the glass produces a coarse grained material with a highly oriented microstructure (Figure 22). Columnar growth of crystals toward the centre of the specimen results in the formation of large pores along the centre-line of the specimen. Thermal stresses induced by shrinkage in the material cause cracking in the material.

SEM micrographs illustrating the development of the microstructure are shown in Figure 22. The micrographs are of polished and etched sections through the specimens, taken after 120, 1200, and 6000 minutes respectively of heat treatment at 950°C. The samples were sectioned approximately parallel to the axis of growth.

Table 8: Calculated crystallisation parameters for Base Glass.

Glass	Induction period (min)	Avrami exponent	ln K	MIL (micron)
B	60	1.09	-6.55	5.1

Figure 22(a) shows the cellular growth of the crystal front into the glass. The origin of the oriented microstructure is clear. The grain boundaries of newly formed grains are not clearly defined, but after longer soaking periods at 950°C grain boundaries become more clearly differentiated by the etching procedure (Figure 22(b),(c)). This is attributed to the diffusion of impurities (ions whose inclusion in the melilite lattice is not energetically favoured) out of the lattice to grain boundaries. These impurities become visible as exsolution rims around grains, which etch at a different rate to the center of grains, due to differences in composition.

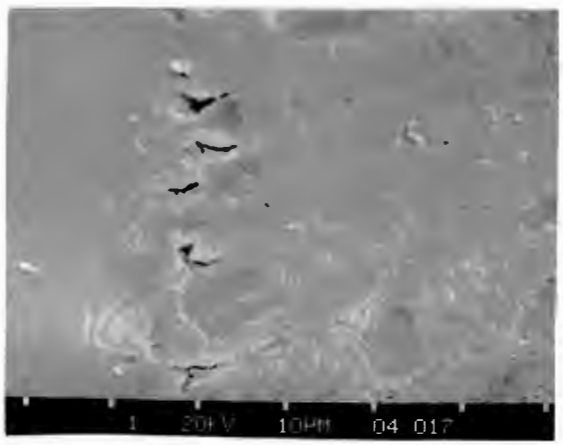

(a) 120 mins

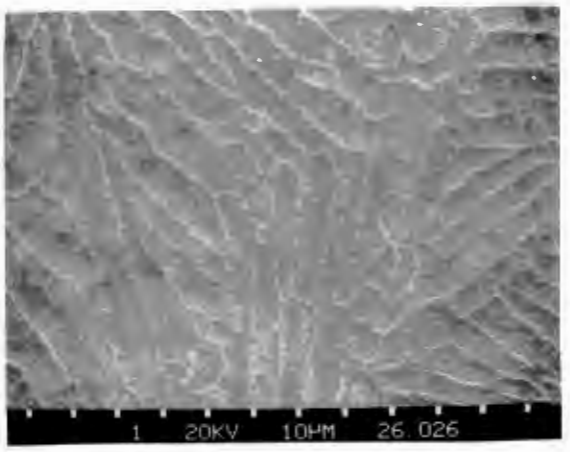

(b) 1200 mins

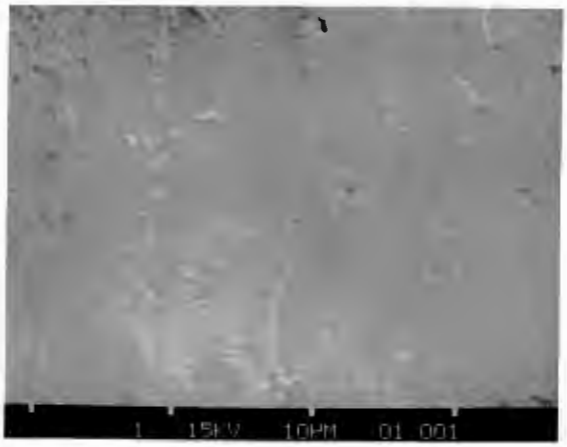

(c) 6000 mins

Figure 22: SEM micrographs of Base Glass.

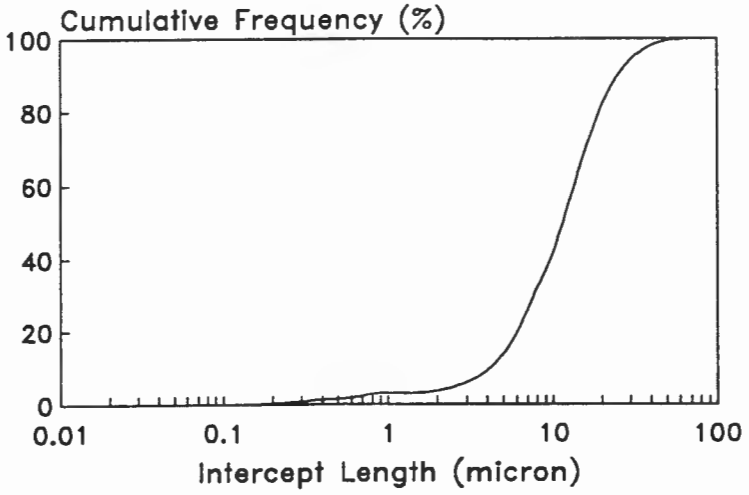

Figure 23: Intercept length distribution of the Base glass after 6000 minutes at 950°C.

The appearance of the exsolution rims coincides with an increase in the sharpness of the XRD peaks. The inclusion of impurities in a crystal lattice gives rise to peak broadening, and the increase in the sharpness of the peaks during heat-treatment implies that solid solution diffusion in the lattice occurs, resulting in partition of impurities to the grain boundaries.

Figure 23 depicts the intercept length distribution of the grains in the material, obtained by measurements on SEM photographs. The material does not show secondary grain growth, and there was no evidence of discontinuous grain growth after 100 hours at 950°C. This could be attributed to the segregation of impurities to the grain boundary, known to reduce boundary mobility by pinning (Christian, 1981).

5.3 Nucleation by Titanium Dioxide (Glasses T10 and T2)

Widely used in silicate systems, TiO_2 is most successful for nucleation of glass systems containing divalent metal ions (Barry, 1979; Scheidler, 1989). The concentration of TiO_2 used to induce nucleation in such glasses has varied, with TiO_2 contents between ranging between 1% and 20% (Stookey, 1960; McMillan, 1979; Partridge, 1982; Maier, 1987).

Crystallisation of the major phase in a glass ceramic is often preceded by formation of $RO.TiO_2$ species in the glass. The existence of such titanate species allows epitaxial crystallisation of the major species due to the similarity of lattice parameters (Lewis, 1979; McMillan, 1979).

Researchers have noted that the efficacy of TiO_2 depends on the oxidation state within the glass (McMillan, 1979). TiO_2 is not as effective in glasses with a reducing environment due to the reduction of Ti^{4+} ions to Ti^{2+}, which prevents formation of the $RO.TiO_2$ species required for nucleation of silicate species. This is important in glass ceramics prepared using PFA as an ingredient, as there is a significant unburned coal content in the PFA, which would produce a reducing environment.

To determine the effect of TiO_2 on the crystallisation of the PFA based glass, melts containing 2% (glass T2) and 10% (glass T10) by mass of TiO_2 were prepared. Table 9 lists the composition of these glasses, with the composition of the Base glass (glass B) and the PFA provided for comparison.

Table 9: Calculated Composition of Glass (mass percent of oxide)

	SiO_2	Al_2O_3	CaO	Fe_2O_3	Cr_2O_3	TiO_2	P_2O_5
PFA	50.8	35.2	4.4	3.4	-	1.7	0.5
Base	25.7	17.8	52.8	1.7	-	0.8	0.1
T2	25.4	17.6	52.2	1.7	-	1.8	0.1
T10	23.3	16.2	47.9	1.6	-	10.0	0.1

A slight degree of surface crystallisation was noted on the air-cooled faces of the materials, while the quenched faces were entirely glassy. The glasses have no detectable crystalline phases when cast, and are similar in appearance to the Base glass.

5.3.1 Crystallisation of the glasses

There are considerable differences in appearance between ceramics prepared from the nucleated glasses (Figure 24) and those prepared from the Base glass (Figure 17). Compared to ceramic B, the ceramics nucleated by TiO_2 are fine-grained, and surface

Figure 24(a): Polished and etched sections through glasses nucleated by TiO_2 - Glass T2.

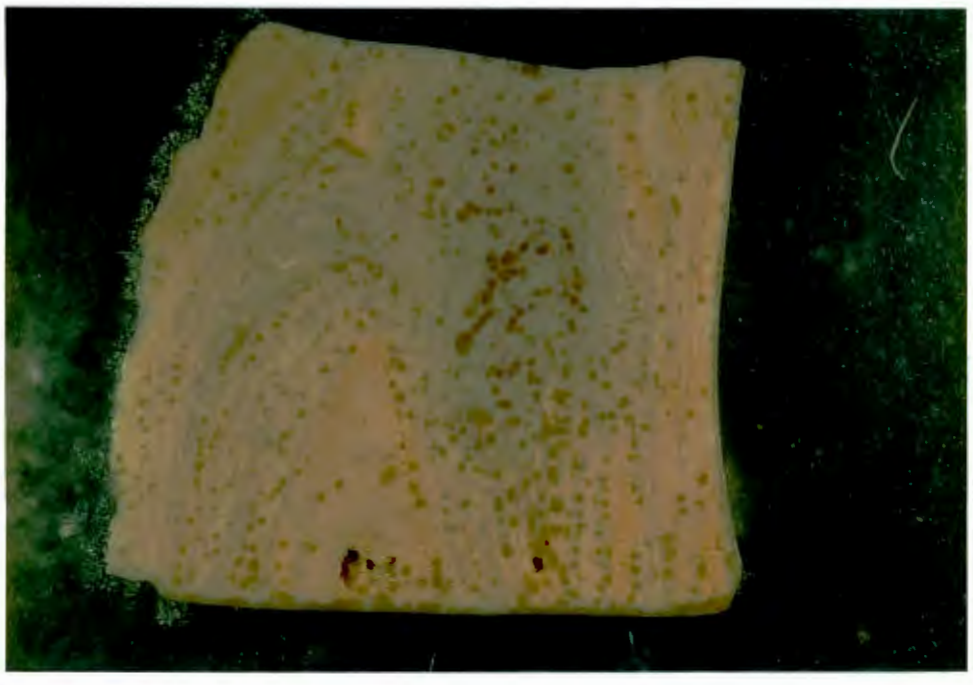

Figure 24(b): Polished and etched sections through glasses nucleated by TiO_2 - Glass T10.

nucleation is minimal. There is less porosity and less cracking, particularly in ceramic T10, containing 10% of TiO_2.

The micrographs in Figure 24 illustrate the spherulitic growth that is characteristic of these two materials. Rounded features are sections through spherulites, and are particularly obvious in ceramic T2 due to their size. A degree of porosity and cracking due to shrinkage during crystallisation is evident in ceramic T2, again a consequence of the large spherulites in this material. Crystallisation in ceramic T10 produced smaller spherulites due to the existence of many more sites for crystal growth.

5.3.1.1 XRD spectrum of glass T10

Crystallisation of the glass containing 10% of TiO_2 produced a two-phase material. The major phase is a melilite solid solution, as in the devitrified Base glass (glass B). Comparing the XRD spectrum of glass T10 (Figure 25) with that of the Base glass (Figure 18) indicates the existence of a second phase. The melilite content of the crystallised material was estimated at greater than 90% of the total volume.

Table 10: JCPDS card file data for Melilite and Fassaite

diffraction angle 2-θ (degrees)	d-spacing (Å)	Melilite (hkl)	Fassaite (hkl)
44.54	2.034		041 402
44.41	2.04	212	
44.21	2.045		202
42.86	2.11	202	
42.80	2.113		421
42.44	2.130		331
40.83	2.21	311	
40.45	2.230		022
39.93	2.258		112
39.34	2.29	112	
39.17	2.30	301	
38.60	2.329		311
37.47	2.40	102	
37.31	2.41	221	
36.68	2.45	310	
35.63	2.52	002	
32.68	2.74	220	
31.27	2.86	211	
29.82	2.996		221
29.09	3.07	201	
27.63	3.228		220
25.67	3.47	210	
23.19	3.71	111	
21.00	4.23	101	
20.07	4.425		020

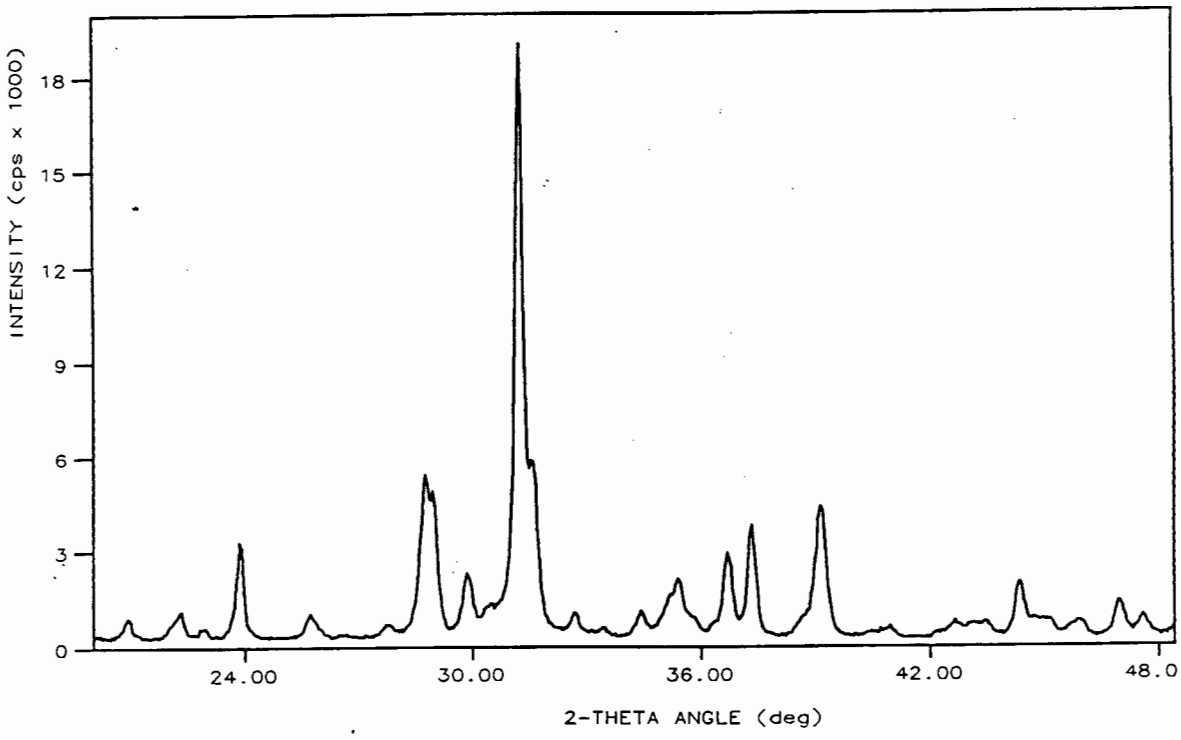

Figure 25: XRD spectrum of specimen T10 after 6000 minutes at 950°C.

Identification of the second phase is complicated by the extent of overlap of peaks in the XRD spectrum. The appearance of this second phase is associated with the addition of TiO_2 to the melt, and it is assumed that the phase is TiO_2-bearing. On this basis the phase could be identified as titan-augite or titanian-fassaite. This is a clinopyroxene, with the generic formula $Ca(Ti,Mg,Al)(Si,Al)_2O_6$, indicating the large degree of solid substitution possible. The closest match to the spectrum in the JCPDS file is card 25-0306, for a specimen with a specific composition. Variations in composition probably account for minor differences between the recorded XRD spectrum and that on the JCPDS card.

The composition of the melilite solid solution is slightly different to that of the phase formed on crystallisation of the Base glass. From the position of the peaks in the XRD spectrum, the composition is closer to G_{50}/A_{50}, i.e the composition intermediate between the two end members. This shift in composition is ascribed to the partitioning of elements between the two phases.

The close association between the peaks of the melilite and those of the second phase indicates similar lattice spacings in the unit cell of both species. This in turn suggests the existence of an orientation relationship between the two phases resulting from epitaxial growth of one phase on the other. As the XRD patterns of the two phases develop simultaneously, it is not possible to conclude that the TiO_2-containing species

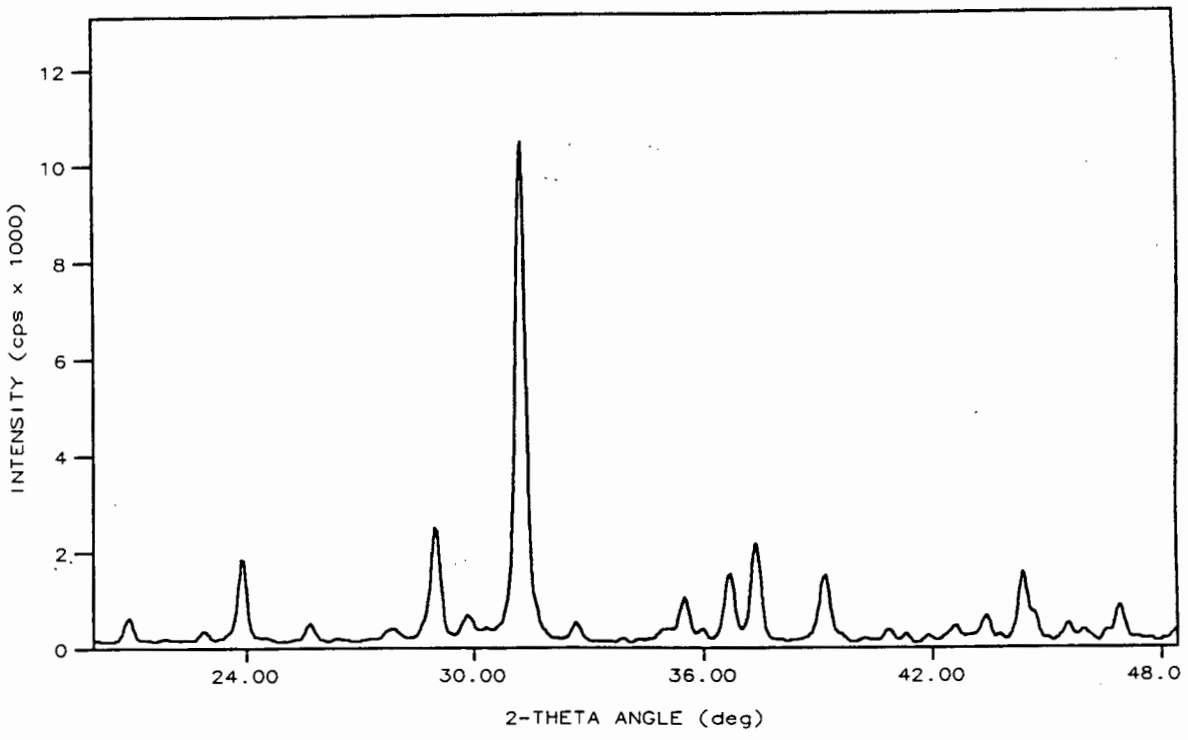

Figure 26: XRD spectrum of ceramic T2 containing 2% of TiO_2 as a nucleating agent.

has acted as a nucleating agent for the melilite solid solution. Microstructural examination leads to the conclusion that the two phases form concurrently by rejection of TiO_2-containing species from the advancing melilite lattice. Detailed experimental work involving direct investigation of the association between the phases would be necessary to investigate the nature of the relationship.

5.3.1.2 XRD spectrum of glass T2

Crystallisation of ceramic T2 containing 2% of TiO_2 does not as clearly crystallise to give two phases. The XRD spectrum does not contain large peaks due to a second phase (Figure 26), but a close comparison with the spectrum of the Base glass shows enough differences between the spectra to reveal the presence of a second phase. Comparison with the spectrum of ceramic T10 indicates that the second phases in ceramics T2 and T10 are similar. Microstructural examination shows a similar relationship between the morphology of the second phases in both these ceramics, indicating that they form by a similar process.

5.3.1.3 Rate of crystallisation

Adding TiO_2 markedly increases the crystallisation rate of the glasses (Figure 27). The glass containing 10% of TiO_2 (glass T10) crystallises much faster than the non-

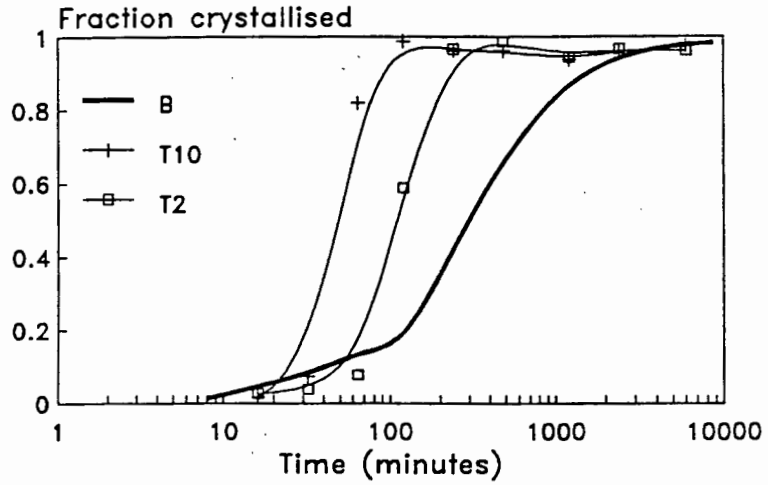

Figure 27: The rate of crystallisation of the glass specimens nucleated by the addition of TiO_2 when heat treated at 950°C.

nucleated Base glass, and crystallisation is practically complete after 120 minutes. Glass T2, containing 2% of TiO_2, crystallises at an intermediate rate, and requires around 240 minutes to complete the process. All the glasses require an induction period before crystallisation begins, which period becomes shorter as the TiO_2 content increases. This time is needed for the formation of sites for growth (Christian, 1975)

Calculation of the rate constant (k) for the Avrami equation shows a large increase in

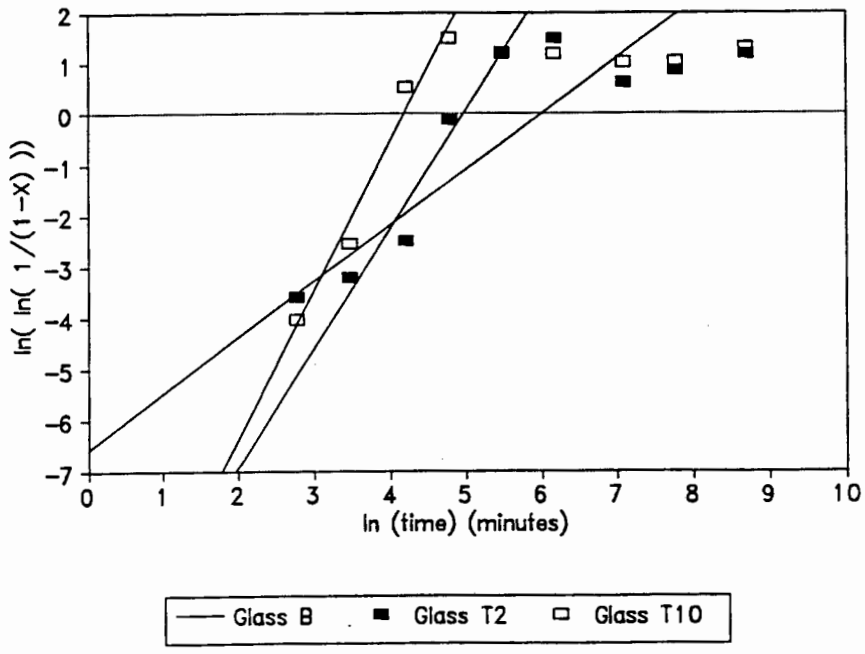

Figure 28: Avrami plot for glasses nucleated by addition of TiO_2.

the rate of crystallisation in TiO_2 containing glass specimens (Table 11). The rate of the crystallisation reaction increases due to changes in both the growth rate of the new species and the number of sites available for growth. In addition, the mode of growth changes from one- to three-dimensional due to the provision of growth sites in the bulk of the material.

Ram (Weyl, 1962) has noted that at 950°C the viscosity of a glass containing TiO_2 will be lower than that of a similar glass containing no TiO_2, to an extent depending on the TiO_2 concentration. The effect is small, but it will contribute to an increase in the rate of growth of the interface.

Table 11: Measured parameters for glass containing TiO_2.

Glass	Induction period (min)	Avrami exponent	ln K	MIL (micron)
B	60	1.09	-6.55	5.1
T2	40	2.3	-11.6	3.3
T10	20	2.9	-12.2	4.6

The calculated value of the Avrami exponent (n), calculated by fitting the crystallisation data to the Avrami relationship, changed markedly on addition of TiO_2 (Table 11). This indicates a change in the mode of crystallisation (McFarlane, 1986), and reflects the appearance of the kinetic plot (Figure 28), which differs markedly from that of the Base glass. This change, attributed to the production of nuclei in the bulk of the specimen, occurs when TiO_2 is added to the glass. It is reasonable to assume that these nucleating species are TiO_2-containing, and that they act by forming metal-titanates as discussed in Section 3.1.4.

In contrast glass B, crystallising via surface nucleation, has an exponent of approximately 1, and has noticeably grown from surface nuclei. Glasses T10 and T2 have Avrami exponents close to 3, reflecting the three-dimensional growth on nucleation sites within the sample (Christian, 1975). Glass T2, with an exponent of about 2.5, crystallised mostly by growth from bulk sites, with a small amount of surface crystallisation.

We see from the microstructures of the crystallised glass ceramics T2 and T10 (Figure 24) that increasing the TiO_2 concentration produces more sites for growth prior to the start of crystal growth. The increase in the rate of growth of the crystals combines with a change in the mechanism of growth in the glass to produce much more rapid crystallisation of the material. The effect of the increase in the number

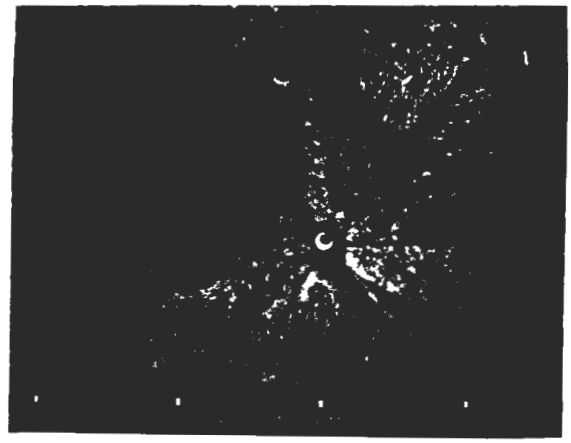

Figure 29: SEM micrograph of spherulite formed during crystallisation of glass T10 at 950°C.

of sites is expected to be the predominant factor in the increase in the rate of crystallisation, but this cannot be confirmed using the current experimental data.

5.3.2 Microstructure

The glasses containing TiO_2 as a nucleating agent crystallised largely by the growth of spherulites in the bulk of the specimen, seen clearly in the micrographs in Figure 24. Figure 29 shows a SEM image of a section through a single spherulite.

The TiO_2 content of the glass affects the size attained by the spherulites. Ceramic T10 has noticeably smaller spherulites than does ceramic T2, again attributed to the generation of more sites for growth as the TiO_2 content increases, so that the individual spherulites cannot grow as large before impingement upon others.

The heating rate used in the crystallisation process affected the microstructure of ceramic T10, but not of ceramic T2. At slow heating rates (2°C/min), ceramic T10 was fine grained and showed fewer spherulites then specimens prepared at high heating rates (Figure 24). At the higher heating rates used to crystallise the specimens prepared for microstructural examination, the difference in the microstructures of ceramics T2 and T10 was less marked, being mostly in the size of the spherulites. Specimens heated slowly spend longer in the temperature range at which nuclei are formed, increasing the number of growth sites, thus producing smaller spherulites.

The microstructure of a specimen that has crystallised via a spherulitic growth process is complex. The spherulites grow to sizes of 0.2 to 2 millimeters in diameter, depending on the conditions of growth, and the spherulites themselves have a fine-scale microstructure. In addition, due to the directional growth of the crystals from

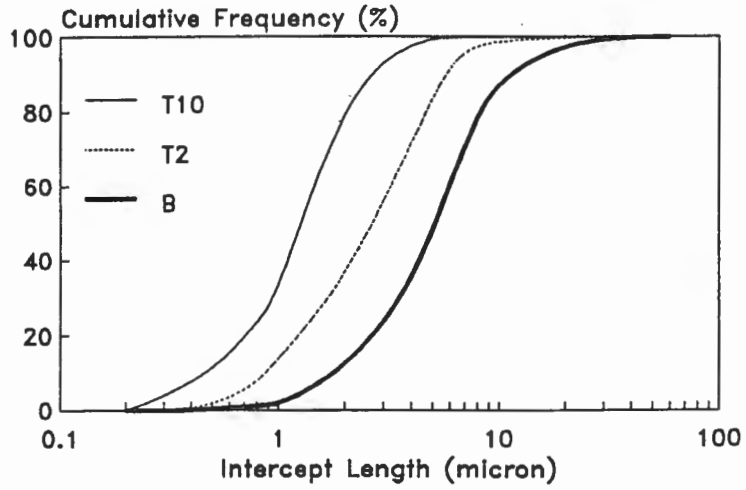

Figure 30: Intercept Length Distribution for glasses nucleated by TiO_2.

the origin the section chosen through the spherulite will influence the apparent microstructure of the material.

Since the presence of grain boundaries between phases has a major effect on crack propagation through the material, microstructural comparisons between ceramics T2 and T10 were made on this scale. Sections through the spherulites perpendicular to the direction of growth were photographed for both specimens, and Figure 31 shows SEM micrographs of the polished and etched sections.

The intercept length distributions of the grains of the major phase in specimens T2 and T10 is shown in Figure 30, and show clearly that increasing the TiO_2 content

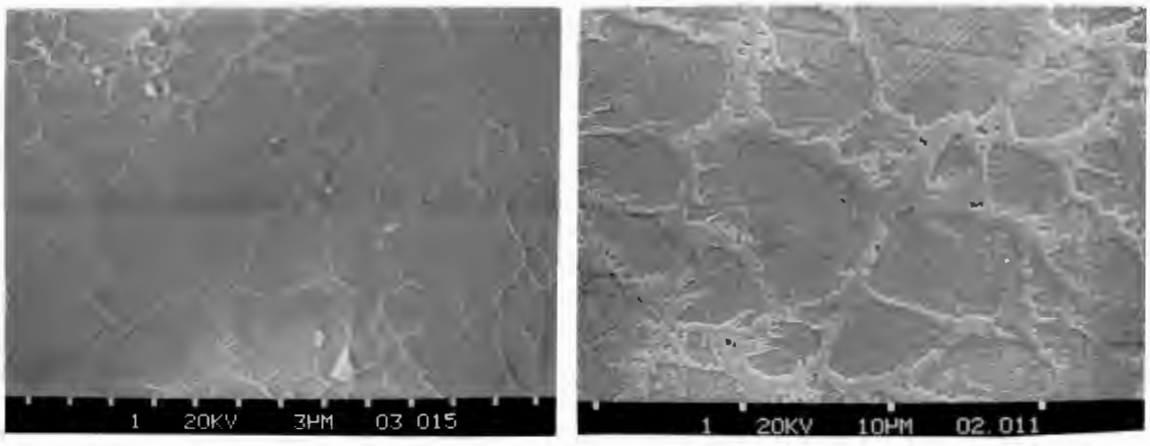

(a) Ceramic T2 (b) Ceramic T10

Figure 31: SEM micrographs of sections through spherulites perpendicular to growth direction. The ceramics were crystallised at 950°C for 1200 minutes.

changes the grain size. Spherulitic growth results in segregation of oxides along the growth path, giving a two phase microstructure with orientation along the growth path. Figure 31 shows the second phase distributed as a rim around the grains of the major phase. The different proportions of second phase in ceramics T10 and T2 results in smaller rims in ceramic T2, providing further evidence that the second phase in the XRD spectra is a crystalline phase containing TiO_2.

5.4 Nucleation by Phosphorous Pentoxide (Glass F)

Phosphorous Pentoxide (P_2O_5) is an effective nucleating agent for glass containing significant concentrations of alkali-earth metal oxides, particularly Li_2O, due to the formation of lithium phosphate species suitable for epitaxial growth of silicate species (James, 1975; Headley, 1984).

Since the Lethabo PFA has very low concentrations of alkaline earth species, P_2O_5 was not expected to be an effective nucleating agent. A glass, with 0.5% of P_2O_5 by mass added to a batch of the Base glass (Table 12) and prepared using standard methods, confirmed this.

Table 12: Nominal Composition of batch used to prepare glass F. (mass percent)

	SiO_2	Al_2O_3	CaO	Fe_2O_3	Cr_2O_3	TiO_2	P_2O_5
PFA	50.8	35.2	4.4	3.4	-	1.7	0.5
Base	25.7	17.8	52.8	1.7	-	0.8	0.1
F	25.7	17.8	52.8	1.7	-	0.8	0.6

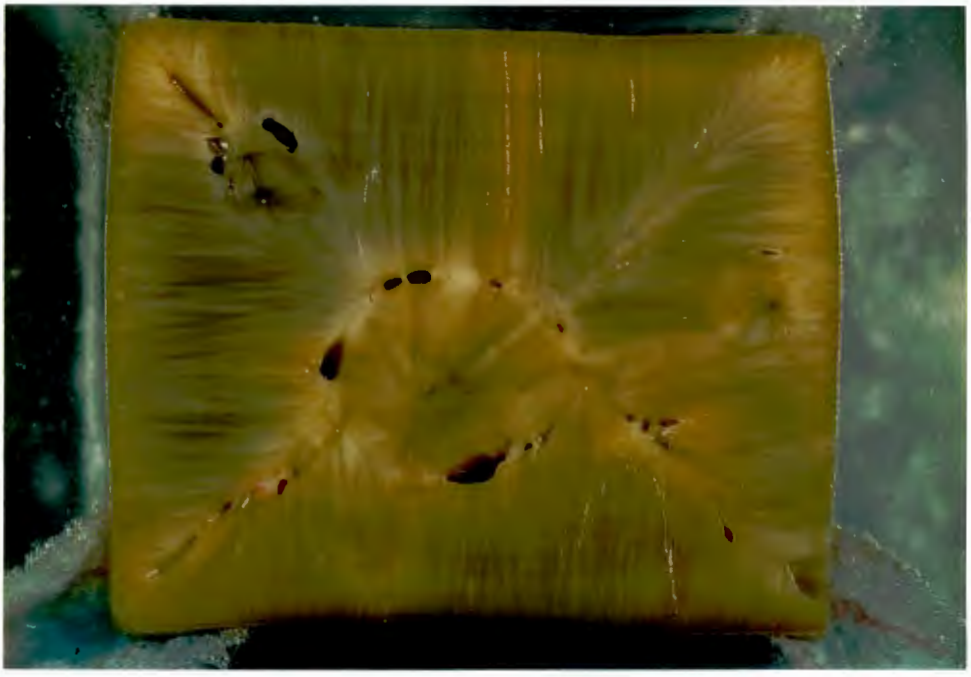

Figure 32: Polished section through Glass F, nucleated by addition of a P_2O_5, after crystallisation at 950°C for 6000 minutes.

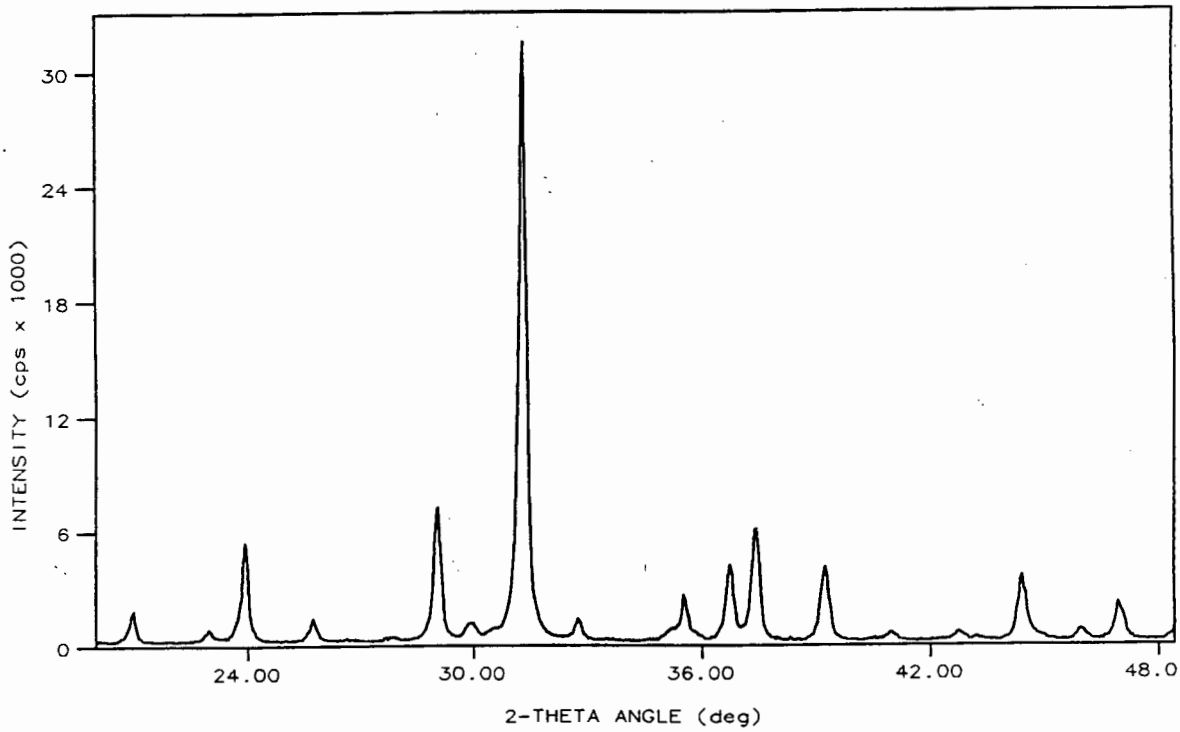

Figure 33: XRD spectrum of fully crystalline glass nucleated by P_2O_5 after heat treatment at 950°C for 6000 minutes.

5.4.1 Crystallisation of the glass

Heat treatment at 950°C resulted in surface crystallisation of the specimen (Figure 32). The resulting ceramic was less friable than the Base glass, but still had a microstructure strongly oriented along the direction of growth.

The crystallisation behavior of this glass is very similar to that of the Base glass. The crystalline phase forming is melilite, and the XRD spectrum is very similar to that of the Base glass (Figure 33). No evidence of a phosphate-containing phase was found. The glass crystallised by growth from the surface of the specimen toward the center. This results in a columnar microstructure, as in the Base glass. There is less porosity and cracking due to shrinkage, possibly due to the effect of P_2O_5 on the viscosity of the glass.

The rate of crystallisation is similar to that of the Base glass, as shown by Figure 34. Data obtained from the XRD spectra of the heat treated specimens was fitted to the Avrami equation, shown in Figure 35, and the values of the constants of the equation are given in Table 13. The value of the Avrami exponent (1.6) is similar to that of the Base glass, a result of the surface nucleation which occurs in both materials.

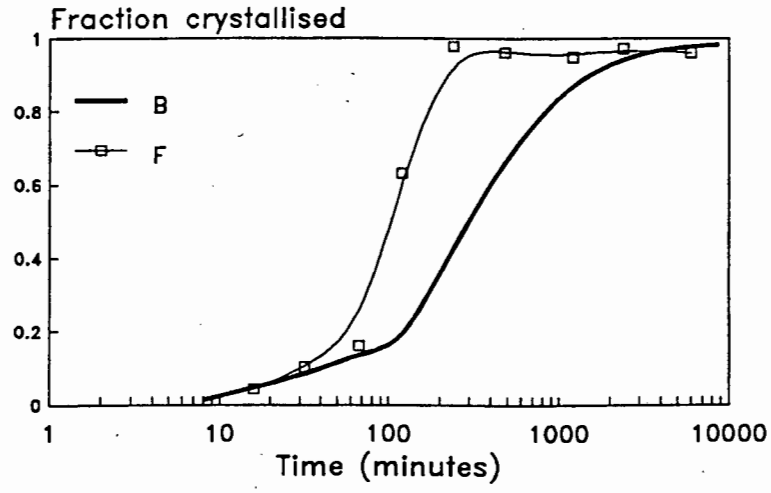

Figure 34: Rate of crystallisation of glass nucleated by P_2O_5, measured using XRD.

The rate of growth of the crystals, described by the rate constant of the Avrami equation (k), shows an apparent increase for the glass crystallised by P_2O_5 relative to the Base glass. No reports of the effect of P_2O_5 on the rate of growth of MCAS glass systems are available.

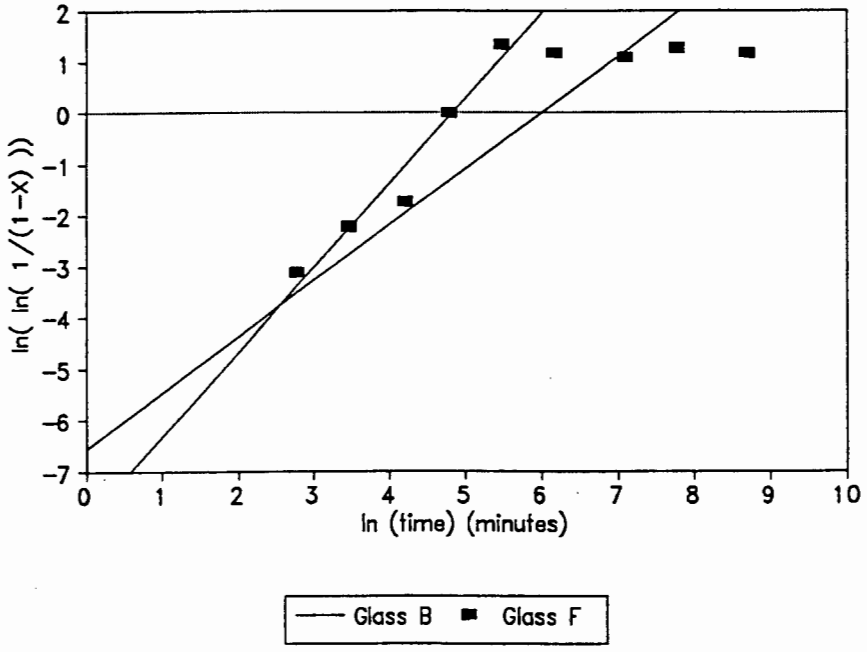

Figure 35: Avrami plot of glass nucleated using P_2O_5.

5.4.2 Microstructure

The microstructure of glass F, nucleated by the addition of P_2O_5, is very similar to that of the Base glass. Surface nucleation has resulted in a columnar microstructure oriented toward the centre of the specimen. A similar cellular growth mechanism is responsible for the oriented microstructure. Exsolution rims appear, exactly as for the Base glass, increasing in definition with the heat treatment time.

Table 13: Calculated constants for glass nucleated by P_2O_5.

Glass	Induction period (min)	Avrami exponent	ln K	MIL (micron)
B	60	1.09	-6.55	5.1
F	40	1.6	-8.00	5.5

The size of the lamellae in glasses B and F are very similar, and it is clear that the addition of 0.5% of P_2O_5 has only a small effect on the viscosity at the glass/ceramic interface of glass F. The size of the lamellae is largely controlled by the diffusion rate, and the growth rate, both of which are viscosity dependent terms (Christian, 1975).

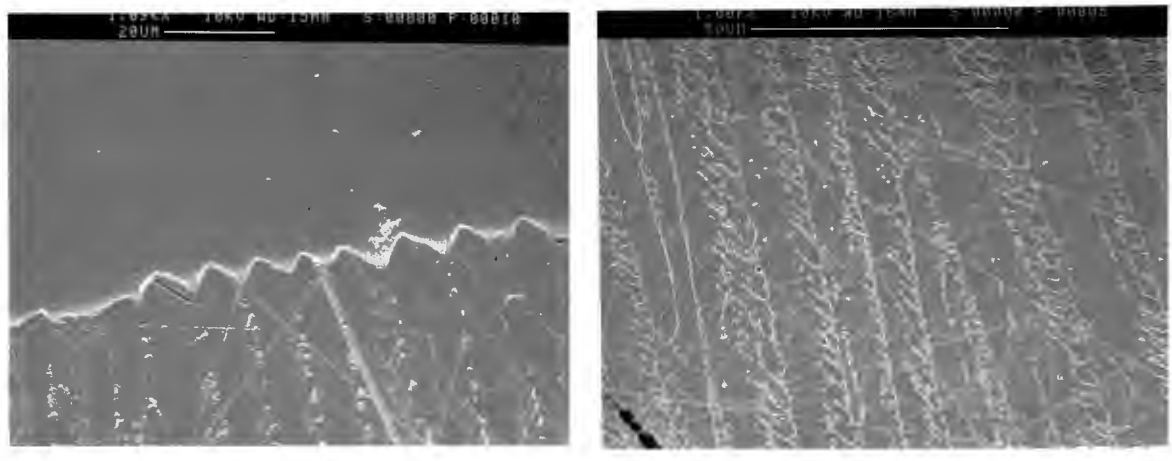

(a) 120 min (b) 6000 min

Figure 36: SEM micrographs of polished and etched sections through glass F, nucleated by P_2O_5

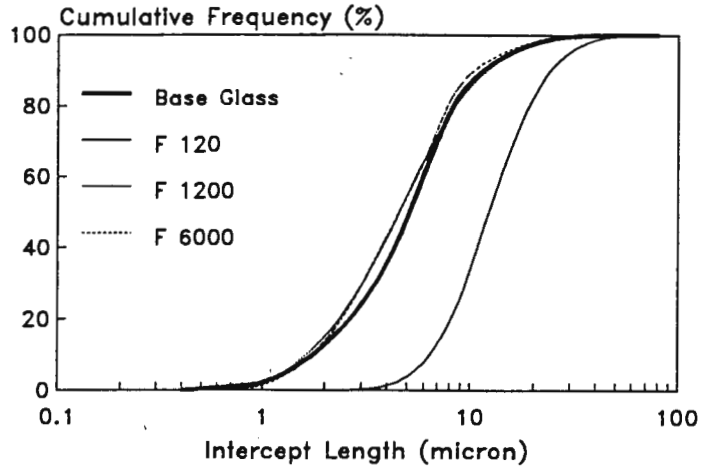

Figure 37: Intercept length distribution of glass F

SEM micrographs of the crystallisation of glass F are shown in Figure 36. The advancing crystal front, giving rise to the elongated crystals is shown in Figure 36(a), while Figure 36(b) shows the surface of the fully crystalline material. The morphology of the crystals is very similar to that of the Base glass, as are the crystal dimensions. The dimensions of the crystals are shown in Figure 37, the intercept length distribution.

5.5 Nucleation by mixed Iron and Chrome oxides (Glass D4)

The oxides of iron and chrome introduce finely disseminated nuclei in silicate melts. These oxides, commonly added as chromite (chrome ore), contain both iron and chrome oxides, and provide nuclei with a spinel structure. This structure, formed in crystals of the type $FeO.Fe_2O_3$ and $FeO.Cr_2O_3$, eases the crystallisation of the silicate phase due to their ability to induce epitaxial growth (Kirsch, 1989).

The nucleating ability of iron oxide is very sensitive to the Fe^{2+}/Fe^{3+} ratio, as this affects the number and size of the crystallites formed (Williamson, 1968). This is a significant factor in nucleation of glasses prepared using PFA as the unburned coal content of the PFA makes the glass very reducing and disrupts the ratio.

A glass melt was prepared to examine the ability of a combination of iron and chrome oxides to nucleate the glass produced from PFA. The glass specimens was prepared by adding equal weights of pure Fe_2O_3 and Cr_2O_3 to the PFA-$CaCO_3$ batch, and melting and cooling under standard conditions.

The compositions of the glass is given in Table 14, with the composition of the Base glass and the PFA provided for reference. The glass was extremely dark in colour, and prone to form a thin layer of crystals on the surface while cooling.

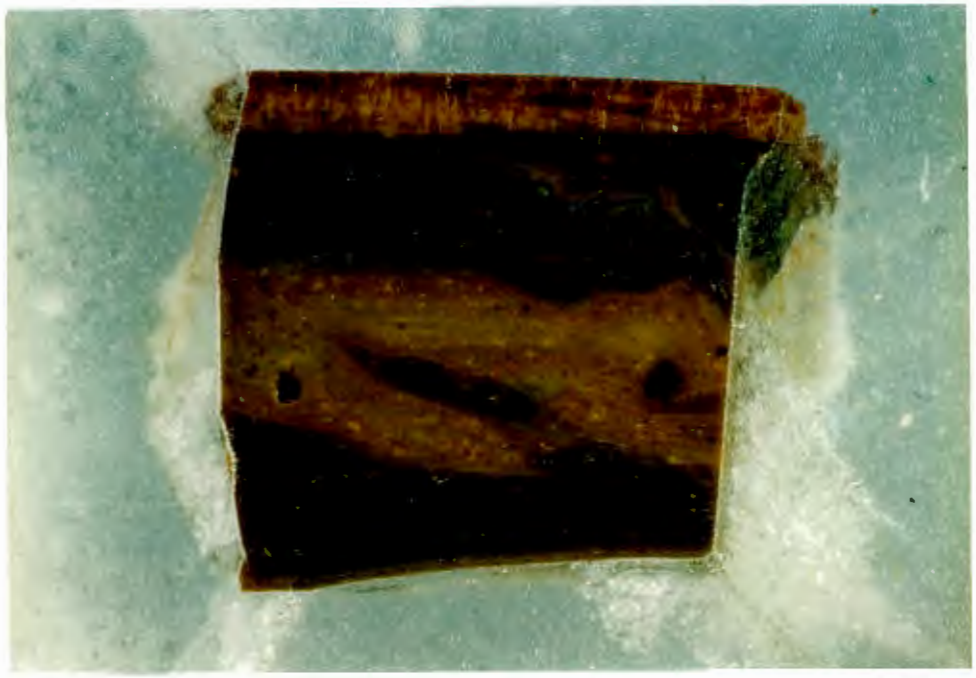

Figure 38: Glass D4, nucleated by addition of a mixed oxide nucleating agent, shown as a polished section after crystallisation.

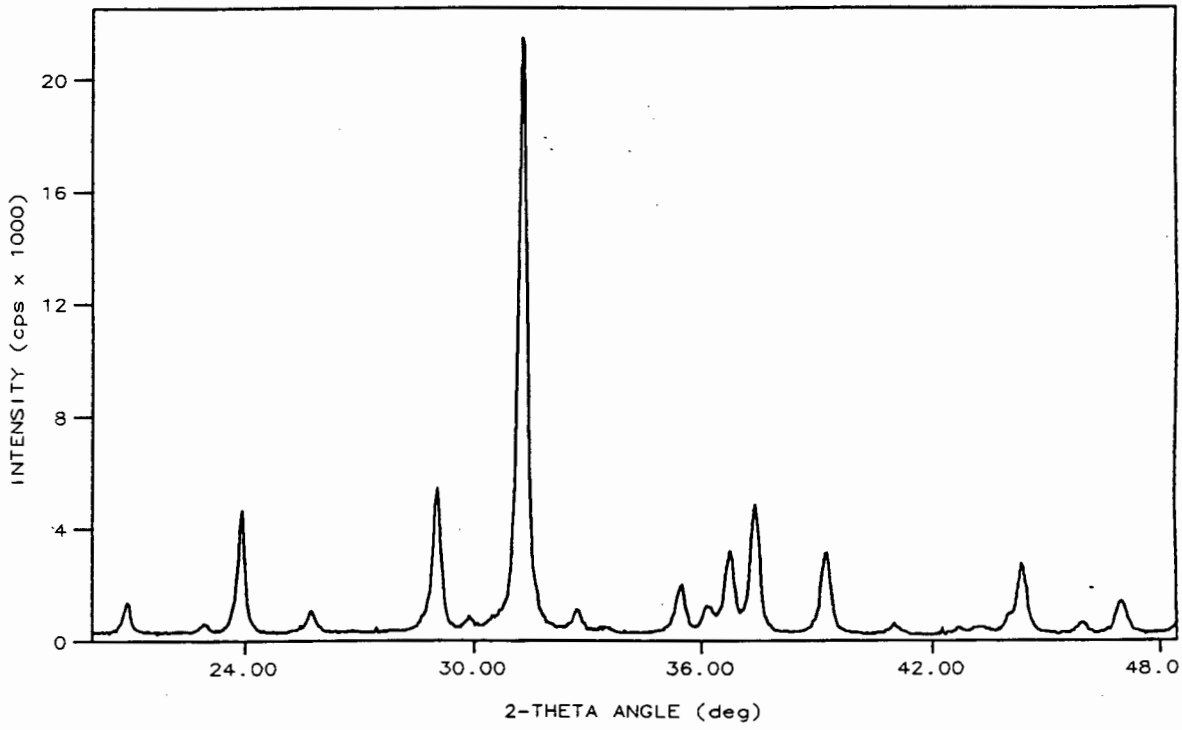

Figure 39: XRD spectrum of fully crystalline specimen D4 after heat treatment at 950°C for 6000 minutes.

Table 14: Nominal Composition of materials used to prepare glass D4 (mass percent)

	SiO_2	Al_2O_3	CaO	Fe_2O_3	Cr_2O_3	TiO_2	P_2O_5
PFA	50.8	35.2	4.4	3.4	-	1.7	0.5
Base	25.7	17.8	52.8	1.7	-	0.8	0.1
D4	24.4	17.0	50.2	4.0	2.4	0.8	0.1

5.5.1 Crystallisation of the glass

Crystallisation of the glass at 950°C produced a dark brown ceramic with no evidence of the columnar microstructure that dominates the microstructure of the Base glass (Figure 38).

Heat treatment of the glass at 950°C quickly produces a wholly crystalline material. The XRD spectrum of the material (Figure 39) shows a single phase identified as a member of the melilite solid solution series *cf* the Base glass (glass B). The addition of Cr_2O_3 and Fe_2O_3 does not produce a detectable crystalline phase, although the uncrystallised glass has low intensity peaks in the XRD spectrum at 36° and 44° 2-theta which do not correlate to peaks of the melilite solid solution. These unidentified peaks are present in the glass prior to any heat-treatment, and forms

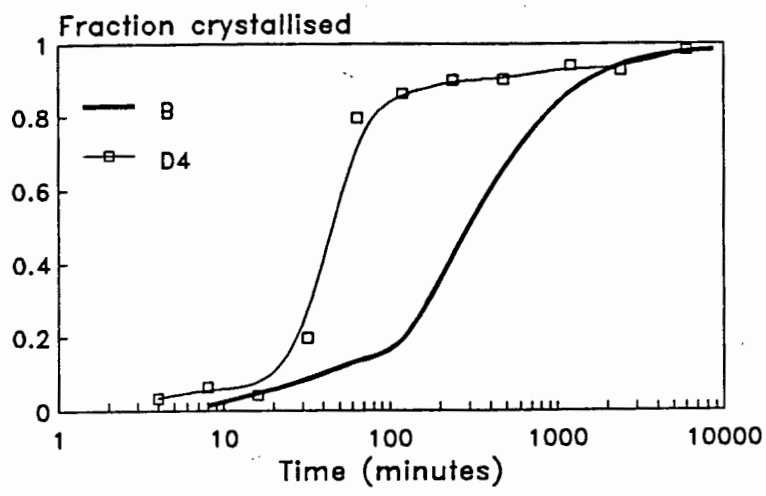

Figure 40: Rate of crystallisation of glass D4.

either as a result of reactions in the glass at high temperatures, or as a result of undissolved solids in the glass. This phase is present in very small amounts and the peaks are only just detectable in the spectrum of the fully crystalline material.
Crystallisation of glass D4 begins and ends sooner than any of the glasses in this study which crystallise with melilite as the only phase. Crystallisation is essentially complete after 60 minutes of heat treatment at 950°C (Figure 40). The rapidity of the crystallisation is attributed the same factors as the glass nucleated by TiO_2, *viz.* an increase in the number of nucleation sites and a decrease in the viscosity of the melt.

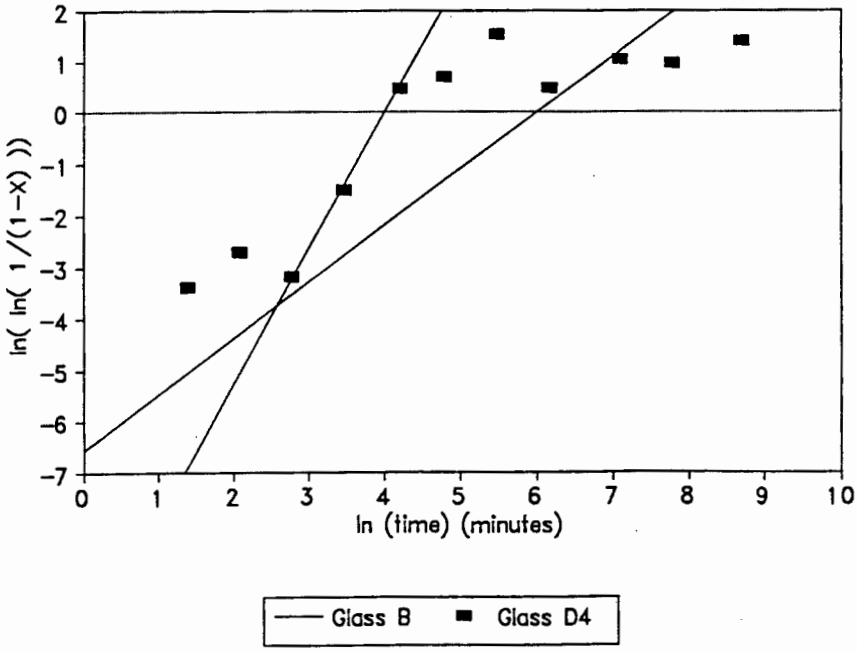

Figure 41: Avrami plot for glass D4.

Davies (1976) showed that the addition of iron oxides to a MCAS glass decreases the viscosity of the glass at 950°C, with a commensurate increase in the rate of crystal growth. This effect is evident in the large value of the crystallisation constant (Table 15).

The increase in the rate of crystallisation of the sample is also due to the change from one-dimensional surface nucleated growth to bulk nucleated, three-dimensional growth. The Avrami expression ($X = 1 - \exp(-kt^n)$) was fitted to the crystallisation data obtained from the XRD spectra of the heat treated specimens of glass D4, and this plot is shown in Figure 41. The Avrami exponent (n) for the crystallisation of this glass has increased to a value of about 3, reflecting the three-dimensional growth of the grains in the material. This is a considerable change from the surface nucleated growth of the Base glass.

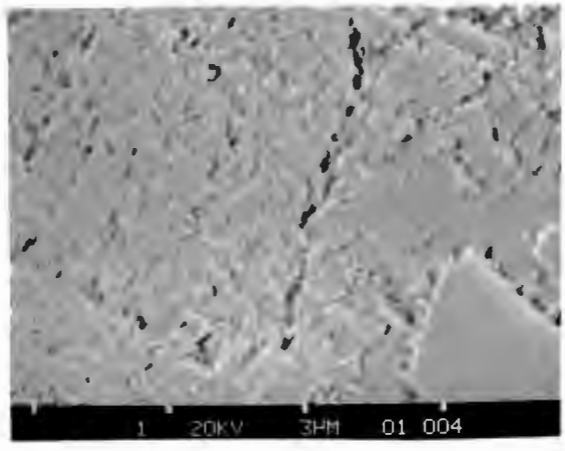

(a) 120 mins

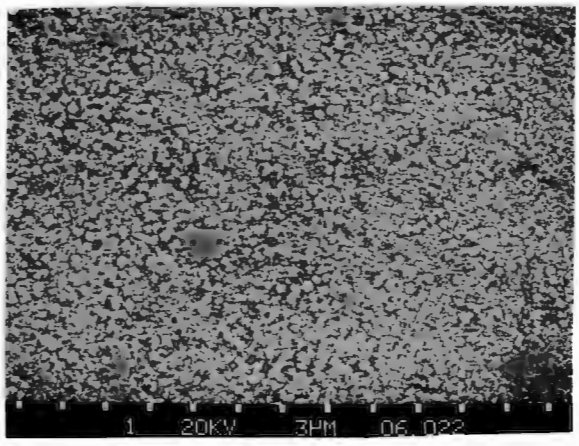

(b) 1200 mins

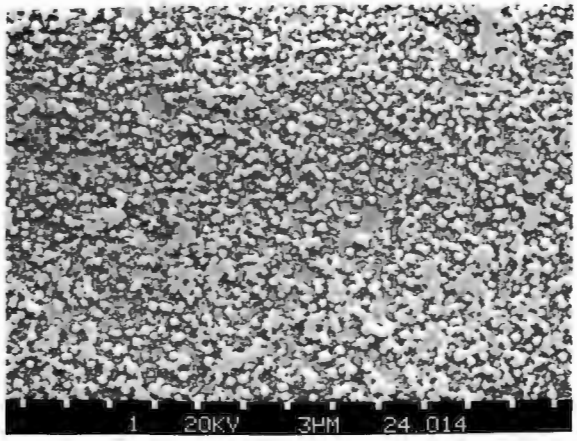

(c) 6000 mins

Figure 42: SEM micrographs of specimen D4 after heat treatment at 950°C.

Table 15: Measured crystallisation parameters for glass D4

Glass	Induction period (min)	Avrami exponent	ln K	MIL (micron)
B	60	1.09	-6.55	5.1
D4	20	2.6	-10.25	0.4

5.5.2 Microstructure

The microstructure of the crystalline material is considerably altered. Figure 42 shows SEM micrographs of polished and etched sections of the crystalline material after 120, 1200, and 6000 minutes of heat treatment at 950°C.

Examination of the microstructure showed the small size of the grains, a consequence of the large number of sites available for growth and the restrictions on crystal growth imposed by the proximity of the surrounding sites. The number of growth sites had increased as a result of the addition of the nucleating agent

The microstructure consists of small crystals which have apparently grown out of a surrounding matrix. Since there is no detectable second phase in the XRD spectrum of the material, the matrix cannot be of a different composition and differences revealed by etching are possibly due to segregation of elements to grain boundaries in a process analogous to the creation of impurity rims in the Base glass.

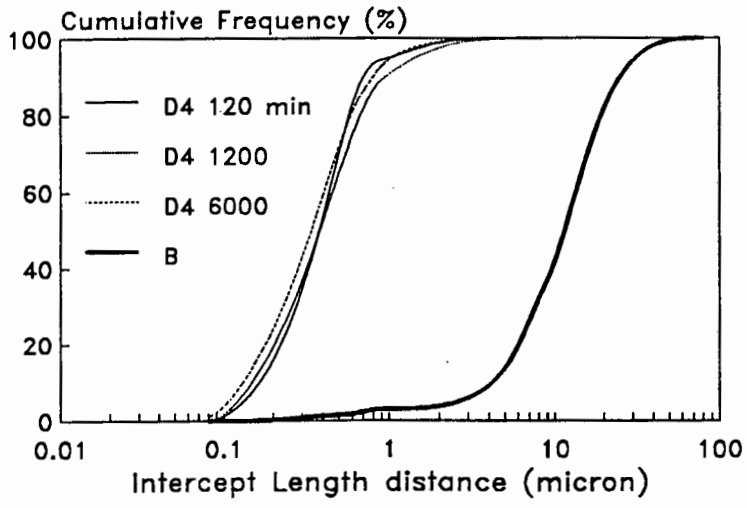

Figure 43: Grain size distribution for the crystallised material nucleated by iron and chrome oxides.

The intercept length distribution is smaller than the Base glass, the average value being almost two orders of magnitude smaller (see Table 15). This is due to the generation of many sites for growth in the glass as a result of the addition of the mixture of iron and chrome oxides.

Secondary grain growth in the material is essentially non-existent. The intercept length distribution after heat treatment for 6000 minutes is unchanged from that at 120 minutes (Figure 43). This is a consequence of the impurities which concentrate at grain boundaries and which act to pin the boundaries in place.

5.6 Nucleation by Titanium Dioxide and Phosphorous Pentoxide (Glass E2)

The combination of TiO_2 and P_2O_5 successfully nucleates some glass ceramics prepared from industrial by-products (Pavlushkin, 1982). Very little information is available on the means by which this combination of oxides is able to provide nuclei in the glass.

Table 16: Nominal Composition of batch used to prepare glass E2 (mass percent)

	SiO_2	Al_2O_3	CaO	Fe_2O_3	Cr_2O_3	TiO_2	P_2O_5
PFA	50.8	35.2	4.4	3.4	-	1.7	0.5
Base	25.7	17.8	52.8	1.7	-	0.8	0.1
E2	23.2	16.1	47.7	1.6	-	9.9	0.6

A glass containing 10% of TiO_2 and 0.5% of P_2O_5 by mass was prepared using standard methods. The glass was physically similar to the Base glass, and had no detectable crystalline phase in the as-cast glass.

5.6.1 Crystallisation of the glass

The glass crystallised by growth on nuclei distributed throughout the bulk of the

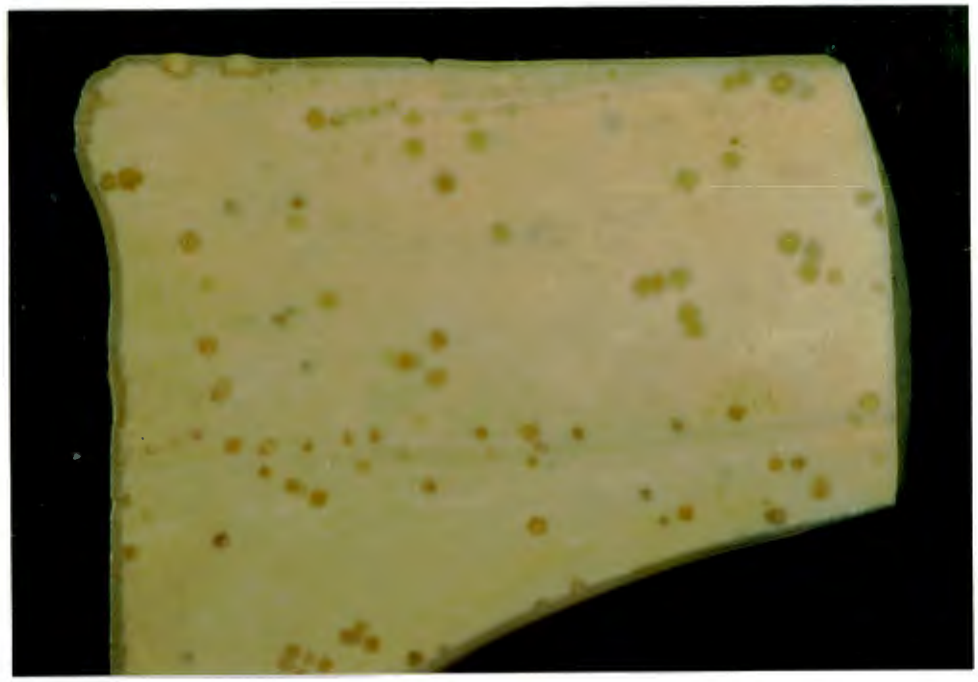

Figure 44: Polished section through glass E2 nucleated by TiO_2 and P_2O_5, after 6000 minutes of heat treatment at 950°C.

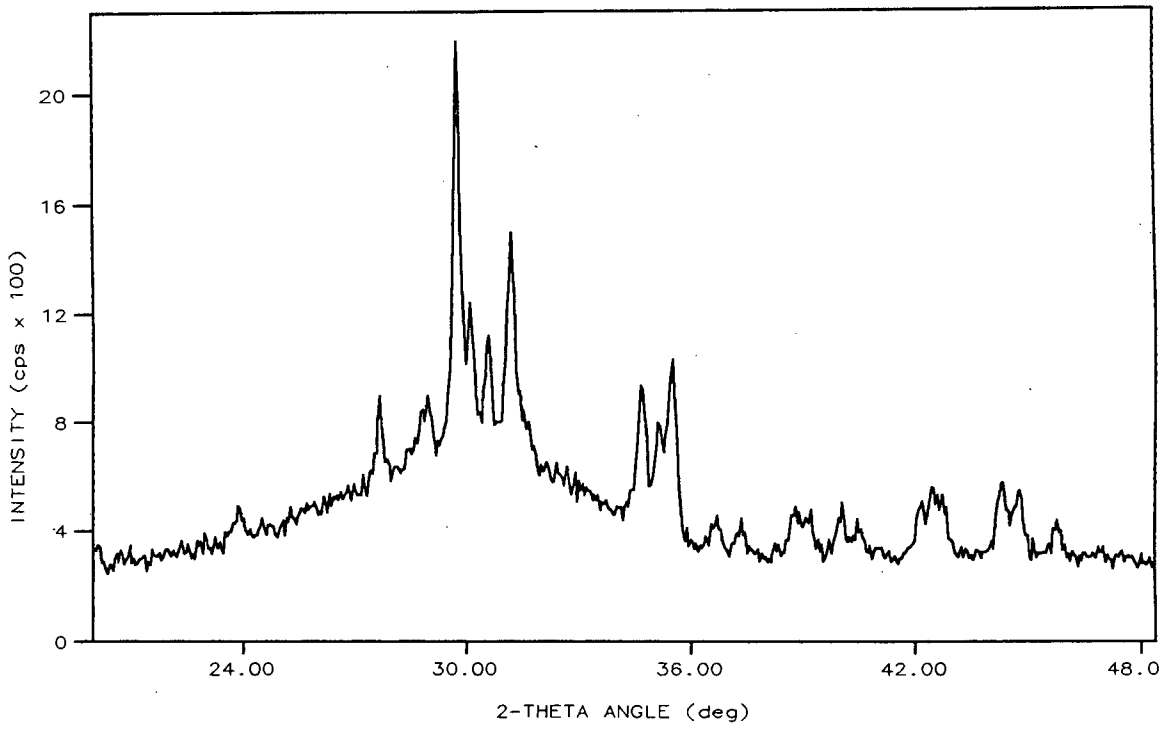

Figure 45: XRD spectrum of ceramic nucleated by TiO_2 and P_2O_5 after 32 minutes at 950°C.

specimen to give a fine-grained ceramic with little porosity and few shrinkage cracks. The majority of crystals grow as subhedral crystals, resulting in a material with small, equiaxed grains throughout. Figure 44 shows a micrograph of a polished section through the material taken using a stereo-microscope. A small number of spherulites are evident, as is the fine-grained nature of the matrix. The small spherical regions evident in the photograph do not differ in their microstructure from the surrounding matrix, and their origin is not known.

The material crystallises to give two phases. The initial crystalline phase detected is diopside ($Ca(Mg,Fe)[Si_2O_6]$), which appears after some thirty minutes of heat treatment at 950°C, accompanied by a small amount of melilite with a composition of near G_{50}/A_{50}. Figure 45 shows the XRD spectrum of the material at this stage. Diopside and melilite continue to form as the heat treatment proceeds, until at about 120 minutes the diopside disappears. This is accompanied by a rapid increase in the melilite content, and the appearance of a second phase identified as titanian-fassaite. (Figure 46)

The diopside phase is the first to form, but decomposes to give the equilibrium phase (melilite). Neither diopside or melilite is able to accommodate Ti^{4+} in the lattice, and the buildup of TiO_2 in the residual glass may be a factor in the decomposition. The decomposition coincides with the appearance of a TiO_2 containing phase, titan-augite or titanian fassaite. This sequence is shown in Figure 47, which shows the

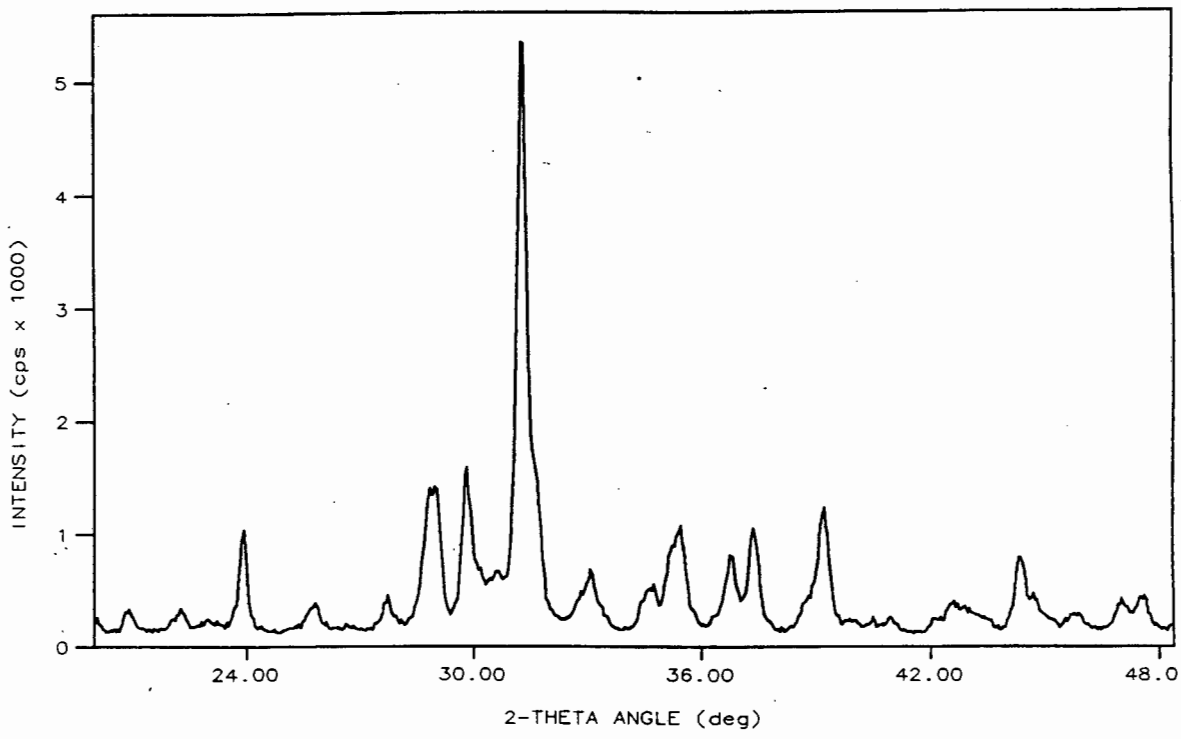

Figure 46: XRD specimen of glass nucleated by P_2O_5 and TiO_2 after 6000 minutes of heat treatment at 950°C.

change in the peak height of the phases present in the glass during the crystallisation process.

The distinction between diopside and fassiate is largely artificial, as both are clinopyroxenes existing in a solid solution series. However, diopside does not accept Ti^{4+} into the lattice as augite (fassaite) does. On this basis it is proposed that the diopside changes to a new phase by a combination of decomposition to melilite and reaction with TiO_2 to produce a TiO_2-bearing phase.

The unusual sequence of events in the crystallisation of this glass occurs only in the glass which has P_2O_5 added. Rogers (1969) found a similar sequence of crystallisation in a MCAS glass, where a metastable diopside phase was the first to form, and converted after extended heat treatment (15 hours) to melilite. The glasses prepared by Rogers are of a quite different composition, and contained iron oxides as the nucleating agent. Due to the difference in conditions under which the two glasses crystallised, the sequence of crystallisation cannot be definitely be ascribed to the presence of TiO_2 and P_2O_5 in the PFA-containing glass.

Nucleation by TiO_2 or P_2O_5 alone does not produce this sequence of events, and this may imply some interaction between the two oxides which favours the formation of diopside rather than the (equilibrium) melilite phase.

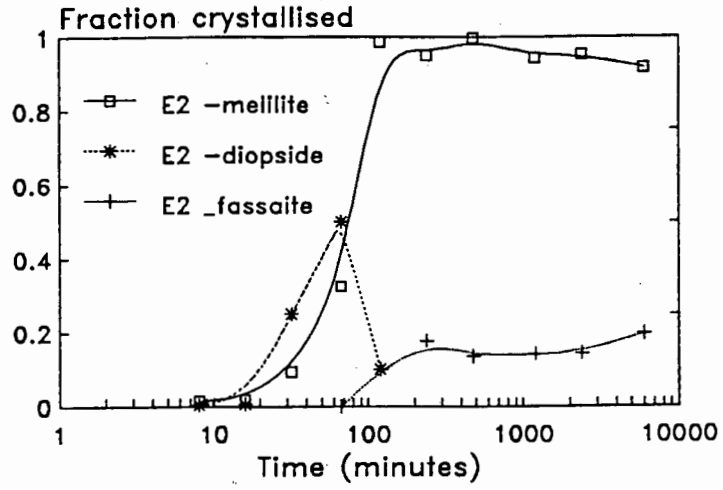

Figure 47: The sequence of the formation of the phases present during the crystallisation of glass E2 (axes not to scale)

5.6.2 Calculation of crystallisation rates

This two stage crystallisation process complicates the calculation of the rate constants, as growth may not be by the movement of an interface, and in this case the model used may have no physical significance. The following assumptions were made to relieve this difficulty. The diopside forms by an interfacial growth process, as it is the first phase to appear in the glass. The diopside later decomposes to give a melilite solid solution in a process that must involve a large degree of atomic rearrangement. This occurs by movement of an interface through the diopside, and can be represented by the interfacial growth model.

The calculated constants for the growth of melilite are shown in Table 47. The crystallisation of melilite is considerably more rapid than in the Base glass, and is very similar to that of glass T10, as seen in Figure 48. Crystallisation rates for diopside and fassaite were not measured, as too few data points were available. The sequence of formation of the phases is illustrated in Figure 47, which shows that the diopside is the first phase to form, but disappears abruptly as the melilite concentration increases. The calculated value of the Avrami exponent (n) for the growth of melilite again indicates a three-dimensional growth process, resulting from the formation of nuclei in the bulk of the glass. This data is shown in Figure 48.

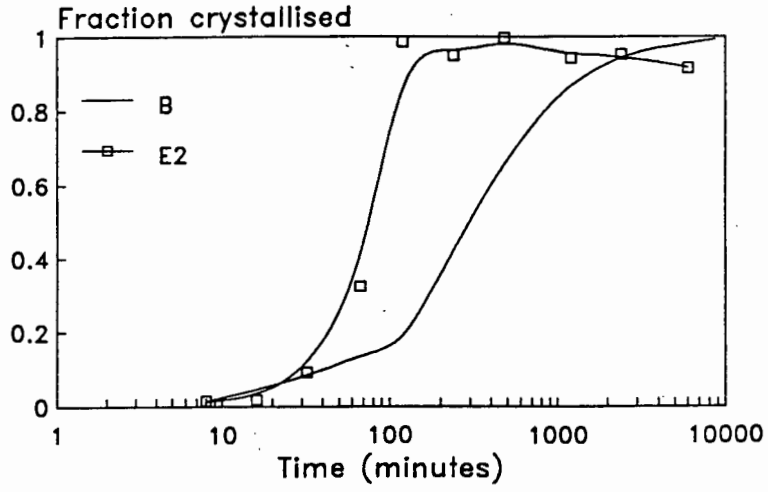

Figure 48: Rate of crystallisation of glass nucleated by P_2O_5 and TiO_2.

Table 17: Calculated constants for glass nucleated by P_2O_5 and TiO_2.

Glass	Induction period (min)	Avrami exponent	ln K	MIL (micron)
B	60	1.09	-6.55	5.1
E2	30	2.6	-11.4	5.9

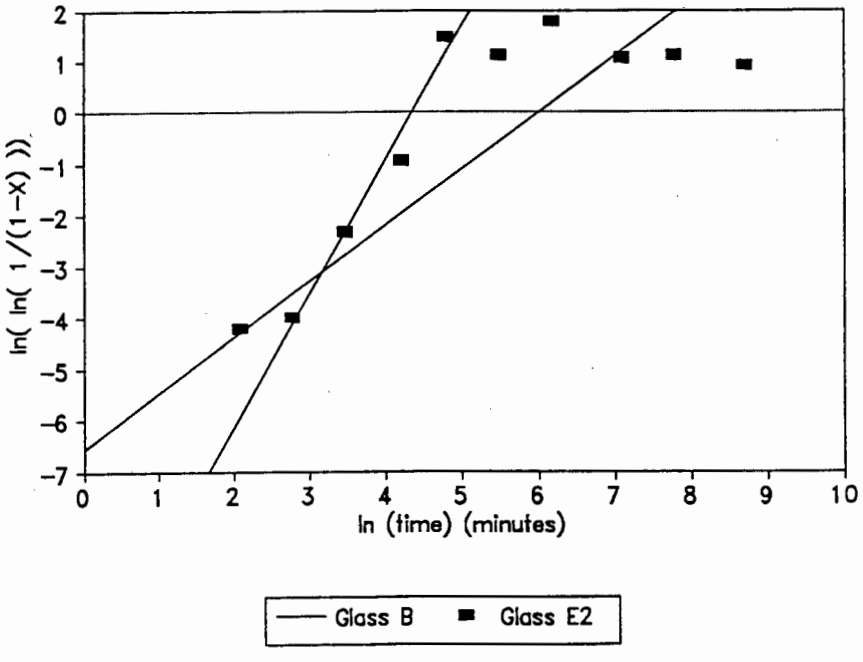

Figure 49: Avrami plot for glass nucleated by P_2O_5 and TiO_2.

5.6.3 Microstructure

The microstructure of the crystallised material consists of small equiaxed grains of the melilite solid solution surrounded by fassaite. SEM micrographs of polished and etched specimens of the glass at various stages of the heat treatment process are shown in Figure 50. The microstructure is very different to that of the other glasses prepared, and this is attributed to the two stage crystallisation of the material. As stated earlier, it is believed that the diopside forms, and then transforms, leading to the segregation of elements, and resulting in the formation of the TiO_2-bearing fassaite phase.

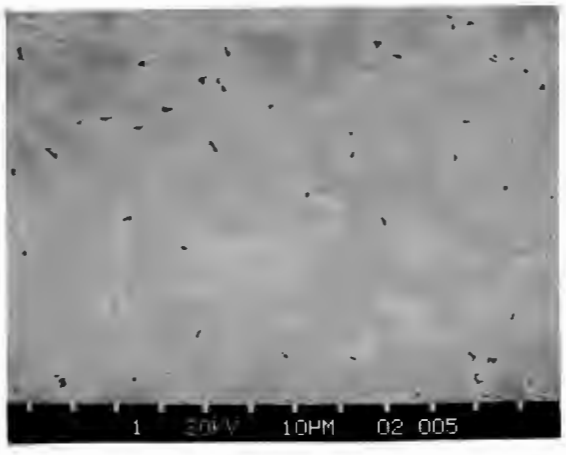

(a) 120 minutes

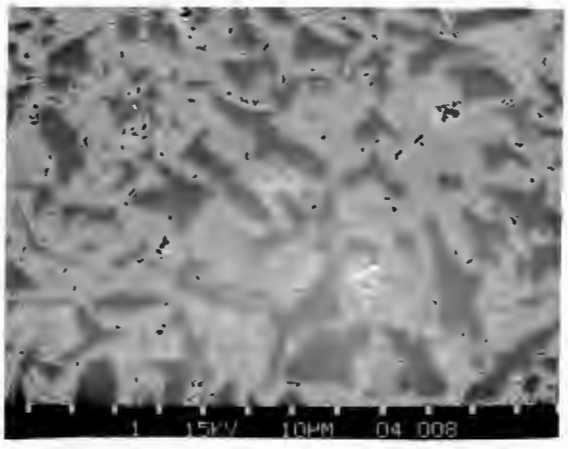

(b) 1200 minutes

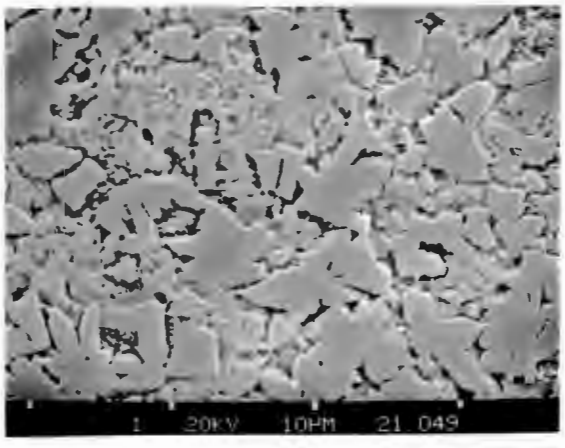

(c) 6000 minutes

Figure 50: SEM micrographs of polished and etched sections of the glass nucleated by TiO_2 and P_2O_5.

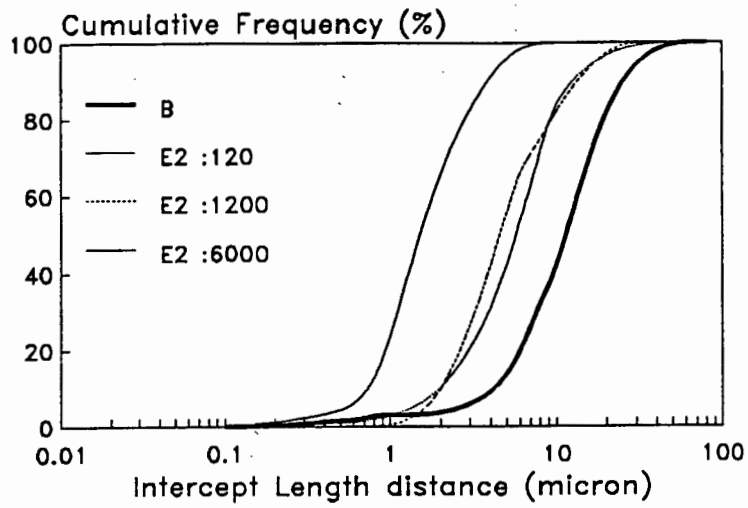

Figure 51: The intercept length distribution of the ceramic prepared from a glass nucleated by P_2O_5 and TiO_2, showing the variation with length of heat treatment.

The microstructure is consistent through the material, and there is no evidence of orientation of the grains. The average grain size of the material is smaller than that of the ceramic prepared from the Base glass (ceramic B). The grain size distribution is narrow (Figure 51), with few large grains, while the porosity is negligible. The material shows a tendency for the average grain size to decrease with heating. This may be due to changes in the melilite/fassaite ratio.

5.7 Erosion resistance of the Glass Ceramics

To asses the wear resistance of the materials, machined specimens were subjected to controlled erosion by air-blown particles (See Appendix 8.4). A number of materials, selected from a range of materials commonly used as wear-resistant surfaces, were tested to establish their erosion resistance relative to that of the materials prepared in this study. These are listed in Table 18, along with their measured erosion resistance, calculated relative to that of the least resistant material, Cast Basalt.

Table 18: Identification of materials tested

NAME	MATERIAL	RELATIVE EROSION RESISTANCE (ex CB)
SC	Silceram	1.615
DX	Deranox (97.5% Alumina)	3.602
MOH9	97% Alumina	2.401
C2	Coors (85% Alumina)	2.798
DID	Didier (98% Alumina)	3.367
CB	Cast Basalt	1.000
DGC1	Glass ceramic #1 prepared from PFA by commercial concern	1.322
DGC2	Glass ceramic #2 prepared from PFA by commercial concern	2.126
B	Base glass prepared using PFA	1.193
F	PFA glass containing 2% of TiO_2	1.266
T2	PFA glass containing 0.5% of P_2O_5	1.790
T10	PFA glass containing 10% of TiO_2	2.400
D4	PFA glass containing 5% of iron and chrome oxide	1.661
E2	PFA glass containing 10% of TiO_2 and 0.5% of P_2O_5.	1.745

The relative erosion resistance of these materials is plotted in Figure 52. The Cast Basalt is the least resistant of the materials tested, due largely to the high porosity of

the material as well as the low degree of crystallinity. The alumina materials are the most resistant, as would be expected due to their high hardness and small grain size.

The materials prepared using PFA show a wide variation in their erosion resistance. The materials which have crystallised by surface nucleation have the lowest erosion resistance, due largely to the large-grained, oriented microstructure which results in shrinkage cracks and low fracture toughness. The addition of nucleating agents to the glass can improve the erosion resistance considerably. This is attributed largely to an increase in fracture toughness as it is unlikely that the relatively small additions to the glass will affect the hardness of the glass ceramics to any large extent.

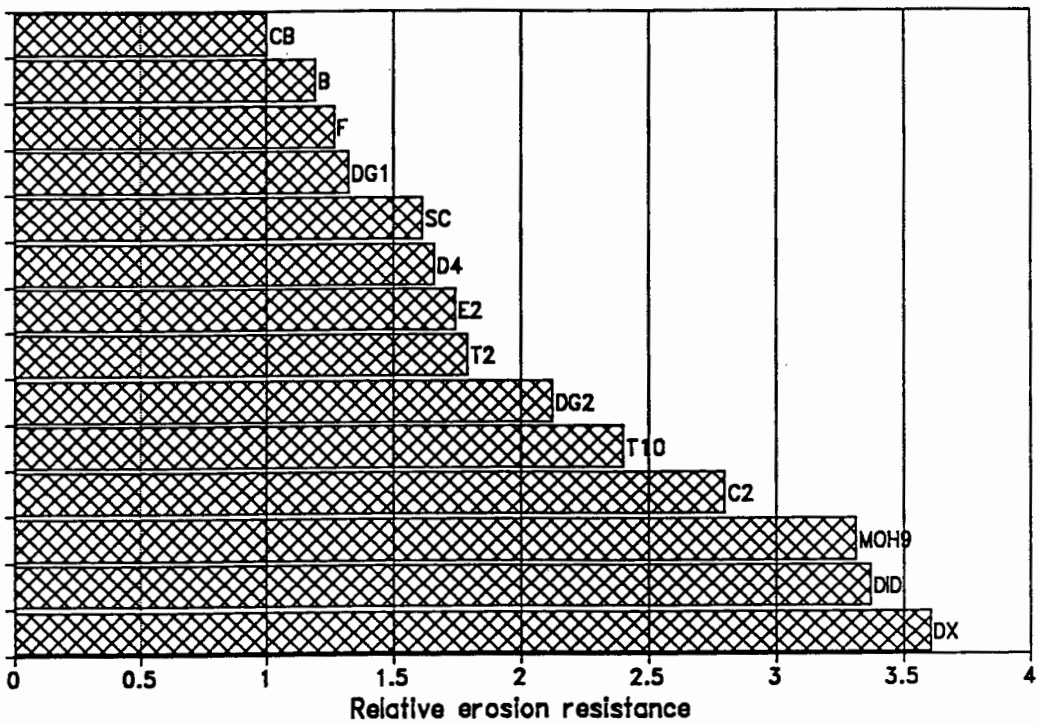

Figure 52: Graphical illustration of the relative erosion resistance of the materials tested.

The high erosion resistance of the PFA-based materials with a two-phase microstructure (specimens T2, T10 and E2) is particularly noticeable. Such materials are more resistant to the passage of cracks than are single phase materials, possibly due to stresses that build up at phase boundaries as a result of differences in thermal expansion coefficients between the phases (Rice, 1977). This results in an increase in the fracture toughness of the material.

The grain size of the material affects the wear resistance of the material due to a similar effect. An example of this is the difference in erosion resistance between ceramics B and D4, both with a similar composition and consisting of only a single phase. There is a large difference in the average grain size of the material, as seen in

Figure 43. This results in an increase in the wear resistance of the material, as the crack path becomes more tortuous.

This effect, combined with thermally induced interfacial stresses, makes ceramic T10 more wear resistant than ceramic T2. Increasing the proportion of second phase (as the TiO_2 content increases) will increase the degree of stress between the phases, acting to increase the fracture toughness. The increase in wear resistance that occurs when a second phase is introduced into the ceramic produced from PFA material do not stem from an increase in the hardness the material, as the fassaite phase has a similar hardness to the melilite (Deer, 1964).

6. DISCUSSION

The PFA from the Lethabo power station is refractory, but forms a glass when mixed with calcite, which provides CaO as a fluxing agent. This glass, referred to in this study as the Base glass, melted easily at 1550°C to give a stable glass which reacts only moderately with the crucible. The short working range and the high softening temperature of the glass makes it very suitable for conversion to a ceramic, as deformation during crystallisation will be negligible.

6.1 Crystalline Phases in the Base glass

The Base glass is very high in CaO and devitrified to give a calcium alumino-silicate material, melilite. Melilite is a Ca-Mg solid solution with gehlenite and Åkermanite as the respective end members. Pure gehlenite ($Ca_2[Al_2SiO_7]$) does not form when the glass is crystallised, due to the MgO contained within both the PFA and the calcite. It is likely that there is between one and two percent of MgO in the glass, and the melilite phase forms with a composition between G_{100} and G_{75}/A_{25}. According to the JCPDS data, G_{75}/A_{25} requires only 3% of MgO in the lattice.

In the glasses prepared in this study which crystallise to give only one phase, the composition of that phase is close to G_{75}/A_{25}. The materials which crystallise to give two phases show a shift in the composition of the melilite phase, nearer to G_{50}/A_{50}. The second phase present in the fully crystalline specimens containing two phases was identified as a pyroxene group mineral known as titan-augite, or more specifically titanian-fassaite. The shift in composition of the melilite phase implies that the second phase contains little Mg^{2+}, which agrees with the description of fassaite given by Deer (1964). Fassaite is formed by the substitution of [Si,Al] for [Mg,Si] in pyroxene materials, and is always low in Mg^{2+}.

The mechanical properties of the crystalline phase formed on crystallisation will influence the properties of the crystalline specimen, regardless of the influence of the microstructure of the material. Factors such as the ease of cleavage and the hardness of the individual crystals may have a large effect on the properties of the specimen as a whole. Melilite is a ring silicate, consisting of $[MgO_4]^{6-}$, $[SiO_4]^{4-}$ and $[AlO_4]^{5-}$ tetrahedra arranged in layers, which are joined by Ca-O linkages. Such a structure has planes of weakness, and will not be a tough material. Improved mechanical properties can be found in glasses with SiO_2 and Al_2O_3 contents high enough for the glass to crystallise as a chain silicate, such as wollastonite or diopside.

6.2 Devitrification of the Base glass

The Base glass, containing only PFA and CaO, devitrified by growth of crystals from the surface, resulting in an oriented microstructure and poor mechanical properties despite the presence of oxides known to act as nucleating agents from the PFA. As received, the PFA contains significant quantities of titanium and iron oxides, but they do not act as nucleating agents in the Base glass, despite the large amount of literature indicating that they could be expected to do so.

There are several possible reasons for the poor nucleation of the Base glass by the entrained oxides. The concentration of the species may be too low to be effective, or the process of producing the glass may result in segregation of these species to give large crystalline assemblages which are not able to act as nuclei, or loss of these oxides by volatilisation during the manufacture of the glass is possible. The most plausible explanation is that reduction of these oxides occurs, resulting in ions that do not form suitable nuclei on heat treatment.

The reduction of the oxides in the PFA in the glass to a lower oxidation state will affect the ability of these oxides to nucleate the glass. McMillan (1979) notes that titanium is unable to nucleate silicate glass ceramics, when reduced from Ti^{4+} to Ti^{2+}. Similarly Williamson (1969) found that glass specimens containing only ferrous ions (Fe^{2+}) crystallised from the surface, with bulk nucleation occurring only when the glass contained large proportions of ferric ion (Fe^{3+}).

The analysis of the Lethabo PFA by Willis (1987) showed that the material contained 2,25% of uncombusted organic material, referred to as the unburned carbon content. At elevated temperatures carbon is an extremely effective reducing agent and the TiO_2 and Fe_2O_3 contained in the PFA may be converted to lower oxidation states by reactions similar to the following:

$$2TiO_2 + C \rightarrow 2TiO + CO_2$$
$$2Fe_2O_3 + C \rightarrow 4FeO + CO_2$$

A brief calculation based on the stochiometry of the above reactions shows that there is sufficient unburned coal in the PFA for the complete reduction of the potential nucleating agents contained within the PFA by the carbon (3.4% of Fe_2O_3 and 1.7% of TiO_2). It is therefore necessary to add extra nucleating agents to the glass in quantities too large for complete reduction to occur.

The root of the problem is the carbon content of the PFA, and the problem may be alleviated by oxidation of the carbon prior to melting the batch. This could be done by calcining the PFA at about 800°C in an oxidising atmosphere, either before or

after mixing with the other oxides. Alternatively, addition of an oxidising agent to the batch and holding the glass at high temperatures for a sufficient length of time will ensure complete oxidation of the carbon in the glass.

6.3 Controlled nucleation of the glass

To control the crystallisation behaviour of the glass, a series of glass specimens were prepared by adding oxides to the glass batch prior to melting. These oxides, selected by reference to the literature for their known ability to nucleate crystallisation in glass ceramics, were:

Oxide	Amount	Glass
Titanium Dioxide (TiO_2)	10% and 2%	T10, T2
Phosphorous Pentoxide (P_2O_5)	0.5%	F
Iron and chrome oxides	5%	D4
TiO_2 + P_2O_5	10% + 0.5%	E2

The nominal composition of the glass batches prepared for these glasses is shown in Table 19.

Table 19: Nominal batch composition of glasses prepared using PFA

	SiO_2	Al_2O_3	CaO	Fe_2O_3	Cr_2O_3	TiO_2	P_2O_5
PFA	50.8	35.2	4.4	3.4	-	1.7	0.5
Base	25.7	17.8	52.8	1.7	-	0.8	0.1
T2	25.4	17.6	52.2	1.7	-	1.8	0.1
BT	23.3	16.2	47.9	1.6	-	10.0	0.1
D4	24.4	17.0	50.2	4.0	2.4	0.8	0.1
E2	23.2	16.1	47.7	1.6	-	9.9	0.6
F	25.7	17.8	52.8	1.7	-	0.8	0.6

The formation of nuclei following the addition of oxides to a glass is presumed to occur by growth of small crystallites which have a high degree of lattice registry with the major crystal phase. Epitaxial growth of the major phase on these crystallites reduces the thermodynamic barrier to nucleation, enabling nucleation on a large number of sites. In TiO_2-nucleated systems, these crystallites are of the form $RO.TiO_2$, where RO is commonly MgO or FeO, while in iron or chrome oxide nucleated systems nucleation occurs by the formation of chromite species such as $FeCr_2O_4$.

The PFA based glasses contain sufficient MgO and Fe_2O_3 for the formation of such titanite and spinel species. Crystallites which act as nuclei need to be very small to

provide suitable sites for the nucleation of a second species and the overall volume fraction of such nucleating species will in the glass be very low. Unfortunately, the techniques generally used for phase analysis (XRD and SEM) do not permit the detection of phases present in such low concentrations.

6.4 The microstructure of the crystallised glass

The glasses prepared using PFA could be divided into two broad groups: those which devitrified by growth from the surface of the specimen and those which crystallised via growth on nuclei in the bulk of the sample. Glasses which devitrify from the surface of the specimen rely on solid/air interfaces to provide sites from which growth can begin and this results in the growth of a relatively small number of large and highly orientated crystals toward the center of the specimen. Those glasses where growth begins on a large number of sites dispersed throughout the glass are said to be bulk-nucleated and have a fine-grained microstructure. Thus the addition of metal oxides able to act as nucleating agents converts the coarse grained, oriented microstructure of the surface nucleated specimens to a more fine-grained material.

It is difficult to get a meaningful measurement of grain size on the materials which have oriented microstructures, as the crystals may be up to 1000 microns in length, and only 4 - 5 microns wide. This is the case where the glasses devitrify by growth from nuclei on the sample surface, as well as those glasses which crystallise with a spherulitic morphology. To provide a basis for comparison among the diverse microstructures, measurements were made perpendicular to the direction of growth as this gives the smallest grain size for the material (a best-case measurement). This measurement was not able to discriminate between the glasses crystallised by surface nucleation and those which grew from nuclei in the bulk of the specimen. It is clear from the micrographs that there is a large difference in the shape of the crystals, but this is not reflected in the digitised values.

The glasses doped with titanium dioxide crystallised by spherulitic growth on a relatively small number of nuclei in the bulk of the glass. Spherulitic morphology often results during crystallisation of glasses and this mechanism has been attributed to the presence of impurities in the glass/ceramic interface. This type of growth is commonly found in glasses with slow diffusion and low growth rates (Keith, 1963). The analysis of the Lethabo PFA by Willis (1987) shows that the PFA contains small concentrations of a number of different ionic species which can not be included in the melilite lattice, and can thus be considered as impurities in the glass. Spherulitic growth of crystals in the Base glass might therefore be anticipated, but is not found. The composition of the crystal phase is very similar to that of the glass, requiring little diffusion for the glass to crystallise, conditions which do not promote the formation of

spherulites. Conversely, the TiO_2 containing glasses separate into two phases on crystallisation, a process which requires a great deal of diffusion, and the glasses are thus more prone to spherulitic growth. A similar effect was found by Hayward (1987) in glass ceramics designed for the entrapment of radioactive wastes (the so-called SYNROC material). These materials showed spherulitic growth when the glass contained less than 30% of waste materials.

Phosphorous pentoxide, when used on its own, is not an effective nucleating agent for the glasses prepared from PFA, but it has a large effect on the crystallisation of the glass containing TiO_2. Glasses T10 and E2, both containing 10% of TiO_2, crystallised with very different microstructures, with glass T10's spherulitic morphology contrasting strongly with the small, equiaxed crystals forming the matrix of glass E2, containing 0,5% of P_2O_5. It is likely that this change in the morphology of glass E2 is due to a change in the viscosity at the interface between the glass and the growing ceramic phase, due to rejection of P_2O_5 ahead of the silicate lattice. This would result in an increase in the rate of crystallisation of the phase, making the formation of spherulites unlikely.

The glass D4, nucleated by the addition of a mixture of iron and chrome oxides, crystallised by equiaxial growth of crystals in the bulk of the specimen. There was no evidence of spherulitic growth. Only a single phase crystallised, due to the similarity in composition between the glass and the crystalline phase, and only short range diffusion of the species is required. Keith (1963) has noted that diffusion limited growth is necessary for formation of a spherulitic morphology.

6.5 Crystallisation Kinetics

The efficacy of the oxides added as nucleating agents to nucleate the crystallistaion of the PFA containing glasses was compared by analysis of the kinetics of crystallisation, using the Avrami equation ($X = 1 - \exp(-kt^n)$). The efficiency of a nucleant was quantified by measuring its ability to change the mode of growth of a glass, indicated by exponent (n) of this equation. The provision of nuclei in the bulk of the glasses changes the mode of growth from the 1-dimensional surface nucleated growth found in the Base glass to growth on nuclei in the bulk of the sample, i.e. 3-dimensional growth.

The kinetic plots for the glass specimens are shown in Figure 53, and it is clear that there are two distinct groups of materials. Glasses B and F, without nucleating agents, and nucleated by 0,5% of P_2O_5 respectively, have low values of the exponent of the above equation ($n \simeq 1$), indicating that growth occurs almost entirely from the surface of the specimen (these figures are listed in Table 20). This is borne out by

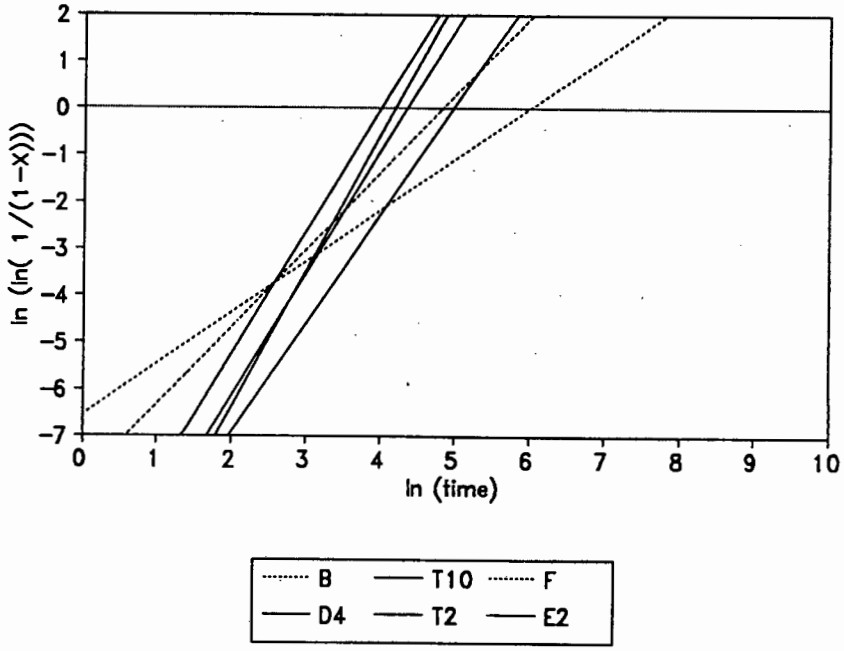

Figure 53: The Avrami Plots for all the glasses prepared using PFA

the microstructures of these materials, and it is clear that the nucleation efficiency in these materials is poor. The second group of specimens shows much higher values of the value of the exponent in the Avrami equation. Glasses T10, T2, D4 and E2 grow from nuclei formed in the bulk of the sample as a result of the addition of the oxides.

Table 20: Calculated parameters for crystallisation of glasses prepared from PFA

Glass	Induction period (min)	Avrami exponent	ln K	MIL (micron)
B	60	1.09	-6.55	5.1
T2	40	2.3	-11.6	3.3
T10	20	2.9	-12.2	4.6
D4	20	2.6	-10.25	0.4
F	40	1.6	-8.00	5.5
E2	30	2.6	-11.4	5.9

It may be noted that the measured values of n for the bulk nucleated materials lie in a cluster between 2.5 and 3, while the theoretical value is for unobstructed growth on nuclei is 3. It is suggested that this discepancy is due to experimental error. The glass specimens crystallised so rapidly that only a few (three or four) heat treatments provided data suiable for analysis. Only data points obtained while the crystals are growing should be used, and any data points which are slightly off the growth curve will reduce the calculated value of the exponent.

The value of the rate constant (k) is a strong indicator of the overall rate of crystallisation of the sample and it is again clear that two groups of materials exist. Those glasses which are surface nucleated (glasses B and F), have slow growth rates,

while the bulk nucleated glasses (T2, T10, D4, E2) have rapid growth rates (see Table 20). The difference in the rate of growth is dramatic, and the time taken for complete crystallisation is much reduced, from 1200 minutes for glass B, to about 80 minutes for glass T10.

6.6 Erosion Resistance

There is, in general, a correlation between the grain size of the materials and their erosion resistance. A trend to higher erosion resistance as the measured mean intercept length of the crystallised glasses decreases is visible (Figure 54). Clearly, the relationship between the erosion resistance and the microstructure is more complex than a simple grain size dependence. Wiederhorn (1983) pointed out that the erosion resistance is also affected by the hardness and fracture toughness of the material.

The fracture toughness particularly is related in a complex manner to the microstructure. Rice (1977), in a review of the relationship between mechanical properties and microstructure, noted that fracture toughness is strongly affected by the presence of a second phase in the material. This effect is even more marked when differences in thermal expansion between the phases give rise to interfacial stresses or cracks in the material, as these act as a crack blunting mechanism, with a consequent increase in fracture toughness and wear resistance. The extent of the effect depends on the chemical composition, size, shape, and location of the second phase. These factors vary widely among the materials in this study, and this no doubt contributes to the poorly defined nature of the relationship between microstructure and erosion resistance.

It is again possible to broadly divide the materials prepared using PFA into two groups, one with poor erosion resistance and the other with good erosion resistance. The materials with poor erosion resistance are those which crystallised by growth from the surface of the specimen, while specimens which crystallised by growth from nuclei in the bulk of the sample are much more resistant to erosion by particle impact. The low erosion resistance of the surface nucleated specimens (glasses B and F) is attributed to the depth to which cracks caused by the impact of particles penetrate into the specimen. Due to thermal stresses along the grain boundaries, planes of weakness exist within the material, and thus cracks formed by particle impact will extend deep into the specimen. The amount of material removed per impact will be high, and the low erosion resistance of these materials is thus a consequence of the oriented microstructure.

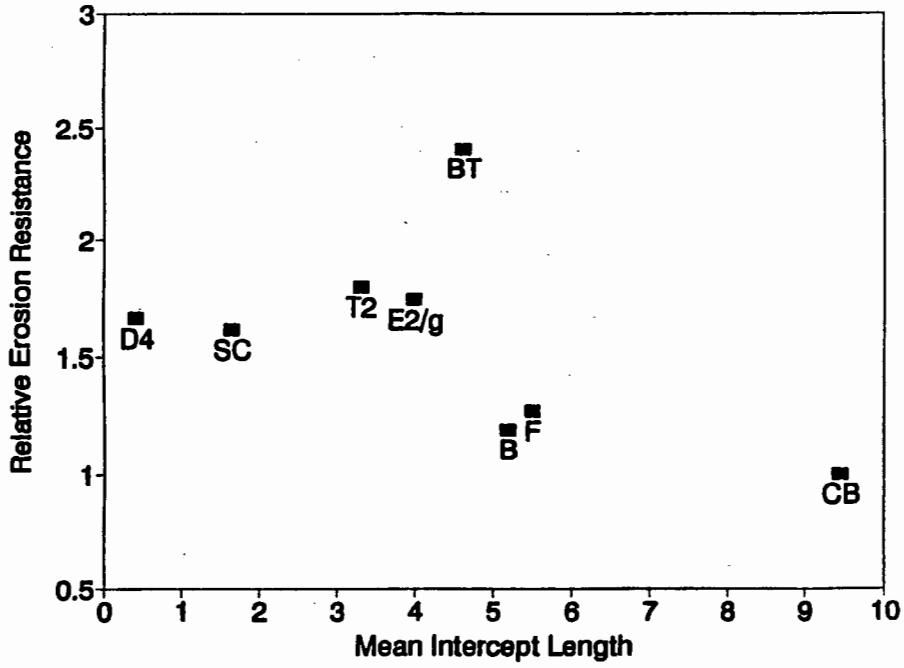

Figure 54: The relationship between microstructure and erosion resistance demonstrated by the glass ceramics prepared using PFA

The improved erosion resistance of the specimens which were bulk nucleated springs from two sources. The decrease in grain size causes an increase in fracture toughness and the hardness of the material. Similarly, the existence of a two phase microstructure where one phase is dispersed throughout the second phase may cause an increase in fracture toughness (Rice 1977). Both these effects are believed to be operating in these glass ceramic materials.

Ceramic D4 illustrates the influence of grain size. The phase assemblage in this material is identical with that of the Base glass, but due to the addition of a nucleating agent the glass has a much smaller average grain size. Since there is no second phase, the increase in the wear resistance is attributable only to the change in grain size of the material.

The marked effect on the erosion rate of the material by the presence of a second phase is be shown by comparing the erosion resistance of ceramics B, T2 and T10, containing 0, 2, and 10% of TiO_2 respectively. The ceramic T2 has a considerably higher erosion resistance than does ceramic B. Further increasing the TiO_2 content increases the erosion resistance, presumably since the higher proportion of the second phase in the material results in higher internal stresses, as well as a smaller grain size. Both these factors act to increase the fracture toughness and thus the wear resistance.

6.7 Summary

Pulverised Fuel Ash from the Lethabo power station will form a stable glass when mixed with $CaCO_3$ and melted at 1550°C. The resultant glass devitrifies on heat treatment at 950°C by crystal growth from nuclei on the surface of the glass to give a friable material with a columnar microstructure and a high degree of porosity.

The glass may be bulk nucleated by additions of titanium dioxide and iron and chrome oxides, to produce a fine grained and erosion resistant material. Phosphorous pentoxide is ineffective as a nucleant in these glasses, although it has some effect on the microstructure of the crystalline materials. The major phase present in all the glasses prepared was melilite, a calcium-magnesium alumino-silicate solid solution.

Glasses containing titanium dioxide crystallised to give two phases, melilite and a second phase containing titanium, titaian-augite. The added titanium dioxide acted as a nucleating agent, providing nuclei throught the bulk of the glass for crystal growth. The resultant glass was mechanically strong, and the erosion resistance, measured using solid particle impact, was much higher than the un-nucleated glass, due largely to the two phase microstructure.

The glass nucleated by a mixture of iron and chrome oxides crystallised to give a fine grained, single phase material which is more robust and has a greater resistance to erosion than the glass without additions.

It was clear that tough and wear resistant ceramic materials could be prepared using PFA as a raw material. The solid particle erosion tests indicated that the material containing titanium dioxide was the most resistant of the materials prepared, and is much more resistant to erosion than some commercially used materials.

7. BIBLIOGRAPHY

Alberts L. (1987)
South African minerals and waste products.
Proc. International Symposium on Ash - a Valuable Resource, CSIR, Pretoria, 1987.

Avrami M. (1939).
J. Chem. Phys. 9, 177.

Barry T.I. (1979).
The Mineralogy of Glass-Ceramics.
Brit. Ceram. Soc. Proc., 29, 1-22.

Barry T.I., Cox J.M., Morrell R. (1978).
Cordierite Glass-ceramics - effect of TiO2 and ZrO2 content on phase sequence during heat treatment.
J. Mater. Sci., 13, 594-610.

Beall G.H. and Duke D.A. (1969).
J. Mater. Sci., 4, 340.

Becker R. (1938)
Ann Phys, 32, 128

Becker R., and Doerning W. (1935)
Ann Phys, 24, 719

Bek M.V., Pona M.G., Givlyvel N.W. (1981)
Use of power station fuel slags for making ceramic tiles.
Sleklo Keram., 7, 4-5.

Boswell J.E.S. (1987)
The disposal of power station ash by ESKOM in South Africa.
Proc. International Symposium on Ash - a Valuable Resource, CSIR, Pretoria, 1987.

Bronkala W.J. The selection and application of magnetic seperation equipment. Proc. International Symposium on Ash - a Valuable Resource, CSIR, Pretoria, 1987.

Burnet G. Alumina recovery from Fly Ash by the lime-soda-sinter process. Proc. International Symposium on Ash - a Valuable Resource, CSIR, Pretoria, 1987.

Cahn J.W. and Charles R.J. (1965).
Phys. Chem. Glass, 6, 181

Carter S., Ponton C.B., Rawlings R.D., Rogers P.S. (1988).
Microstructure, chemistry, elastic properties and internal friction of Silceram glass ceramics.
J. Mater. Sci., 23, 2622-2630.

Cervinka L, Dusil J. (1975).
Determination of crystallinity in crystallized glasses by XRD .
J. Non-Cryst. Solids., 21, 125-16, 1975.

Chen Q.Q., Gai P.L., Groves G.W. (1982).
Microstructure and grain growth in Li_2O-Al_2O_3-SiO_2 glass ceramics
Journal of Materials Science 17 (1982) 2671-2676.

Christian J.W (1975)
The theory of transformations in metals and alloys, 2nd edition, Part 1. Pergamon, Oxford. ISBN 0-08-018031-0

Clarke D.R. (1987),
Ann. R. Mater., 17, 57-74.

Dalton R.H. (1947).
U.S. Patent No. 2 422 472.

Davies M.W., Kerrison B., Gross W.E., Robson M.J., Wichall D.W. (1970).
Slagceram : A glass ceramic from blast furnace slag.
J. Iron and Steel Inst., 208, (4), 348-370.

Davis D.E.
Fly ash utilization in cement bonded products - a general view.
Proc. International Symposium on Ash - a Valuable Resource, CSIR, Pretoria, 1987.

Deer W.A, Howie R.A., Zussman J. (1966). An introduction to the rock forming minerals. 1st ed, 12t impression. Longman UK.
ISBN 0582 44210 9.

Deguire E.J, Risbud S.H. (1984).
Crystallisation and properties of glasses prepared from Illinois coal fly-ash.
J. Mater. Sci., 19, 6, 1760-6, 1984.

DeVekey R.C., Majumar A.J. (1973).
Metastable zoning in cordierite-based glass-ceramics.
Mater. Res. Bull., 8, 9, 1073-78.

DeVekey R.C., Majumdar A.J. (1975).
The influence of TiO2 on the properties of cordierite glass ceramics.
Brit. Ceram. Soc. Proc., 25, 1-11.

Doherty P.E., Lee D.W., Davis R.S. (1967).
Direct observation of the crystallisation of Li2O - Al2O3 - SiO2 glasses containing TiO2.
J. Amer. Ceram. Soc., 50, 77.

Doremus R.H. (1973)
'Glass Science', p.90,
John Wiley and Sons,New York.

Englebrecht E. (1987)
Methods applied by ESKOM to revegetate ash dams in South Africa.
Proc. International Symposium on Ash - a Valuable Resource, CSIR, Pretoria, 1987.

Evans A.G (1978)
Impact damage mechanisms: solid projectiles.
Treatise on Materials Science and Technology, Vol 16, p1-67

Faber J.H and Babcock A.W. (1987)
50 years of ash marketing and utilization in the USA.
Proc. International Symposium on Ash - a Valuable Resource, CSIR, Pretoria, 1987.

Flanagan R.C. (1977) Ash particle formation in pulverised coal combustion. Paper 77-4, Spring meeting of the Western States Section, Seattle, Washington, The Combustion Inst.

Frith V. and Heckroodt R.O. (1984) The reliability of a digitiser system for image analysis.
Pract. Met., 21, 595-601

Goodman C.H.L. (1986).
The structure of silica glass and its surface.
Phys. Chem. Glass., 27, 1, 27.

Goodman C.H.L. (1987).
A new way of looking at glass.
Glass Tech., 28, 1, 19-29.

Gutzow I., Zlateva E., Alyakov S., Kovatscheva T. (1977).
Kinetics and mechanism of crystallisation in enstatite-type glass ceramics.
J. Mater. Sci., 12, [6], 1190-1202.

Hammetter W.F., Loehman R.E. (1987).
Crystallisation tendencies of complex lithium-silicate glass-ceramics.
J. Amer. Cer. Soc., 70, 8, 577-82, 1987.

Harper H. James P.F., McMillan P.W. (1970). Discuss. Faraday Soc. 50, 206.

Harper H. and McMillan D.W. (1972)
The formation of glass ceramic microstructures.
Phys. Chem. Glass, 13, [4], 97.

Hayward P.J., Vance E.R., Coren D.C. (1987).
DTA / SEM study of crystallisation in sphene glass-ceramic.
Am. Ceram. Soc. Bull., 66, 11, 1620-26.

Headley T.J., Loehman R.E. (1984).
Crystallisation of a glass ceramic by epitaxial growth.
J. Am. Ceram. Soc., 67, [9], 620-5.

Heckroodt R.O. and Robinson A.N. (1987)
Erosion by Pulverized Fuel Ash in power generating units.
Proc. International Symposium on Ash - a Valuable Resource, CSIR, Pretoria, 1987.

Heinichen D. and Walton K. The potential for exploiting two of the chemical attributes of Pulverized Fuel Ash (PFA) in South Africa. Proc. International Symposium on Ash - a Valuable Resource, CSIR, Pretoria, 1987.

Hing P. (1975)
The Strength and fracture properties of Glass-ceramics.
Brit. Ceram. Soc. Proc., 25, 13-25.

Hing P., McMillan P.W. (1973).
The strength and fracture properties of glass-ceramics.
J. Mater. Sci., 8, 1041-1048.

Hing P., McMillan P.W. (1973a).
A transmission electron microscope study of glass ceramics.
J. Mater. Sci., 8, 340-348.

Humphreys K.K. and Lawrence W.F. (1970)
Producing mineral wool from by-products.
Minerals Processing, March.

James P.F, McMillan P.W. (1970).
Phys. chem. glass., 11, 59.

James P.F. (1975).
Review: Liquid-phase separation in glass-forming systems.
J. Mater. Sci., 10, 1802-1825.

James P.F., McMillan P.W. (1970).
Quantitative measurements of phase separation in glasses using TEM. Part 2. A study of lithia-silica glasses and the influence of phosphorous pentoxide.
Phys. Chem. Glass. 11, 3, 64-70.

Johnson W.A., Mehl R.F. (1939).
Trans. Am. Inst. Min. (Metall.) Engrs. 135, 416.

Karayakin V.A., Gapeka L.F., Turusheva G.Y. et al. (1980)
Synthesis of glass ceramics from thermoelectric power plant ashes and slags.
Steklo Keram., 6, 6-7.

Karayakin V.A., Turusheva G.Y., Nagornava E.A., Kruchinin Y.D. (1975)
Glass ceramic material from fly ash of heat and electric power plants.
Steklo Keram., 10, 34-35.

Karlsen T.M. (1985).
The erosive characteristics of SA pulverised coals.
MSc Thesis, UCT.

Keith H.D. and Padden F.J. (1963).
J. Appl. Phys. 34, 2409

Kim H.S., Rawlings R.D., Rogers P.S. (1989), Quantitative determination of crystalline and amorphous phases in glass ceramics by X-Ray diffraction analysis. Brit. Ceram. Soc. Trans. J. 88 21-25

Kirby M.J. (1987)
Mineral Wool from PFA
BSc(Hons) Thesis, UCT.

Kirsch M., Berger G., Banach U., Huber. (1988). Vitroceramics - A Non-Conventional type of ceramic. Interceram. 3, 34-38.

Klug H.P. and Alexander L.E. (1974)
X-Ray Diffraction Procedures for Polycrystalline and Amorphous Materials. (2nd Ed.)
J. Wiley & Sons NY.

Kruger D. (1987)
Ash - an aggregate for polymer concretes - some research results.
Proc. International Symposium on Ash - a Valuable Resource, CSIR, Pretoria, 1987.

Krüger J.E. (1987)
Research at the NBRI on the utilization of fly ash: an overview.
Proc. International Symposium on Ash - a Valuable Resource, CSIR, Pretoria.

Lauf R.J. (1982)
Microstructure of Coal Fly Ash Particles.
Am. Ceram. Soc. Bull., 61, [4], p 487-490.

Lavie A. (1987)
Ash utilization in Israel.
Proc. International Symposium on Ash - a Valuable Resource, CSIR, Pretoria, 1987.

Lesch W. and Cornell D.H. (1987)
The mineralogy and morphology of Fly Ash from South African Power Stations.
Proc. International Symposium on Ash - a Valuable Resource, CSIR, Pretoria, 1987.

Levin E.M., Robbins C.R., McMurdie, H.F. (1964).
"Phase Diagrams for Cermists".
American Ceramic Society.

Lewis M.H, Metcalf-Johansen J., Bell P.S. (1979),
Crystallisation mechanisms in glass ceramics.
J. Am. Ceram. Soc. 62 278-288

Li J.H., Uhlmann D.H. (1971).
J Non-cryst solids, 5, 328.

Lorenzato A.G and Blackbeard P.J. (1987)
Collection, storage and transport of ash at large power stations in South Africa.
Proc. International Symposium on Ash - a Valuable Resource, CSIR, Pretoria, 1987.

MacFarlane D.R. and Fragoulis M. (1986).
Theory of devitrification in multicomponent glass forming systems under diffusion control.
Phys. Chem. Glass. 27, 6, 228-234.

Maier V., Muller G. (1987).
Mechanism of Oxide nucleation in Lithium AluminoSilicate glass-ceramics.
J. Am. Ceram. Soc., 70, 8, C176-8.

Maier V., Muller G. (1988).
Nucleation and crystallisation in Mg-Al-Silicate Glasses.
cfi/Ber, 65, 6/7, 208-212.

Manz O.E. (1984).
Utilization of By-Products from western coal combustion in the manufacture of mineral wool and other products.
Cement and Concrete Research, 14, 513-520, 1984.

Marshall G.D, Robèrt R.V.D, Burden K.J. (1987)
Gallium - it's determination and distribution in South African Fly Ash.
Proc. International Symposium on Ash - a Valuable Resource, CSIR, Pretoria, 1987.

Matusita K., Sakka S., Maki T., Tashiro M. (1975).
Study on crystallisation of glass by differential thermal analysis. Effect of added oxide on crystallization of Li2O-SiO2 glasses.
J. Mater. Sci. 10 94-100

Maurer R.D. (1962).
J. Appl. Phys. 33, 2132.

Mazurin O.V., Kluyev V.D., Roskova G.P. (1970).
Phys. Chem. Glasses. 11, 192.

McColm I.J. (1983).
Ceramic Science For materials technologists.
Leonard Hill, Glasgow, 1983. ISBN 0-412-00351-1.

McMillan P.W., Partridge G. (1969).
Brit. Patent No. 1 151 860.

McMillan P.W. (1982).
The crystallisation of glasses.
J. Non-Cryst. Solids., 52, 67-76.

McMillan P.W. (1974).
Proc X Intl. Cong. on Glass., 14, 1.

McMillan P.W. (1974).
The glass phase in glass ceramics.
Glass Tech., 15, 1, 5.

McMillan P.W. (1979).
Non-Metallic Solids Volume 1. Glass Ceramics. (second edition).
Academic Press London 1979 ISBN 0-12-485660-8

McMillan P.W. and Partridge G. (1972).
J. Mater. Sci. 7, 847.

McMillan P.W., Peter W.J. (1982),
Crystallisation of glasses.
J. Non-Cryst. Solids. 52 [1-3 67-76

Motsareva E.G., Pavlushkin N.M.
Tr Mosk Khim Technol, In-ta Im. D.I. Medeleev, No 92, p 35, 1976.

Ohlberg S.M. and Strickler D.W. (1962),
Determination of percent crystallinity of partly devitrified glass by X-Ray Diffraction.
J. Am. Ceram. Soc. 45 4 170-171

Orren M.J., Wyrley-Birch J.M. and Maree P.J.C. (1987)
Environmental utilization of ash - an agricultural opportunity?.
Proc. International Symposium on Ash - a Valuable Resource, CSIR, Pretoria, 1987.

Partridge G. (1982).
Nucleation and crystallisation phenomena in low expansion Li2O Al2O3 SiO2 glass ceramics.
Glass Tech., 23, [3], 133-8.

Pavlushkin N.M., Sarkisov P.D., Orlova L.A. (1982).
Process of catylysing the crystallisation of glass and the synthesis of glass ceramic.
Zh. Vses. Khim. O-va., 27, [5], 510-18.

Ponton C.B., Rawlings R.D., and Rogers P.S. (1986),
Mechanical properties of 'Silceram' Glass ceramics
Brit. Ceram. Soc. Proc. 37 229-234

Rabinovich E.M. (1982)
Glass-Ceramics from Israeli Slag and Coal Ash.
Adv. Ceram. (4), 334, 1982.

Ray C.S., Huang W., Day D.E. (1987)
Crystallisation kinetics of lithia silica glasses: effect of composition and nucleating agent.
J. Amer. Cer. Soc., 70, 8, 599-603.

Ray C.S., Huang W., Day D.E. (1987).
Crystallisation kinetics of lithia silica glasses: effect of composition and nucleating agent.
J. Am. Ceram. Soc., 70, 8, 599-603.

Ray S and Muchow G. (1968).
J. Amer. Cer. Soc., 51, 678.

Rice R. (1977).
Microstructure dependence of mechanical behaviour. in: Properties and Microstructure (Treatise in materials science and technology). Ed McCrone R.K.
Academic Press London.
ISBN 0-12-341811-9.

Rindane G.E. (1962).
J.Am. Ceram. Soc. 45,7.

Rogers P.S. and Williamson J. (1969).
The nucleation of crystalline phases in silicate glasses containing iron oxides.
Glass Technol., 10, 5, 128-133.

Ruff A.W and Wiederhorn S.M.(1979)
Erosion by solid particle impact.
Treatise on Materials Science and Technology, Vol 16 p69-126.

Sandrelli C. and Paoletti-Gualandi M. (1987)
The industrial use of coal ash in Italy.
Proc. International Symposium on Ash - a Valuable Resource, CSIR, Pretoria, 1987.

Sarsby R.W. and Marshall C.B. (1987)
Field Performance of a retaining wall composed of reinforced Pulverised Fuel Ash.
Proc. International Symposium on Ash - a Valuable Resource, CSIR, Pretoria, 1987.

Scheidler H. and Rodek E. (1989)
Li2O-Al2O3-SiO2 Glass-Ceramics.
Ceramic Bulletin, 68, 11, 1926-1930.

Shelestak L.J. Chavez R.A., McKenzie J.D., Dunn B.S. (1978)
J NonCryst Solids, 27, 83.

Smith M.A. and Harris M.R. (1987)
Fly Ash disposal and utilization: Environmental considerations.
Proc. International Symposium on Ash - a Valuable Resource, CSIR, Pretoria, 1987.

Stavreka D.A and Patsovska A.P. (1987)
Glass Ceramic and glass crystal materials from thermal power plants.
Proc. 5th Natl. Conf. on mechanics and Technology of Composite Materials.
Varna 1987.

Stewart D.R. (1972).
TiO2 and ZrO2 as nucleants in a Lithia-Aluminosilicate glass. Advances in nucleating and crystalline glass.
Amer. Ceram. Soc. Spec. Publ. 5. Ed Hench, L.L., and Freiman, S.W., p251, 1972.

Stookey S.D. (1960). British Patent 829447.

Stookey S.D. (1960)
British Patent 829447, 1960.

Stookey S.D. (1950a).
U.S. Patent NO. 2 515 275.

Stookey S.D. (1950b),
U.S. Patent No. 2 515 941.

Stookey S.D. (1956).
Brit. Patent No. 752 243.

Stookey S.D., Maurer R.D. (1962).
"Progress in Ceramic Science", Vol. 2, p. 77. Pergamon Press, New York.

Swift H.R. (1947)
J. Amer. Ceram. Soc. 30, 165.

Topping J.A. (1976).
Fabrication of glass ceramic material based on blast furnace slag - a review.
J. Can. Ceram. Soc., 45, 63-67.

Turnbull D. and Vonnegut B. (1952).
Indstr Engng Chem, 44, 1292.

Uhlmann D.R.,
J. Non-Cryst Solids 7, 337.

Uhlmann D.R., (1971).
Advances in Nucleation and Crystallization in Glasses p 91. American Ceramic Society.

Utsumi Y., Sakka S. (1970).
J. Amer. Cer. Soc. 53, 286.

Veasey T.J. (1973).
Recent developments in the production of Glass-Ceramics.
Miner. Sci. Engng., 5, 2, 92-107.

Verbaan B. (1987)
The utilization of South African Power Station Fly Ash for the recovery of Alumina products.
Proc. International Symposium on Ash - a Valuable Resource, CSIR, Pretoria, .

Vonnegut B (1947)
J Appl Phys, 18, 593.

Wagner H. (1987)
Mining Applications of Fly Ash.
Proc. International Symposium on Ash - a Valuable Resource, CSIR, Pretoria, 1987.

Wakabayashi A. (1987)
Manufacture of lightweight aggregate utilizing Fly Ash.
Proc. International Symposium on Ash - a Valuable Resource, CSIR, Pretoria,.

Wert C. and Zener C. (1950)
J. Appl. Phys., 21, 5]

Weyl W.A. (1951).
"Coloured Glasses".
Soceity of Glass Technology.

Weyl W.A. (1962)
Conditions of glass formation among simple compounds.
Symposium on Nucl and Cryst in Glasses and Melts p37-38.

Weyl W.A. and Marboe E.C. (1962) The constitution of glasses: A dynamic interpretation. Vol II, Part I: constitution and properties of some representative glasses. ???

Wiederhorn S., Hockey, B.J. (1983),
Effect of material parameters on the erosion resistance of brittle materials
J. Mater. Sci. Lett. 18 766-780

Williamson J., Tipple A.J., Rogers P.S. (1968).
Influence of Iron oxides on kinetics of crystal growth in $CaO-MgO-Al_2O_3-SiO_2$ glasses
J. Iron Steel Inst. 206, 898.

Willis J.P. (1987)
Variations in the composition of South African Fly Ash.
Proc. International Symposium on Ash - a Valuable Resource, CSIR, Pretoria,.

Zdaniewiski W. (1973).
Crystallisation and properties of a MgO-Al2O3-SiO2-TiO2 glass-ceramic.
J. Mater. Sci., 8, 192-202.

Zdaniewski W.A. (1975).
DTA and X-Ray analysis study of nucleation and crystallisation of MgO-Al2O3-SiO2 glasses containing ZrO2, TiO2, and CeO2.
J. Am. Ceram. Soc., 58, 5-5, 163-169.

Zdaniewski W.A. (1978).
Microstructure and kinetics of crystallisation of MgO-Al2O3-SiO2 glass ceramics.
J. Am. Ceram. Soc., 61, 5-6, 199-204.

Zelowski J. (1987)
Generation of ash by hard coal power stations and problems of its utilization in the Federal Republic of Germany.
Proc. International Symposium on Ash - a Valuable Resource, CSIR, Pretoria.

8. APPENDICES

8.1 Composition of the Pulverised Fuel Ash

Table A1: XRF Analysis of Lethabo Mixed ash

Oxide	Wt.%	Element	ppm	Element	ppm
SiO_2	50.77	Ba	868	Sr	746
Al_2O_3	35.23	Cu	59	Th	29
CaO	4.36	Nb	42	U	10
Fe_2O_3	3.41	Ni	92	Y	94
TiO	1.67	Pb	72	Zn	81
MgO	1.20	Rb	47	Zr	468
Na_2O	0.28	Sc	43		
K_2O	0.46				
P_2O_5	0.36				
Loss on ignition : 2.25% (residual coal) Analysis by Geochemistry Dept, UCT.					

8.2 Preliminary investigation of Glass crystallisation

The following glass batches were prepared, melted and specimens cut and heat treated. Specimens were heat treated for times of 15, 60, 120, 1200, and 6000 minutes, and then mounted in a thermoplastic medium, polished, etched, and examined by microscope.

The specimens were classified as 'good' or 'bad' according to their microstructure, meaning the extent of porosity, of cracking and the grain size of the material. A few specimens were selected from this list for further examination.

Table A2: Composition of specimens (mass percent)

Name	SiO_2	Al_2O_3	CaO	Fe_2O3	TiO_2	MgO	Cr_2O_3	Na_2O	P_2O_5
A1	25.7	17.8	52.8	1.7	0.8	0.6	0.0	0.4	0.1
T10	23.3	16.2	47.9	1.6	10.0	0.6	0.0	0.3	0.1
T5	24.4	17.0	50.2	1.6	5.6	0.6	0.0	0.4	0.1
T2	25.4	17.6	52.2	1.7	1.8	0.6	0.0	0.4	0.1
BN	24.5	17.0	50.3	1.6	0.8	0.6	0.0	5.0	0.1
BT	23.3	16.2	47.9	1.6	10.0	0.6	0.0	0.3	0.1
BTN	22.3	15.5	45.9	1.5	9.5	0.5	0.0	4.5	0.1
C2	31.7	21.9	43.3	1.4	0.7	0.5	0.0	0.3	0.1
C3	35.9	24.8	36.8	1.2	0.6	0.4	0.0	0.3	0.1
C4	47.5	35.7	14.9	0.9	0.4	0.3	0.0	0.2	0.1
C5	60.3	9.5	28.2	0.9	0.5	0.3	0.0	0.2	0.1
D2	25.2	17.5	51.7	2.7	0.8	0.6	1.0	0.4	0.1
D3	24.4	17.0	50.2	4.0	0.8	0.6	2.4	0.4	0.1
D4	23.3	16.2	47.9	6.2	0.8	0.6	4.6	0.3	0.1
A3	33.5	23.1	34.3	1.1	7.1	0.4	0.0	0.2	0.1
E2	23.2	16.1	47.7	1.6	9.9	0.5	0.0	0.3	0.6
E3	33.4	23.1	34.2	1.1	7.1	0.4	0.0	0.2	0.4
2.3	49.5	12.4	35.6	1.2	0.6	0.4	0.0	0.3	0.1
2.1	32.7	8.2	57.4	0.8	0.4	0.3	0.0	0.2	0.1
5.1	24.0	16.0	59.9	0.0	0.0	0.0	0.0	0.0	0.0
5.3	35.5	24.5	40.1	0.0	0.0	0.0	0.0	0.0	0.0
A4	25.2	17.5	50.6	0.8	5.4	0.3	0.0	0.2	0.1
A5	21.5	14.9	57.0	0.5	5.9	0.2	0.0	0.1	0.1

8.3 The commercial materials

8.3.1 Silceram

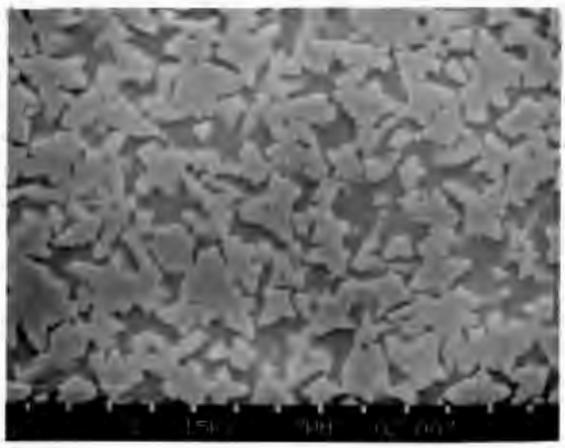

Figure A1: SEM micrograph polished and etched section through SILCERAM

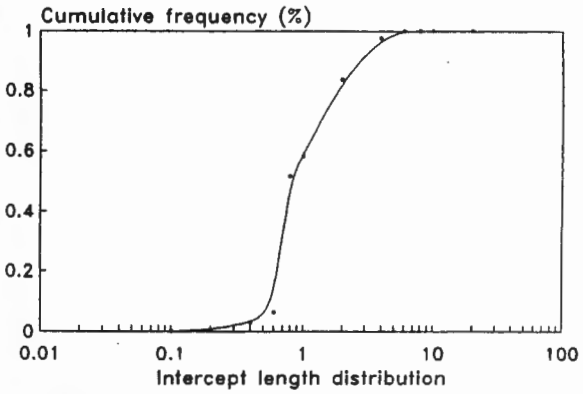

Figure A2: Intercept length distribution of SILCERAM

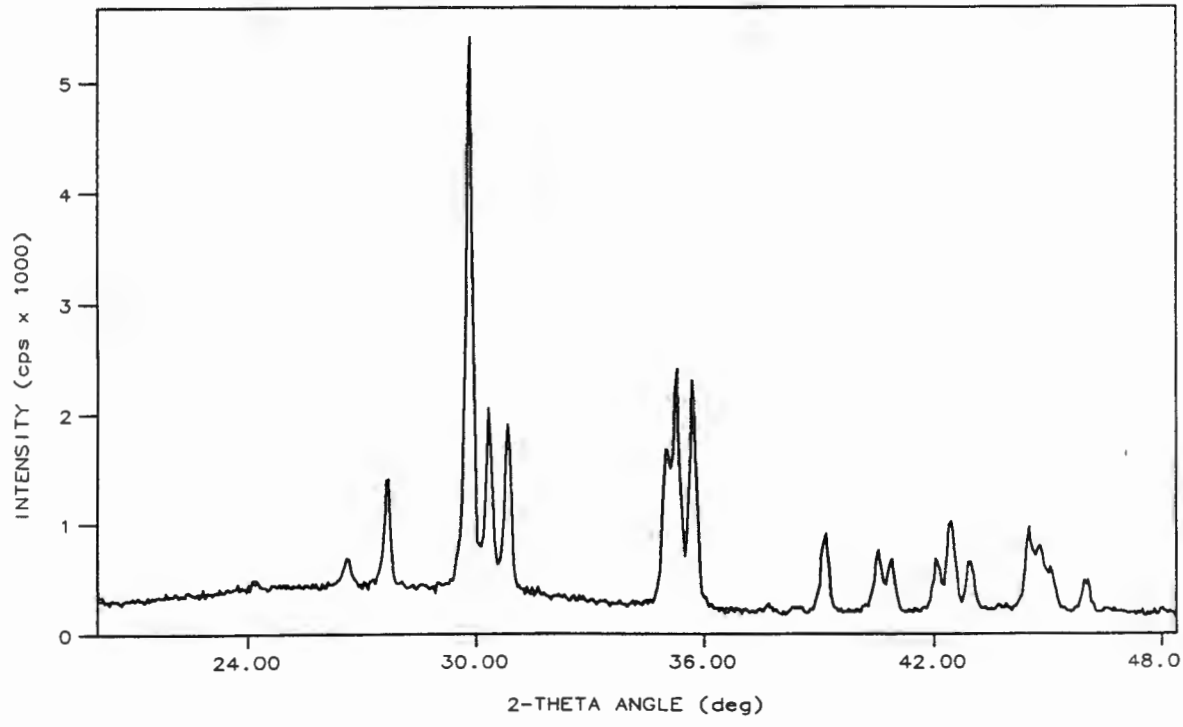

Figure A3: XRD spectrum of SILCERAM.

8.3.2 DGC1

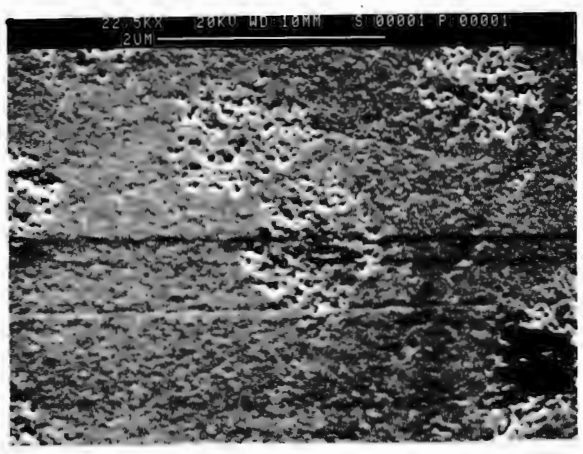

Figure A4: SEM micrograph polished and etched section through DGC1

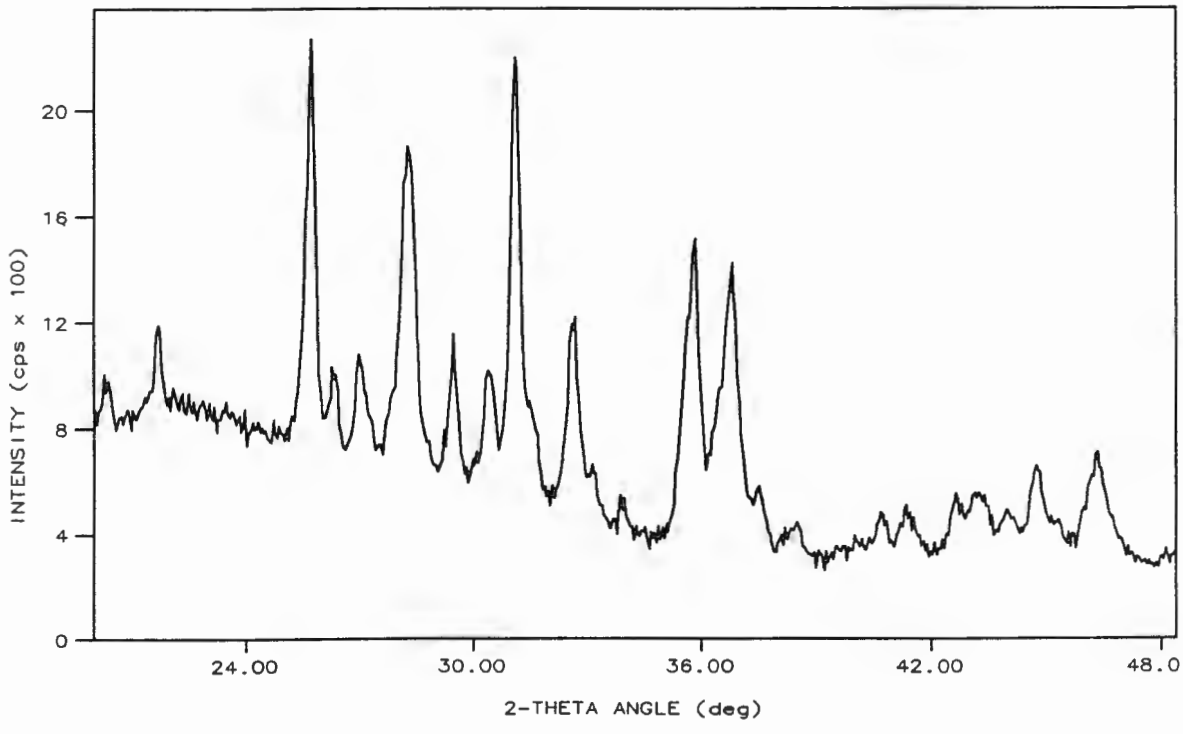

Figure A5: XRD spectrum of DGC1

8.3.3 DGC2

Figure A6: SEM micrograph polished and etched section through DGC2

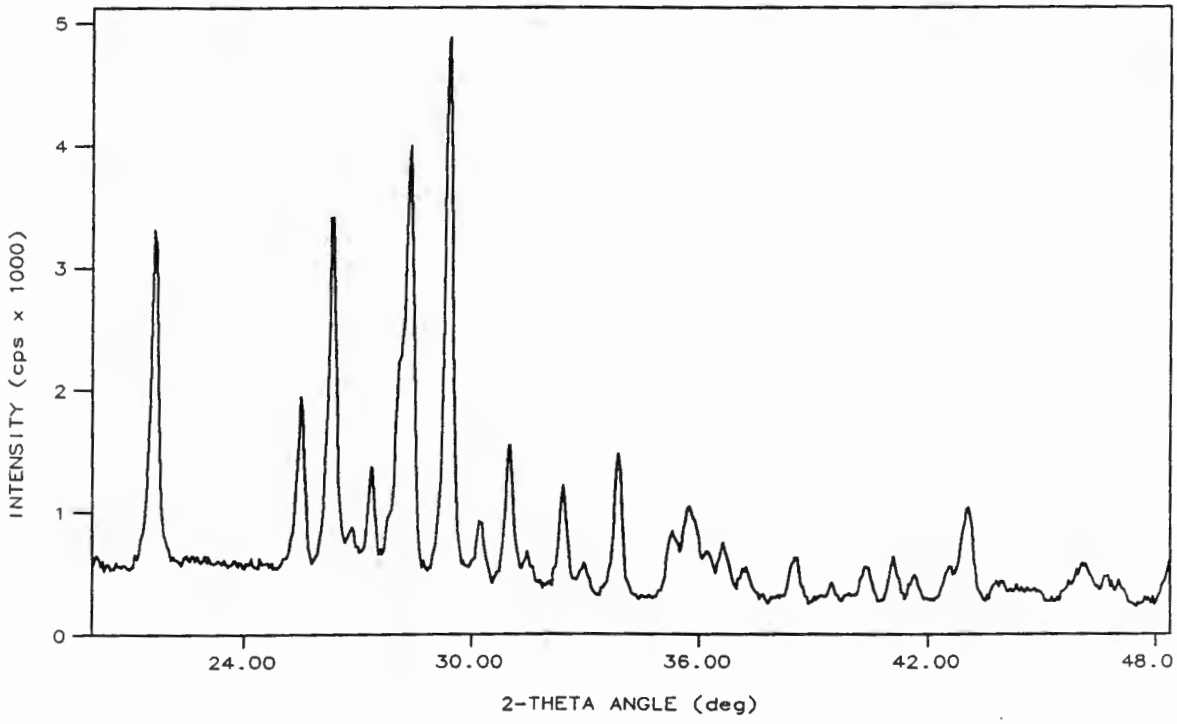

Figure A7: XRD spectrum of DGC2

8.3.4 Cast Basalt

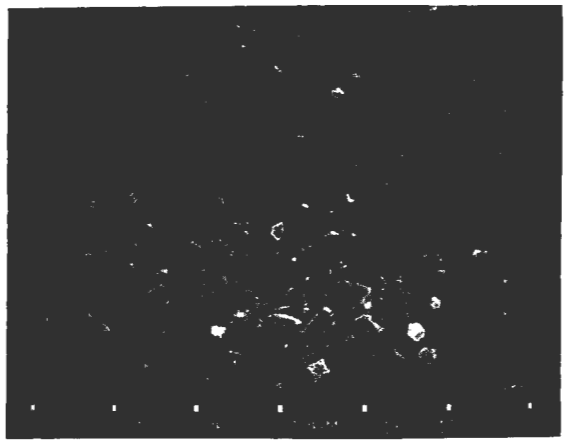

Figure A8: SEM micrograph polished and etched section through CAST BASALT

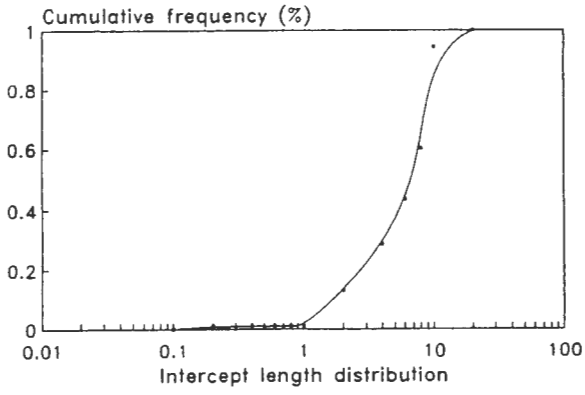

Figure A9: Intercept length distribution for CAST BASALT

8.4 Experimental Conditions.

8.4.1 Heat Treatment

The specimens for microstructural analysis and erosion testing were heat-treated using the High Temperature Furnace designed by the department. The heating profile of this furnace is controlled via a RS232 link to an (IBM compatible) computer, and can be set to any desired combination of ramp and soak profiles using the control software developed in the department (FIRE.EXE, G.Evans and M.Kirby). High reproducibility and accuracy are features of this system.

The specimens for isothermal crystallisation were heated by insertion into a small tube furnace at the temperature required for crystal growth (950°C). After the required soak time, the sample was removed and quenched into water. The heat treatment cycle for these specimens is shown in Table 3. No nucleation treatment was given as earlier microstructural examination showed that this had little effect.

The samples for erosion were ramped slowly to prevent thermal stresses in the material, as large blocks of glass were used. No nucleation period was given to these specimens, as the slow rate of heating through the temperature region where nucleation occurs was felt to be sufficient.

Table A3: Heat treatment of samples prepared.

Specimen	Rate (°C/min)	Nucleation	Crystal growth
Microstructure	20	800°C / 1hr	950°C / as rqd
Erosion	2	-	950°C / 6000 mins
Crystall'n rate	>900	-	950°C / as rqd

8.4.2 Grinding and Polishing

The samples were mounted in a transparent thermoplastic using a mounting press, and polished through coarse grit to a 1/4 micron finish.

A standard polishing procedure was used for all samples. Firstly, rough grinding on a water lubricated rotating wheel on bonded carborundum papers, starting at #80, and followed by #120, #240, #320, #480 and #600. Specimens were given approximately 1 minute on the coarser grits, and 5 minutes on the two finest. The specimens were thoroughly rinsed with water between papers.

For the polish, specimens were polished on diamond impregnated textile pads lubricated with a polishing oil. Each specimen was given one hour on each of the 15 micron, 7 micron, 3 micron and 0.25 micron diamond pastes. The specimens were thoroughly cleaned between each grade of paste, and examined by optical microscope to ensure that scratches from the previous grade had been removed.

8.4.3 Etching

Due to the fairly reactive nature of the major phase of the material (melilite) toward hydrochloric acid, an acid etch consisting of 5% of HCl + 2% of HF was used for all samples.

The wide range of compositions encountered in the materials prevented the establishment of a standard etching procedure. Instead, a sample was etched for 10 seconds, then washed and dried, and the degree of etch evaluated using the optical microscope. This process continued until the etching became evident.

This procedure was successful on the ceramics with microstructures on a scale resolved by the microscope, but the samples with a very fine grained microstructure tended to be slightly over-etched for SEM evaluation.

8.4.4 X-ray Diffraction

XRD measurements were made using a Philips PW1400 diffraction spectrometer. Due to the inaccuracies inherent in the chart drive, spectra were collected by digitally by counting at discrete two theta increments and transferring the results to a floppy disk via the RS232 port. Communication software (COLLECT.EXE), written to facilitate this is available at the XRD instrument. A standard set of instrumental conditions was used to record the spectra:

Radiation:	Cu Kα, 40 kV, 30 mA.	
Slits:	receiving	0.5°
	divergent	0.5°
	scattering	1°
Step Size:	0.05° 2-theta.	
Count Time	10 seconds.	

To reduce the effect of instrumental variations on the data, the automatic sample changer was used to collect data overnight as this allowed all the samples in a series to be recorded without pause.

8.4.5 Optical Microscopy

Micrographs were recorded on a Reichert-Jung Polyvar, using the automatic camera system and Ilford FP4 film (125 ASA). Developing was done by a commercial concern, and printed in the darkroom of the Civil Engineering Department using the (very old) enlarger on Ilford Multispeed paper, grade 4. Standard procedures for developing and printing were used throughout.

8.4.6 Scanning Electron Microscope

SEM micrographs were recorded using the Cambridge S180 Stereoscan system of the Electron Microscopy Unit at UCT. The electron optic parameters necessary for adequately high resolution were established, and all photographs taken on the S180 were taken using these settings. The magnification of the microscope was calibrated by photographing standards of known dimensions.

The demise of the S180 in the late stages of the project required a certain amount of photography to be done using the S200 in the same department. Unfortunately, the electron optic parameters could not be controlled to the same extent, and the pictures were not taken under identical conditions.

Samples were sputter-coated with Au-Pd for normal imaging. The micrographs of the sample were taken using 120mm Ilford FP4 film (125 ASA).

The electron optical parameters for the S180 were :

kV	20.0
C1	1.1A
C2	0.8A
Beam Current	250×10^{-6} A
Aperture	#1
Working distance:	4.437 mV on voltmeter
Rise time	100×10^{-6} seconds
Tilt	0°

The working conditions on the S200 were as kept similar as possible. The working distance was shorter, and the tilt could not be kept under 35°, due to the design of the specimen chamber.

8.4.7 Erosion

Samples were prepared for erosion by machining a flat surface using a rotating diamond-bonded facing wheel lubricated by water. Shaped specimens were cleaned using ultrasound, dried and weighed. Each sample was then placed in the test rig,

and eroded by the passage of 10.0 grams of #120 grit SiC carried in an air stream with a pressure of 300kPa at the inlet. The particle velocity was previously measured to be above 50 ms^{-1} and the impact angle 20° from the normal. The sample was then weighed to record the mass loss. This procedure was repeated three times for each sample and the average value reported.

8.5 Measurement of Intercept Length Distribution

Photographs of polished and etched specimens were obtained as described previously. These photographs were analysed using software written for image analysis, called <IMAGE.EXE> (Author: M Kirby). The program, once started, allows entry of parameters such as the date, sample name, and other information needed for record purposes.

The photograph for analysis is fastened onto the table, with a suitable grid of lines overlaying. This study used a grid of lines ruled 5mm apart due to the small features of the photographs. The effective magnification of the photograph is calculated using the scale bar on SEM photos, or a previously photographed graticule for optical micrographs. The total distance of all line segments of interest is measured, followed by the measurement of the segments of the phase of interest. The length of each of these segments is recorded, and the complete data file written to disk when the measurement is complete.

This data is then transferred to a spread sheet, where a frequency distribution is derived from the individual line lengths using the statistical functions provided by the worksheet. The data may then by plotted as a cumulative frequency histogram.

8.6 Measurement of Rate of crystallisation

Under isothermal conditions, the kinetics of the crystallisation of a glass specimen can be described by the Avrami expression:

$$X = 1 - \exp(-kt^n) \qquad [1]$$

X = volume fraction of crystallisation species
k = materials constant (rate constant)
n = mechanism description
t = time

The constant n may be used to evaluate the mechanism of growth (McFarlane, 1986).

Samples of glass approximately 1x1x1 cm (carefully selected for consistent sample properties) were heat treated at 950°C. The samples were inserted directly into the furnace at 950°C from room temperature. They were soaked for a predetermined length of time, after which they were removed and quenched into cold water. The samples were then crushed in a Sieb Technik swingmill for 5 minutes to produce a fine powder.

A step scan from 20° to 50° 2-theta, with a step size of 0.05° and a count time of 10 seconds was used to record the spectrum. Selected peaks were analysed using software designed for the purpose. This software <XPROC.EXE> (Author M Kirby) provides background stripping, peak height and integrated peak area for peaks specified. The XRD data file is written with a 6 line header, as below, and the first line must contain the name of a second file containing information specifying the processing required.

<FILE B6000.XRD>

```
B.XRS          (name of description file)
DATA LINE
DATA LINE
DATA LINE
DATA LINE
      601    20.0000    50.0000    0.0500   10.0000STEP202311 291
    2000      113    10000
    2005      142    10000
    2010      137    10000
    2015      149    10000
      .
      .
      .
    5000      100    10000
```

The description of the position of peaks and the background associated with each peak are in an associated file. The description file must contain the following information in order: the start and end 2-theta angles of the first region to be used as data; the start and end angles of the second background region; the start and end regions of the region to be analysed as a peak. An example is presented below. This file (B.XRS specifies that 4 peaks will be analysed. The background for the first is measured from 23.20 - 23.4° 2θ, and 24.8 - 25.2° 2θ. The peak will be measured between 23.6 and 24.4° 2θ.

<FILE B.XRS>

```
2320   2340   2480   2520   2360   2440   - 1st peak for analysis
2780   2800   2950   3050   2830   2950   - 2nd peak for analysis
3000   3020   3400   3480   3040   3220
3400   3480   3800   3860   3600   3700
```

Peak start and end angle

Background 2 start and end

Background 1 start and end

Each peak was analysed as follows:

The local background under the peak is calculated by fitting a line through backgrounds 1 and 2 of the scan. The intensity of the background at any point under the peak is determined by interpolation.

To determine the position and intensity of the peak maximum, a subset of data was extracted, comprising 5 points around the largest number in the peak data set. The peak maximum was evaluated by fitting a curve to this subset of data, and calculating the maximum using the derivative, i.e. evaluating the position of theta for $f'(\theta) = 0$.

This gave the position of the maximum, and the value was obtained by substitution into the fitted curve. The background evaluated at the position of the peak maximum was subtracted to give nett peak heights. The area of the peak was evaluated by summing the area under the curve, with the background subtracted at each point.

The output of the program is a data file called <File.XRO>, with the following format:

<FILE B.XRO>

```
Processing file: B6000.XRD

#   THETA D_SPACE    HEIGHT    AREA    HEIGHT    AREA
1   23.906   3.723    290.18   79.08    286.23   75.98
2   28.813   3.099    438.66  176.35    454.93  195.47
3   31.292   2.859   1814.09  713.60   1768.60  638.08
4   36.721   2.448    219.62   59.55    235.90   75.71
```

straight line

polynomial

d space and angle of peak

There are two values for each peak area and peak height. These are calculated using a straight line and 2nd order polynomial respectively. The straight line is useful where the peak intensity is very low, as the noise inherent in the measurement my cause strange artifacts in the values calculated if a polynomial is used.

Corrected peak intensities (or peak areas) may then be used to evaluate the coefficients in the Avrami kinetic equation.

8.7 The measurement of the constants of the Avrami (kinetic) equation

Specimens of the cast and annealed glass were cut into pieces of equal size, approximately 1x1x1 cm. These were heat-treated by inserting the specimen into a hot furnace for a fixed length of time, and quenching the specimen into water.

The specimens were heated for times of 1, 2, 4, 8, 16, 32, 64, 120, 240, 480, 1200, 2400 and 6000 minutes.

The heat treated specimens were then ground, and the XRD spectrum recorded. Software developed for the purpose was used to calculate the maximum peak height and peak area of selected peaks in the specimen.

The samples were assumed to be 100% crystalline after 6000 minutes at 950°C, and the fraction crystallised was calculated as the ratio of the peak height (or area) at time t to the peak height (or area) at 6000 minutes.

The value $\ln(-\ln(1-X))$, where X is the fraction crystallised, is then plotted against ln(time).

ln k and n were evaluated over a selected subset of the data. The long time range over which the data set extends meant that crystallisation may not have started, or not have finished for some values and these were excluded, as the equation is only valid while crystallisation is in progress.

By selection of those points which are measured during the crystallisation process, a least-squares fit to the above equation can be made, allowing the constants k and n to be evaluated.

8.8 Derivation of the Avrami equation

The symbols to be used are:

^{v}I	: nucleation rate per unit volume
τ	: induction period
t	: time
T	: growth rate (assumed isotropic)
$V\beta$	: volume of phase α transformed to new phase β
ξ	: volume fraction transformed at time t.
V	: total volume of system

The volume fraction E is defined as:

$$\xi = \frac{V\beta}{V} \qquad [A2]$$

Assuming isotropic growth of an isolated spherical region, the volume of the region transformed to phase β after a time t is:

$$V = (4\pi/3)\ T^3\ (t-\tau)^3 \quad (\ t > 0\ ) \qquad [A3]$$

The total volume transformed in a time period is the sum of the volume of all the regions transformed in this time including growth on new nuclei formed during this time. The total volume transformed after a time TR is:

$$V\beta = (4\pi V/3) \int_0^t {}^{v}I\ T^3\ (t-\tau)^3\ dt \qquad [A4]$$

Growth of a number of separate nuclei will eventually lead to mutual interference as the particles grow into each other. In transformations in solid media, the growing regions will develop a common interface, and growth along this interface will cease. The overall rate of the transformation will be reduced by a factor depending on the extent of interaction.

The derivation by Johnson & Mehl (1939) and Avrami (1939; 1940, 1941) which is summarised by Christian (1975) treats this by proposing that an "extended" volume ($V\beta_e$) of transformed material be given by:

$$V\beta_e = (4\pi V/3) \int_0^t {}^{v}I\ T^3\ (t-\tau)^3\ dt \qquad [A5]$$

The extended volume is the volume of material that would have transformed in the absence of impingement of the growing particles. It is geometrically related to the volume that actually transforms, and a relationship can be found between V^{β}_{e} and V^{β}:

$$V^{\beta}_{e} = -V \ln(1 - (V^{\beta}/V)) \qquad [A6]$$

By using the equations A5 and A6 we can calculate:

$$-\ln(1 - \xi) = (4\pi V/3) \int_0^t {}^{V}I \; T^3 \; (t-\tau)^3 \; dt \qquad [A7]$$

Integration of this equation is possible only if the time dependance of the nucleation rate is known.

Avrami (1941) proposed a description of the rate of nucleation that is applicable to certain reactions. By assuming that nucleation only occurs at certain preferred sites, and that these sites become gradually exhausted, the rate of disappearance of such sites in a time dt will be given by:

$$d({}^{V}N) = -{}^{V}N_0 \; dt \qquad [A8]$$

Or:

$${}^{V}N = {}^{V}N_0 \exp(-v_1 \; t) \qquad [A9]$$

where:

- ${}^{V}N_0$: Number of sites/unit value initially
- ${}^{V}N$: Number of sites remaining after time t
- v_1 : Frequency at which a site becomes a nucleus

The nucleation rate (^{V}I) is then given by:

$${}^{V}I = -\frac{d({}^{V}N)}{dt} = {}^{V}N_0 \; v_1 \exp(-v_1 \; t) \qquad [A10]$$

Substitution of (7) into (10) and integrating gives a large cumbersome equation, solution of which requires knowledge of the time dependance of ^{V}I and v_1:

$$\xi = 1-\exp\left[(8\pi {}^{v}N_0 T^3/v_1{}^3)\left\{\exp(-v_1 t)-1+v1t - \frac{(v1t)^2}{2} + \frac{(v1t)^3}{6}\right\}\right] \qquad [A11]$$

There are two limiting conditions for this equation, corresponding to a constant rate of nucleation (small $v_1 t$), and to a rapid decrease of the rate of nucleation, which gives effectively a zero rate of nucleation for the reaction. These two possibilities reduce to the following equations:

For the case of constant nucleation:

$$\xi = 1 - \exp\left\{-(\pi/3)\ {}^{v}I\ T^3\ t^4\right\} \qquad [A12]$$

For the case where nucleation is effectively zero:

$$\xi = 1 - \exp\{-(4\pi/3)\ {}^{v}N_0\ T^3\ t^3\ \} \qquad [A13]$$

Avrami (1941) proposed a general form of the above equations, which has become known as the Johnson-Mehl-Avrami equation, or the Avrami equation:

$$\xi = 1 - \exp\ (-kt^n)$$

The meaning of the value k will vary considerably according to the nucleation mechanism.

8.9 The XRD spectra of gehlenite and akermanite

The diagrams below show the schematic spectra of gehlenite and Åkermanite imposed on the XRD spectrum of the Base glass.